KU LEUVEN

FACULTEIT WETENSCHAPPEN

The response of alanine dosimeters in small fields and low kV X-rays

Burak YALVAC

Promotor: Prof. dr. Brigitte Reniers
Hasselt University/ KU Leuven

Co-promotor: Prof. Edmond Sterpin, PhD, Ir
KU Leuven

Proefschrift ingediend tot het behalen van de graad van Master of Science in de Medische Stralingsfysica

Academiejaar 2019-2020

The response of alanine dosimeters in small fields and low kV X-rays

Preface

Alanine/EPR dosimetry has been used for many decades for the measurement of ionising radiation in various applications such as food irradiation, sterilisation and medical dosimetry in radiotherapy quality assurance (QA). Recently, lots of advancements are happening in the preclinical radiotherapy research with small animal irradiators where they are using beams with smaller fields and kV X-rays. These small animal irradiators are gaining much interest in conducting radiobiology experiments to understand the effect of radiation biologically. To be able to use alanine detectors in those conditions, their response should be characterised. In this thesis, the response of alanine detectors has been determined in 50 – 225 kV photon beams and in small fields. This way, I hope that this thesis can provide insight so that alanine detectors can be implemented for QA in small animal irradiators and other applications using low energies, e.g. brachytherapy or even for QA in radiology departments in the future.

This thesis would not have been possible to finalise without the support of many people. First, I would like to thank my promotor, prof. dr. Brigitte Reniers for her amazing support and guidance during this project. Next, I want to thank my co-promotor, prof. dr. Edmond Sterpin for his amazing guidance and support during this project. I want to thank NuTeC and UHasselt for access to the lab and materials and equipment. I want to thank UZ Leuven and Maastro in Maastricht, The Netherlands for access to the departments and the irradiators.

I am very grateful to prof. dr. Wouter Crijns and prof. dr. Nathal Severijns for their help and constructive feedback during the writing of this thesis.

I am very grateful to my family and friends for their help, patience and tremendous support during this project. Finally, I want to mention my late grandfather, Halil Konakci, who passed away on the 23rd of February 2020. One of the most independent and proud people I knew.

Summary

Introduction

Alanine/EPR dosimetry has been used for many decades for dosimetry QA in radiotherapy. The Nuclear Technology Centre (NuTeC) from the University of Hasselt is using alanine/EPR dosimetry for providing audit services for MV photon beams and MeV electron beams. Lots of improvements are happening recently in the preclinical research for radiotherapy where they are working with small animal irradiators. These machines use medium and lower kV X-rays and small fields. Besides, electronic brachytherapy sources using miniature X-ray sources are also gaining interest. To use alanine/EPR dosimetry in these conditions, its response must be characterised. The goal of this thesis is to investigate the relative response of alanine/EPR dosimetry at 50 – 225 kV X-rays and small fields. This way, NuTeC could extend its audit services to small animal irradiators.

Materials and methods

Alanine and film dosimeters were irradiated on two different small animal irradiators: the SARRP and the X-RAD 225CX. The detectors were irradiated with beams of 50 – 225 kV X-rays and with field sizes of 13.6 x 13.6 cm² to 1 x 1 cm². Both detectors were placed at the same location and depth as close as possible. The dose measured by the alanine pellet was compared to the dose measured by the film. This was defined as the relative response of the alanine detector. The film detectors were investigated for energy dependence by measuring PDD's in water and RW3. MC simulations with the DOSRZnrc user code from the EGSnrc code system were performed to compare with the experimental results.

Results

The relative response of the alanine dosimeters drops to 0.795 at photon beams with a mean energy of 78 kV and it drops further to 0.665 at photon beams with a mean energy of 35 kV. The relative response increases with 1.5% when the field size decreases to 1 x 1 cm². The simulated results are approximately 4.5 % higher than the experimental results. The intrinsic efficiency of the alanine detectors should be known to reproduce the experimental results correctly.

Conclusion

The relative response of the alanine detectors drops significantly with decreasing photon energy in the kV range while the relative response increases slightly with decreasing field sizes. It is possible to characterise this behaviour in function of parameters such as the mean energy or the HVL of the photon spectra. It is feasible to use alanine detectors for dosimetry QA of small animal irradiators and therefore it is possible to use it for auditing purposes of these machines.

Samenvatting

Inleiding

Alanine/EPR dosimetrie wordt al enkele decennia gebruikt voor dosimetrische QA in de radiotherapie. Het nucleair technologisch centrum (NuTeC) van Uhasselt maakt gebruik van alanine/EPR dosimetrie voor MV fotonenbundels en MeV elektronenbundels. De laatste tijd is er veel vooruitgang gemaakt in het veld van preklinisch onderzoek voor radiotherapie waarin ze werken met bestralingstoestellen van kleine dieren. Deze toestellen gebruiken fotonenbundels van lagere energieën in het kV bereik. Daarnaast worden elektronische brachytherapietoestellen met mini X-ray bronnen populairder. Om alanine/EPR dosimetrie te kunnen gebruiken voor deze toestellen moet hun respons gekarakteriseerd worden. Het doel van deze thesis is om de relatieve respons van alanine/EPR dosimetrie te onderzoeken voor 50 - 225 kV fotonenbundels en in kleine bestralingsvelden. Zo kan het mogelijk worden dat NuTeC audits kan ontwikkelen voor bestralingstoestellen van kleine dieren.

Materialen en methodes

Alanine en film detectoren werden bestraald met 2 verschillende toestellen voor kleine dieren: de SARRP en de X-RAD 225CX. De detectoren werden bestraald met 50 – 225 kV bundels en veldgrootten van 13.6 x 13.6 cm² t.e.m. 1 x 1 cm². Beide detectoren werden zo goed mogelijk geplaatst op dezelfde locatie en diepte. De dosis gemeten door de alanine pellet werd vergeleken met de dosis gemeten door de film. Dit werd gedefinieerd als de relatieve respons. De film detectoren werden ook onderzocht voor energie-afhankelijkheid door het meten van PDD's in water en RW3. MC simulaties met de gebruikerscode DOSRZnrc van de EGSnrc package werden uitgevoerd om te vergelijken met de experimentele resultaten.

Resultaten

De relatieve respons van de alanine detectoren zakt naar 0.795 bij fotonenbundels met een gemiddelde energie van 78 kV en het zakt verder naar 0.665 bij bundels met een gemiddelde energie van 35 kV. De relatieve respons stijgt met 1.5 % bij veldgrootten van 1 x 1 cm². De

gesimuleerde resultaten zijn ongeveer 4.5 % hoger dan de experimentele resultaten. De intrinsieke efficiëntie van de alanine detectoren moet gekend zijn om de experimentele resultaten te kunnen reproduceren met simulaties.

Conclusie

De relatieve respons van de alanine detectoren zakken behoorlijk bij dalende fotonenenergie in het kV bereik. De relatieve respons stijgt lichtjes voor kleinere velden. Het is mogelijk om de alanine detectoren te karakteriseren met parameters zoals de gemiddelde energie of de HVL van het fotonenspectrum. Hieruit blijkt dat het mogelijk is om alanine detectoren te gebruiken voor dosimetrische QA van bestralingstoestellen van kleine dieren. Dus het is ook mogelijk om alanine detectoren te gebruiken voor audits van deze toestellen.

Vulgarising summary

Cancer patients receiving radiation therapy are usually irradiated with photon beams of very high energies. The clinical energy range is in the megavolt (MV) range. To verify if the prescribed dose to the patient is accurate and correct, measurements must be performed with detectors that measure the absorbed dose from radiation. This is part of the quality assurance (QA) protocols. These tests happen on a periodical basis. There are also independent QA tests which means that an external company performs dosimetry measurements with their detectors in a radiotherapy department. These measurements usually happen as a dosimetry audit. This makes it possible to compare results from several clinics. Recently, lots of advancements are happening in the preclinical research where they are developing machines for irradiating small animals such as mice to conduct research. These small animal irradiators are used for radiobiology experiments and to test novel treatment techniques on animals before translating it to human research. This is comparable to drugs research that is first tested on small animals before moving to experiments on human subjects. Different from conventional treatment machines for cancer treatment is that these small animal irradiators use beams of lower energy in the kilovolt (kV) range and the field size of the beams are much smaller due to the small size of the animals that are irradiated compared to the size of humans. These small animal irradiators also need QA measurements to control if the delivered doses from these machines are accurate. This means suitable detectors must be found for this purpose. Alanine/EPR dosimetry is a technique where small pills of the amino acid alanine are irradiated that forms free radicals (that contain free electrons) in the pills dependent on the received radiation dose. These free electrons can be measured with electron paramagnetic resonance (EPR) spectroscopy which can be related to the absorbed dose. These alanine pills are already used for decades for QA measurements on conventional radiotherapy machines used to treat humans. To use the alanine detectors for dosimetry on small animal irradiators, its response should be characterised for the beams coming out from these machines. So, the alanine detector response must be characterised in kV beams and small fields. In this study, the response of alanine detectors was investigated with 2 commercial small animal irradiators. Alanine and film detectors were placed at the same location and depth as close as possible, and these were then irradiated by these machines with different beams. The dose measured by

the alanine detectors was compared to the dose measured by the films. The results show that the relative response of alanine detectors can drop down to 0.665 for these lower energy photon beams. For small fields, the response increases with 1.5 %. It seems possible to characterise the response of alanine detectors in these conditions and thus it is possible to use alanine/EPR dosimetry for small animal irradiators.

Vulgariserende samenvatting

In de radiotherapie worden patiënten meestal bestraald met fotonenbundels van hoge energieën. Het klinische bereik van de energieën is in megavolt (MV). Om te controleren of de voorgeschreven dosissen correct worden toegediend aan de patiënt moeten metingen worden uitgevoerd met detectoren die de geabsorbeerde dosis kunnen meten. Dit is een onderdeel van de quality assurance (QA) protocollen. Deze testen worden periodiek uitgevoerd. Er worden ook onafhankelijke QA metingen uitgevoerd door externen met hun eigen detectoren in radiotherapie afdelingen. Dit word meestal als een audit uitgevoerd. Dit maakt het mogelijk om resultaten te vergeleken tussen verschillende klinieken. De laatste tijd is er veel vooruitgang gemaakt in het preklinische onderzoek voor radiotherapie waarin er toestellen worden ontwikkeld om kleine dieren te bestralen zoals muizen. Deze toestellen worden gebruikt voor radiobiologie experimenten alsook om nieuwe technieken te testen vooraleer dit op mensen wordt gebruikt. Dit is vergelijkbaar zoals farmaceutisch onderzoek waarbij medicijnen eerst bij dieren worden getest en daarna pas bij mensen. In tegenstelling tot conventionele bestralingstoestellen voor kankerbehandeling worden bij bestralingstoestellen van kleine dieren gewerkt met bundels van lagere energieën in het kilovolt (kV) bereik en de veldgrootten zijn veel kleiner omdat de bestraalde dieren veel kleiner zijn dan mensen. Deze bestralingstoestellen van kleine dieren hebben ook QA metingen nodig om te controleren of de dosimetrie correct is. Dit betekent dat er gepaste detectoren gevonden moeten worden. Alanine/EPR dosimetrie is een techniek waarbij kleine pilletjes van het aminozuur alanine worden bestraald zodat er vrije radicalen (die vrije elektronen bevatten) gevormd worden. Deze vrije elektronen kunnen gemeten worden met elektron paramagnetische resonantie (EPR) spectroscopie en dat kan gerelateerd worden tot de geabsorbeerde dosis. Om alanine detectoren te kunnen gebruiken op de bestralingstoestellen van kleine dieren moet hun respons gekarakteriseerd worden voor de bundels die uit die toestellen komen. Dus voor kV bundels en kleine veldgrootten. In deze studie werd de respons van alanine detectoren onderzocht met 2 verschillende commerciële bestralingstoestellen. Alanine en film detectoren werden zo goed mogelijk geplaatst op dezelfde locatie en diepte. Deze werden dan bestraald met verschillende bundels. De dosis gemeten door de alanine detectoren werd vergeleken tot de dosis gemeten door de film

detectoren. De resultaten tonen dat de relatieve respons van alanine detectoren daalt tot 0.665 voor lagere fotonenbundels en voor kleine veldgrootten stijgt de respons met 1.5 %. Het is mogelijk om de respons van alanine detectoren te karakteriseren in deze omstandigheden en dus is het ook mogelijk om alanine/EPR dosimetrie te gebruiken voor bestralingstoestellen van kleine dieren.

List of abbreviations and symbols

List of symbols

$\overline{A_D}$:	dose-normalised amplitude
B_0:	Magnetic field
c_T:	Temperature coefficient
Dw:	Dose to water
E:	Energy
Gy:	Gray
h:	Planck's constant
k_T:	Temperature correction
m_s:	Spin state
r:	relative response
r_Q^{MC}:	Monte Carlo simulation defined relative response
μ:	Electron moment
μ_b:	Bohr magneton
ν:	Frequency

List of abbreviations

AAPM: American Association of Physicists in Medicine

EBT: External beam therapy

EPR: Electron paramagnetic resonance

GUI: Graphical user interface

HVL: Half value layer

IMRT: Intensity modulated radiotherapy

LRA: Lateral response artefact

MC: Monte Carlo

NPL: National Physical Laboratory

NuTeC: Nuclear Technology Centre

PDD: Percentage depth dose

PMMA: Polymethyl methacrylate

PTB: Physikalisch-Technische Bundesanstalt

QA: Quality assurance

RCF: Radiochromic film

SARRP: Small Animal Radiation Research Platform

SRS: Stereotactic radiosurgery

List of figures and tables

List of figures

List of tables

Table of contents

1 Introduction

The Nuclear Technology Centre (NuTeC) is performing dosimetry audits using a combination of alanine/EPR and film dosimetry [1-3]. NuTeC would like to extend their alanine/EPR dosimetry service to medium and lower energy X-rays to offer them for the preclinical research area using small animal irradiators [4] and to brachytherapy machines. It is among others of interest for the electronic brachytherapy sources using miniature X-ray sources with peak voltages of 40-50 kV [5-7] that is presently installed in UHasselt in the context of a European grant.

Recently there has been a lot of development in small animal research platforms [4]. These platforms are used for pre-clinical research of novel techniques before moving on to human subjects. Small animals such as mice are irradiated on these platforms. These platforms should be able to mimic conditions that are used to treat humans with radiotherapy. That means that the radiation beams should be downscaled in geometry and energy. These animals are much smaller than humans e.g. a mice lung measures about 2 cm and the tumours are much smaller. Sub-millimetre precision is required. This means that MV beams that are used in external beam radiotherapy are unsuitable. The build ‘up regions which correspond roughly to the range of secondary electrons in tissue is about 1-2 cm for MV photon beams depending on the energy. If small mice are irradiated with those beams, the build ‘up and build’ down regions would have the same dimensions of the targets in the animal itself. This would make it very difficult to deliver a uniform dose to the tumour. Another issue is the lateral beam penumbra which can extend several mm beyond the geometric field.

The solution is then to **use photon beams in the kV range** below 300 kV. These photon beams have sharp penumbras and steeper build ‘up regions.

1.1 Alanine

The amino acid alanine is one of the 20 amino acids that are used in animals for protein synthesis. Besides its biological function, it was discovered in 1963 [8] that this amino acid could also be used for radiation measurements. When an alanine dosimeter is irradiated, it

induces the formation of free radicals that contain free electrons, which can then be related to the absorbed dose.

There are two structural forms of alanine, α–alanine and β-alanine. α–alanine is used for dosimetry due to its crystalline structure. This gives high stability of the formed free radicals after irradiation. They remain stable for a very long time, spanning over years. Figure 1-1 shows the structure of both forms of alanine.

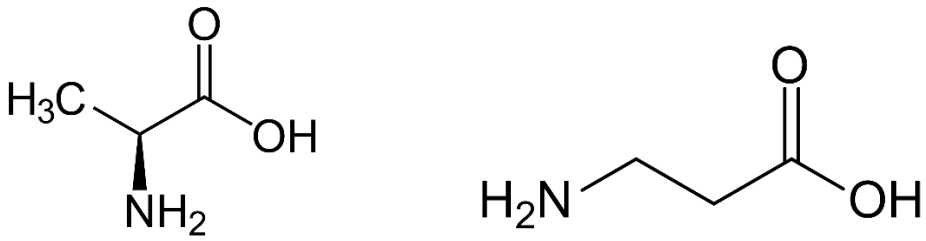

(a) (b)

Figure 1-1: (a): structure of α–alanine and (b) structure of β-alanine.

α–alanine itself exists in 2 different configurations: D and L. Due to practical reasons, only L- α–alanine is used for dosimetry.

α–alanine has an effective atomic number of 6.8, which is very similar to water. This makes it very interesting for applications in clinical dosimetry. The physical density of α–alanine is 1.42 g/cm^3.

Irradiated alanine dosimeters can be read out using electron paramagnetic resonance (EPR) spectroscopy which will be explained briefly in the following section.

1.2 Electron paramagnetic resonance

1.2.1 Theory

According to the laws of quantum mechanics, every atom or molecule has discrete states linked to discrete levels of energy. Spectroscopy consists of measuring and interpreting the transitions between those states by measuring the absorption of electromagnetic radiation by the sample. Thanks to this knowledge, one can gain insight into many properties of the subject

under study (e.g. identity, structure, dynamics). Planck's law states that electromagnetic radiation will be absorbed if ΔE, the difference in energy between the states is exactly:

$$\Delta E = h\nu \tag{1.1}$$

with h Planck's constant and ν the frequency of the electromagnetic radiation. A transition to a higher state from a lower state will occur when there is energy absorption. In conventional spectroscopy, a spectrum is obtained when the frequency is varied and the absorption is measured while in EPR spectroscopy the frequency is kept constant and the magnetic field is varied.

In EPR spectroscopy, the energy differences that are investigated are due to the interaction of unpaired electrons in the sample with a magnetic field B_0 produced by a magnet in the laboratory. This phenomenon is called the Zeeman effect. Electrons act like a compass or a bar magnet when placed in a magnetic field because electrons have a magnetic moment. Free electrons only have two possible states because they are spin 1/2 particles. When presented in an external magnetic field, it has a state of lowest energy when the moment of the electron, μ, is aligned **with** the external magnetic field B_0 and a state of highest energy when the moment of the electron, μ, is aligned **against** the external magnetic field B_0. The parallel state has m_s = -1/2 and the antiparallel state has m_s = +1/2.

The energy difference between the 2 states of the electron for a molecule with one unpaired electron in a magnetic field is described by:

$$\Delta E = g\ \mu_B B_0 \Delta_{m_s} = g\ \mu_B B_0 \tag{1.2}$$

with g the proportionality factor, which is usually 2 for most samples, μ_b the Bohr magneton and Δ_{m_s} the change in spin state. When there is no magnetic field applied, the spin states have the same energy. In case there is a magnetic field applied, the measured energy difference between the two spin states depends linearly on the applied magnetic field. This gives another possibility to perform spectroscopy by keeping the frequency of the electromagnetic radiation constant and varying the magnetic field. When the energy difference of the two states is equal to the energy of the radiation, a peak will occur in the absorption curve (Figure 1-2). This field is then called "field of resonance".

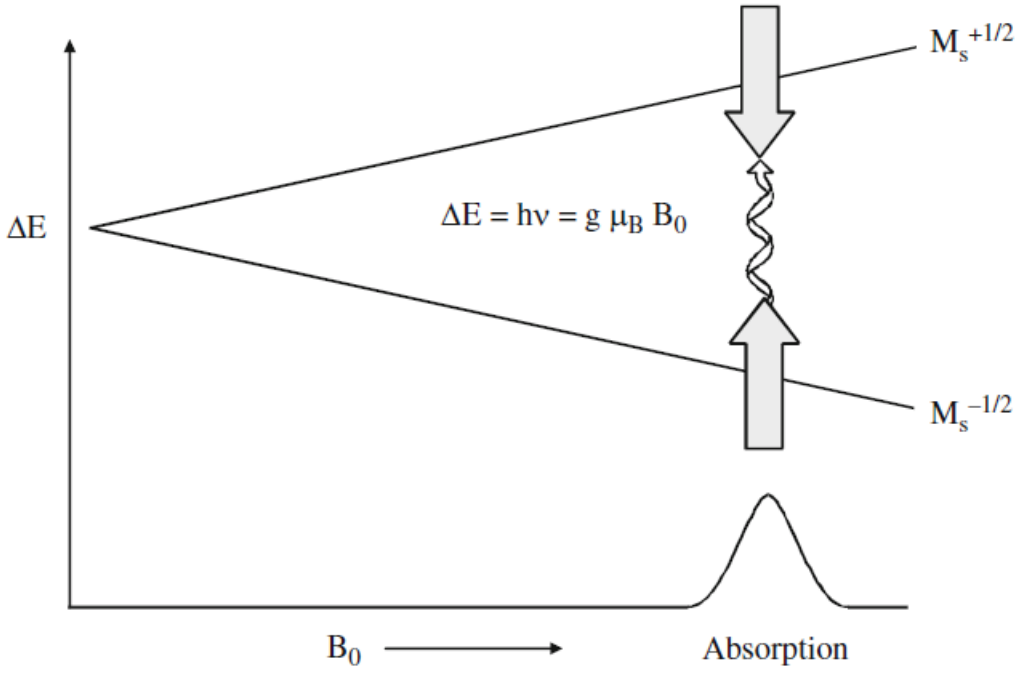

Figure 1-2: The magnetic spin states of the unpaired electrons separate as the magnetic field is scanned. Absorption occurs in the "field of resonance" [9].

It is important to note that the field for resonance is not a unique fingerprint to identify a compound. Spectra can be acquired at different microwave frequencies.

Unpaired electrons are also sensitive to their local environments. The nuclei of the atoms in a complex have a magnetic moment that produces a local magnetic field at the electron. This interaction between the nuclei and an unpaired electron is called a hyperfine interaction. Much useful information can be obtained such as the identity and number of atoms of the samples as well as the distance from the unpaired electron.

These hyperfine interactions lead to splitting of the energy levels, e.g. for a spin ½ nucleus such as hydrogen nuclei, the energy levels split into 2 and then we observe 2 absorptions. Irradiated alanine samples have more hydrogen nuclei which mean that during measurements, we observe exactly five main peaks [8]. Figure 1-3 shows a spectrum of irradiated alanine with 10 Gy.

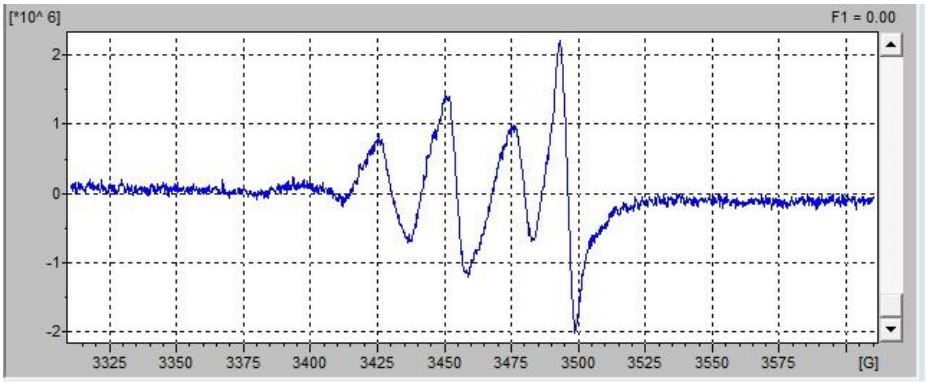

Figure 1-3: A spectrum of irradiated alanine dosimeters with 10 Gy.

1.2.2 EPR spectrometer

The general layout of a typical continuous-wave spectrometer is given in Figure 1-4.

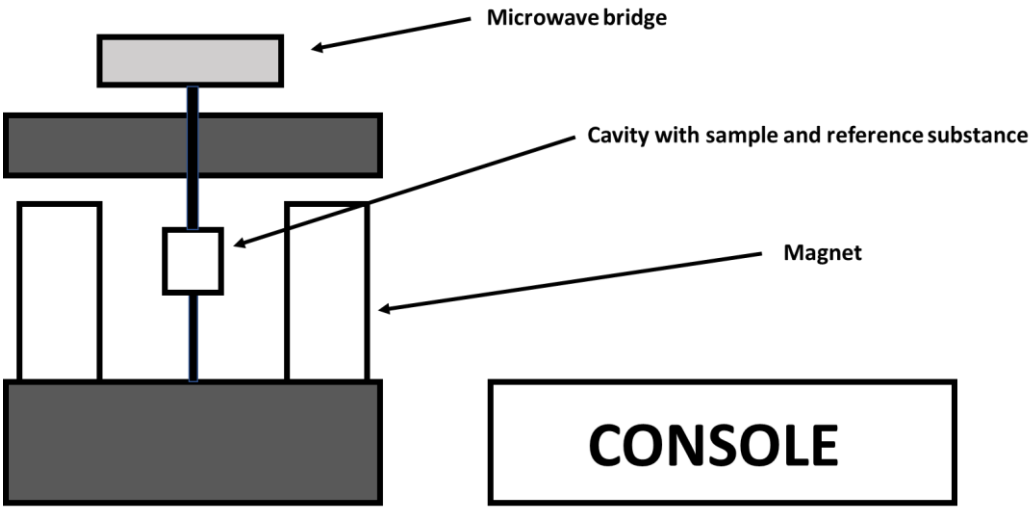

Figure 1-4: The general layout of a spectrometer.

The microwave bridge contains the microwave source and the detector. The investigated sample is placed in a cavity which is a metal box that also helps to amplify weak signals. The reference substance is measured together with the sample and it is used to compensate for the environmental effects. The magnet is used to generate and sweep the magnetic field and finally, the console is used for acquiring spectra and for data analysis.

In essence, the cavity, which is in the surrounding of a magnet with varying strength receives electromagnetic radiation from the microwave bridge. This allows measuring an absorption spectrum as shown in Figure 1-3.

The EPR cavity is used to amplify the weak signals from samples. It is a metal box that resonates with microwaves. When resonance occurs, microwave energy will be stored inside the cavity and no energy will be reflected. Usually, most of the energy will be dissipated as heat instead of being absorbed by the cavity. Cavities are described by their quality factor Q, which describes how efficient the energy storage is inside the cavity.

$$Q = \frac{2\pi\,(energy\ stored)}{energy\ dissipated\ per\ cycle} \tag{1.3}$$

Q factors can be measured easily by expressing it as:

$$Q = \frac{\upsilon_{res}}{\Delta_{\upsilon}} \tag{1.4}$$

ν_{res} is the resonant frequency of the cavity and Δ_{ν} is the width at half height of resonance.

Higher Q value means higher efficiency. It also means a large peak with a very narrow width. The absorption is driven by the magnetic component of the microwave field. The best signal is achieved if the dosimeter is placed in the electric field minimum and magnetic field maximum of the microwave field. Extreme care is required to position the sample inside the cavity with the best signal output.

Field modulation

When acquiring spectra, a smaller modulated field is applied to the magnetic field that is swept, and this results in a signal that is the first derivate of the spectrum. The advantages are a higher signal to noise ratio, improved peak identification and less disturbance from background signals. The modulation amplitude is chosen to be equal to the width of the EPR signal to avoid distorting the signal.

1.3 Alanine/EPR dosimetry correction factors

1.3.1 Temperature effects

A correction for the temperature during irradiation is required because the radiation yield of alanine dosimeters increase at higher temperatures. This factor can be calculated as:

$$k_T = 1 - c_T(T - T_0) \quad (1.5)$$

k_T is the temperature correction factor, T and T_0 are the temperatures during irradiation and the reference temperature (usually room temperature) respectively, and c_T is the temperature coefficient which is dependent on the used sample and is usually supplied by the manufacturer.

1.3.2 Variations of the cavity quality

Environmental conditions within the room containing the spectrometer can cause a change in the measurements of the spectra. Changes in the ambient temperature and humidity can cause unexpected changes to the quality factor of the cavity [10]. The spectrometer should be maintained in a room where the environmental conditions remain constant. This is very difficult to maintain. Another method is to use an adjacent reference sample that is always present in the cavity in a different position than the sample. This reference sample also has a different absorption peak than the investigated sample. The reference sample is measured together with all the test samples and the measurements of the test samples are normalised to the measurements of the reference sample to compensate for the environmental effects. This technique is described by Nagy et al. [11].

1.3.3 Fading

Alanine fading occurs due to the recombination of the irradiation-induced free radicals. Under normal laboratory conditions, the fading is very low, a few per cents per year. The fading of the alanine pellets depends strongly on the humidity level where the irradiated pellets are stored [12-14]. There is minimal effect of the temperature as it was shown that when the post-irradiation temperature was changed to 80° C for approximately 6 hours, there was minimal effect [15].

The next factor that influences the fading is the water content of the dosimeters that is related to the humidity of the environment [13, 14, 16]. It was shown that humidity also affects the sensitivity of the spectrometer [10, 17, 18]. Therefore the detectors should be kept in a dry environment. Another advantage of this system is that the readout of alanine dosimeters is non-destructive, meaning that the detectors can be measured many times without loss of signal.

1.3.4 Anisotropy

When alanine dosimeters are produced, a certain amount of binder material is used to maintain the desired shape of the alanine dosimeter. Inhomogeneity in this binder material can cause variations on the measured signal relative to the orientation of the alanine pellet in the cavity. One solution to take this effect into account is by measuring spectra at different orientations of the alanine pellet and then averaging the measured spectra [17, 19].

1.3.5 Intrinsic linearity

The great advantage of alanine dosimetry is that it shows a linear dose-response to delivered doses up to several kGy [20]. Saturation will occur at very high doses which is probably caused due to the transformation of the alanine pellet due to the immense amount of radicals formed because of the high dose the pellet received. However, for clinical dosimetry, the alanine response can be regarded as linear.

1.3.6 Dose rate dependence

It was examined that there was no significant influence of the dose rate that is used to irradiate the alanine dosimeters [14, 21-23]. It is suggested that using alanine with very high dose rates such as 3×10^{10} Gy/s is still reliable [23].

1.3.7 Tissue equivalency

Alanine has an effective atomic number of 6.8, which is very similar to water. This is very useful for clinical dosimetry.

1.3.8 Energy dependence

Alanine dosimeters have a weak energy dependence to high-energy X-rays and high energy electron beams in the megavoltage range. There is less than 1 % variation in the response of the alanine detector between ^{60}Co (1.25 MeV average energy) and 25 MV X-rays [24-27].

For medium and low energy X-rays, the relative response drops to less than 65 % for beams with mean energies less than 30 kV [28-30] compared to unity for ^{60}Co irradiation.

It was shown by Zeng et al. [26] that the energy dependence of alanine dosimetry can be characterised by the variation of the $(\text{Slope})_Q$ versus energy for a particular beam modality.

1.4 Clinical alanine/EPR dosimetry applications

Alanine/EPR dosimetry has many advantages such as similar radiation transport properties to water, non-destructive read-out, relative small detector size for use in MV beams and no usage of cables since it is a passive dosimeter. This makes it a very convenient dosimeter for reference dose measurements in radiotherapy.

These properties made alanine dosimetry a convenient choice for mailed dosimetry since 1980 for radiation dosimetry Since the 90' alanine is also being used at doses in the therapeutic range [31-33].

Alanine dosimetry is used as a secondary standard for absorbed dose to water (D_w) by metrological institutes such as the National Physical Laboratory (NPL) and the Physikalisch-Technische Bundesanstalt (PTB) [17, 33, 34] for high energy X-rays and MeV electron beams. Alanine dosimeters are also used for dosimetry in advanced radiation therapy modalities such as intensity modulated radiotherapy (IMRT) and other technologies such as CyberKnife and also for stereotactic radiosurgery (SRS) [35-37]. Alanine dosimetry is an excellent choice in these applications because it does not show the perturbations found in ionisation chambers such as directional dependence. Alanine dosimetry is used for mailed dosimetry auditing for decades [2, 3, 34, 37, 38].

Alanine/EPR dosimetry is also used for medium and lower energy X-rays [39-42] (e.g. for brachytherapy). The problem of applying alanine for brachytherapy is the large gradients of the radiation field coupled to the finite size of the detectors which compromises the dosimetry. Accurate knowledge of the relative response to the used radiation quality must be known. Also, the inhomogeneous distribution of the detection probability of the free radicals which are connected to the shapes of the electromagnetic fields inside the resonator of the EPR spectrometer must be taken into account [40].

In recent times, lots of developments happened in the preclinical radiotherapy research using small animal irradiators with small fields and kV X-rays [4]. Alanine is a potential dosimeter to be used for dose measurements, but there are compromises [43]. The relative response at the used energy must be known accurately depending on the X-ray spectra and filtration. The alanine detectors suffer from issues in small fields such as volume averaging [43, 44].

With the development of novel miniature X-ray sources with peak voltages of 50 kV for electronic brachytherapy [5-7], alanine dosimetry could be a potential candidate for reference dose measurements.

1.5 Radiochromic films

Radiochromic films (RCF) were also used in this study in addition to alanine dosimeters. Radiochromic films are used as 2D radiation detectors. They are self-developing, unlike old silver halide films. Radiochromic film detectors have high resolution, are near tissue-equivalent and have a weak energy-dependent response [45, 46]. These characteristics make RCF dosimetry suitable for 2D dose measurements with high dose gradients. They are passive dosimeters. Radiochromic films are also commonly used as reference dosimetry systems [47].

There are several different Gafchromic^{TM} film models available that are used for different dose ranges. Table 1-1 gives a summary of their dose ranges and elemental compositions.

Table 1-1: Gafchromic film models with useful dose ranges and chemical compositions of the sensitive layers [47].

Film model	Dose range (Gy)	Sensitive layer elemental composition by atomic %										Z_{eff}
HD-V2		H	Li	C	N	O	Na	Al	S	Cl	Bi	
HD-V2	10–100	58.2	0.6	27.7	0.4	11.7	0.5	0.3	0.1	0.6		7.63
MD-V3	1–100	58.2	0.6	27.7	0.4	11.7	0.5	0.3	0.1	0.6		7.63
EBT-XD	0.04–40	57	0.6	28.5	0.4	11.7	0.1	1.5	0.1	0.1		7.46
EBT2	0.01–30	56.5	0.6	27.4	0.3	13.3	0.1	1.6	0.1	0.1		7.46
EBT3	0.01–30	56.5	0.6	27.4	0.3	13.3	0.1	1.6	0.1	0.1		7.46
XR-QA2	0.1–20	56.2	1.0	27.6	1.6	11.7				0.1	1.7	55.2

EBT3 films were used in this study. Figure 1-5 shows a diagram of the EBT3 film. This film has a symmetric structure with the active layer of 28 μm sandwiched between 2 layers of matte polyester of 125 μm. It also features anti-Newton ring coatings for enhanced ease-of-use and accuracy.

When radiochromic films are exposed to ionising radiation, polymerisation is initiated of di-acetylene monomers within the sensitive layer due to charged particles depositing energy. This will cause the radiochromic film to become darker depending on the amount of ionising radiation received. By scanning these films with an optical densitometer, it is possible to determine the measured absorbed dose distribution.

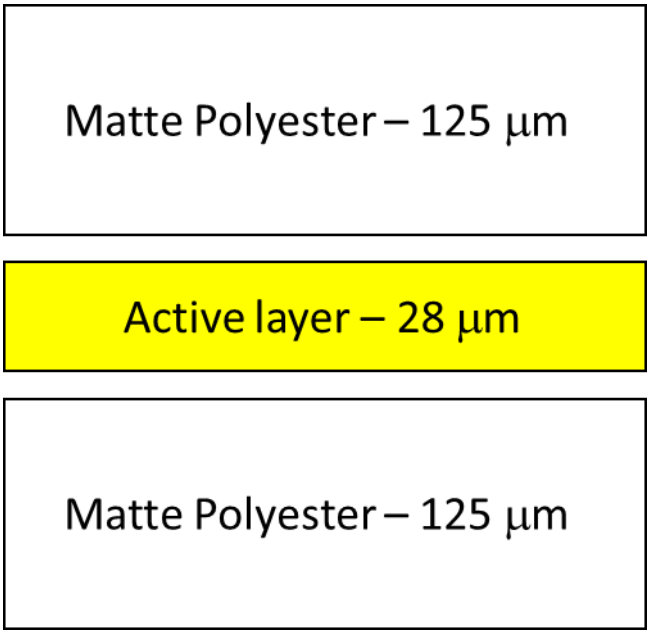

Figure 1-5: Diagram of the Gafchromic™ EBT3 film structure and dimensions.

1.6 Research questions

The goal of this project is to investigate the relative response of alanine dosimeters at X-ray energies between 50 – 225 kV and also in small fields to investigate the possibility to use it as a potential dosimeter for small animal irradiators and electronic brachytherapy sources. In the end, NuTeC could develop a mailed dosimetry auditing service for small animal irradiators and potentially a dosimetry service for electronic brachytherapy sources.

2 Materials and methods

2.1 Study of the relative response of film detectors

2.1.1 Irradiations for the film calibration

To calibrate the EBT3 films at 60 kV, 100 kV and 225 kV, they were irradiated on the Precision X-RAD 225CX small animal irradiator [48, 49] in Maastro in Maastricht, The Netherlands. It has a dual-focus X-ray tube with a 20° angled stationary tungsten target with a 0.8 mm beryllium exit window. It can also be equipped with 0.3 mm Cu and 2 mm Al filter.

The 0.3 mm Cu filter was used for the film calibration. The field size was 4 x 4 cm². The film was placed at the surface of a 2 cm thick tissue-equivalent plastic (WT1) phantom. AAPM's TG-61 protocol was used for the dosimetry [50]. The films were calibrated against the Farmer type ionisation chamber PTW TN30012-10. They were irradiated with doses between 0-8 Gy in a geometric fashion. Table 2-1 shows the beam characteristics used for the calibrations. The half value layers (HVL) and mean energies were calculated with SpekCalc [51-53]. Figure 2-1 shows the spectra.

Table 2-1: Beam characteristics of the energies used on the X-RAD 225CX. The parameters are calculated with SpekCalc [51-53].

Energy (kV)	Filtration (mm Al)	Filtration (mm Cu)	1st HVL (mm Al)	1st HVL (mm Cu)	Mean energy (keV)
60	0	0.3	4.29	0.15	43.3
100	0	0.3	6.93	0.33	58.9
225	0	0.3	11.5	0.946	85.5

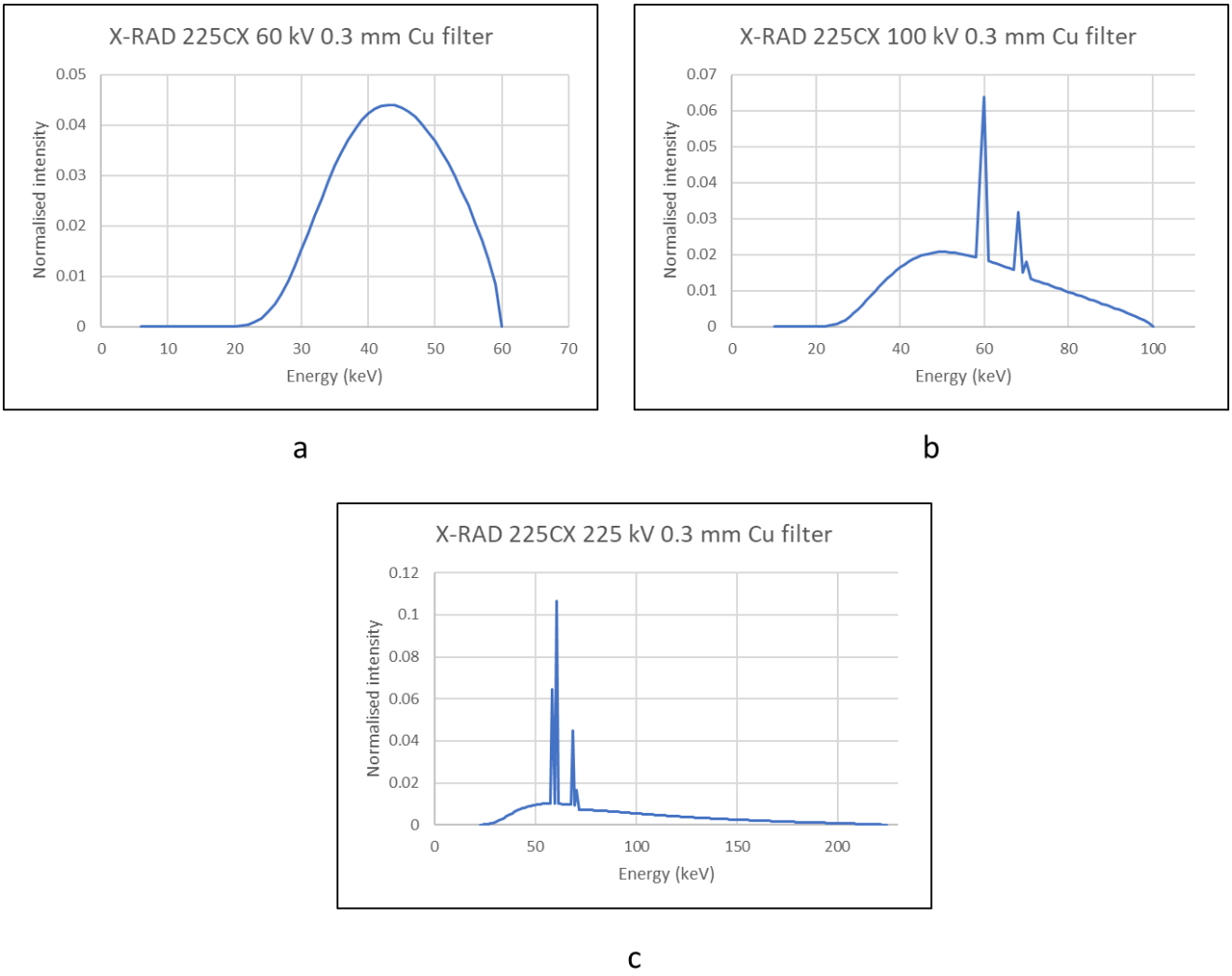

Figure 2-1: Spectra of the X-RAD 225CX used for the film calibrations. All spectra used a 0.3 mm Cu filter. (a) 60 kV spectrum. (b) 100 kV spectrum. (c) 225 kV spectrum.

2.1.2 Study energy dependence

Radiochromic film dosimetry is known for having weak energy dependence in the medium and high energy X-rays [54-57]. It has also been reported that films exhibit some energy dependency in the low kV X-rays [58, 59].

This was investigated in this study by generating calibration curves at energies of 60 kV, 100 kV and 225 kV. Calibration curve files were generated for each energy and these were then used to generate dose maps for films used in the irradiations for the measurements of the percentage depth dose (PDD) curves and determination of the relative response of the alanine pellets. In the final results, it was decided to use the dose maps that were generated using the film calibration curves with the energy that was closest to the energy used during irradiation

of the film with unknown dose distribution (e.g. calibration file of 60 kV was used for the film irradiated with 50 kV).

2.1.3 PDD measurements with the films

The PDD irradiations were performed on the Small Animal Radiation Research Platform (SARRP) at UZ Leuven [60-62]. It has a dual-focus X-ray tube with a 20° angled stationary tungsten target with a 0.8 mm beryllium exit window. The SARRP uses a filtration of 0.15 mm Cu. The open field was used for all the irradiations on the SARRP which has dimensions of 13.6 x 13.6 cm². Table 2-2 shows the characteristics of the beams that were used in this study. The parameters were calculated with SpekCalc [51-53]. Figure 2-2 shows the spectra.

Table 2-2: Beam characteristics of the energies used on the SARRP. The parameters are calculated with SpekCalc [51-53].

Energy (kV)	Filtration (mm Al)	Filtration (mm Cu)	1st HVL (mm Al)	1st HVL (mm Cu)	Mean energy (keV)
50	0	0.15	2.46	0.0794	35.3
100	0	0.15	4.88	0.196	53.4
150	0	0.15	6.94	0.355	65.2
220	0	0.15	9.32	0.637	78.1

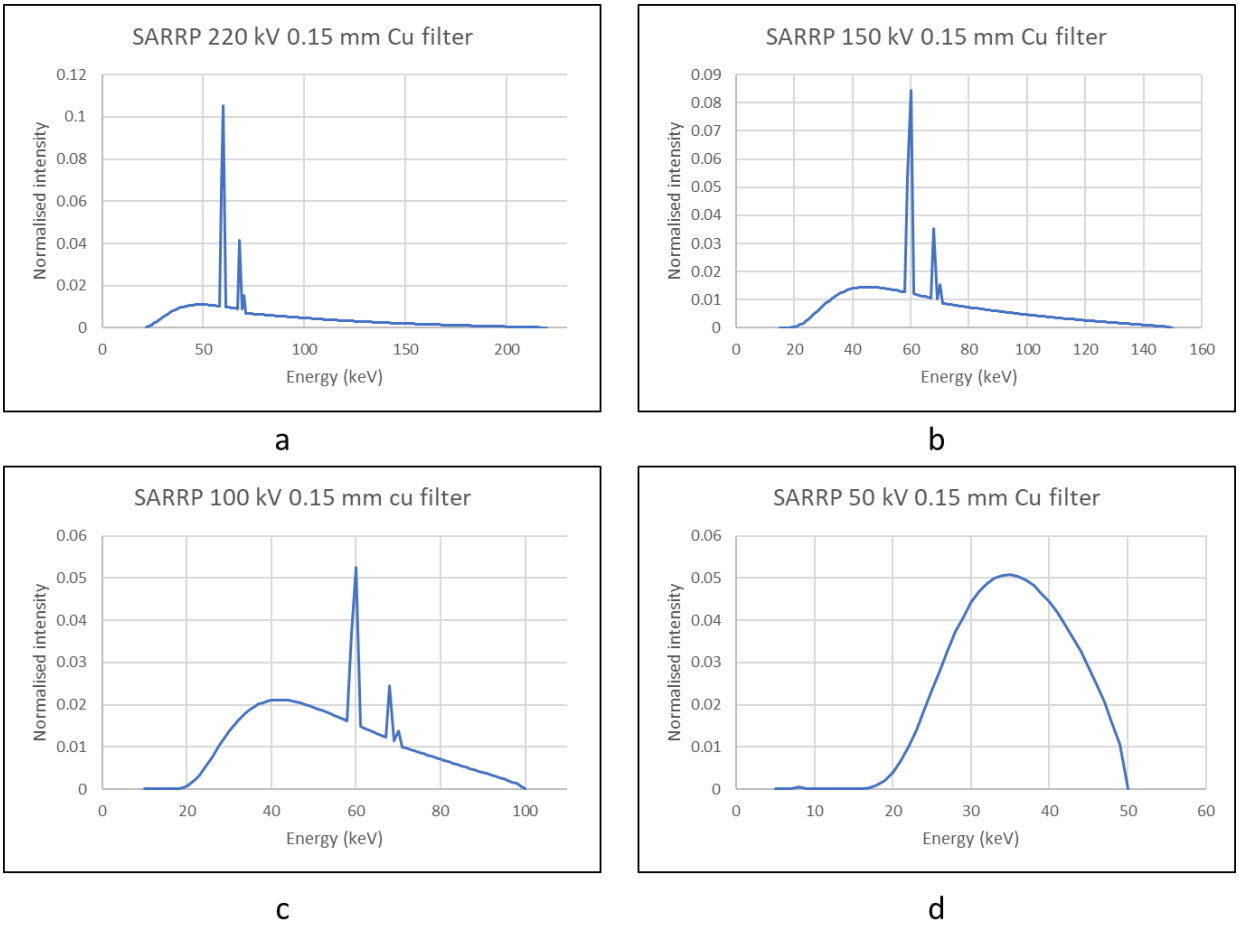

Figure 2-2: Used spectra of the SARRP with 0.15 mm Cu filtration. (a) 220 kV spectrum. (b) 150 kV spectrum. (c) 100 kV spectrum. (d) 50 kV spectrum.

A small polymethyl methacrylate (PMMA) water tank was produced for the PDD measurements in water. This phantom has outer dimensions of 10 x 10 x 10 cm^3 and inner dimensions of 9.4 x 9.4 x 9.4 cm^3. This cube can be filled with water. It has a slit in the middle to place a piece of EBT3 film of dimensions 9.2 x 9.2 cm^2 parallel to the beam direction. Figure 2-3 shows an image of the PMMA cube.

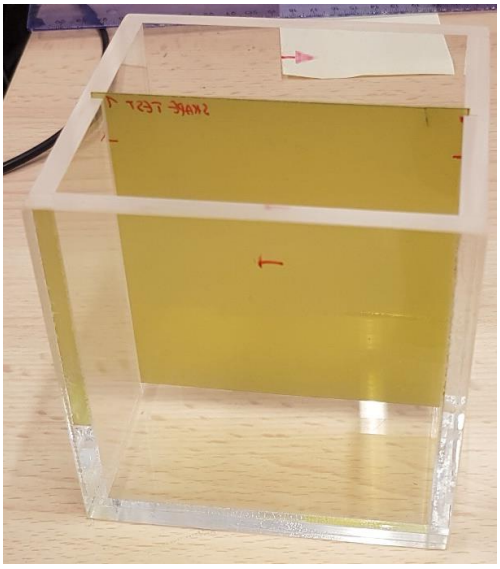

Figure 2-3: Small PMMA water cube with a vertically placed EBT3 film detector.

The small PMMA water cube was filled with water and a film detector was placed parallel to the beam direction. The phantom was placed at a source to surface distance (SSD) of 26.5 cm and 6 Gy was prescribed at the surface. The phantom was positioned using the positioning lasers. Figure 2-4 shows an image of the PMMA cube's placement in the SARRP.

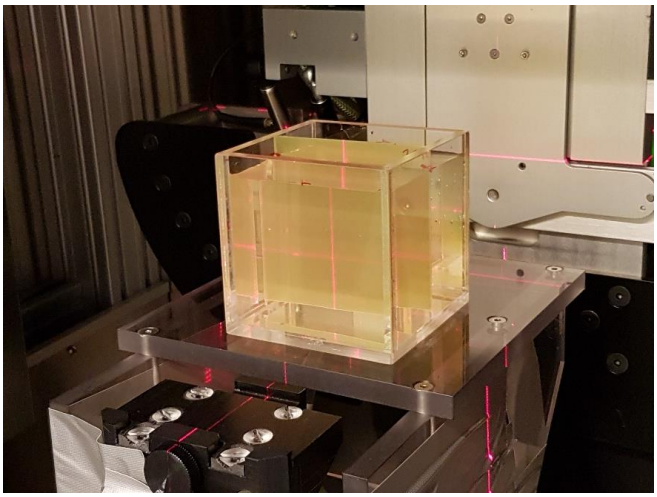

Figure 2-4: Positioning of the PMMA cube under the SARRP.

The detectors were irradiated with the exposure times given in Table 2-3.

Table 2-3: Exposure times of the film detectors at the various energies for the PDD measurements.

Energy (kV)	mAs	Exposure time(s)
50	13	1080
100	13	270
150	13	120
220	13	60

2.2 Study of the relative response of alanine

The irradiations for the calibration of the alanine pellets were performed in PTB in a ^{60}Co reference beam in water against the primary water calorimetry standard at PTB [63]. All the other irradiations were performed on two small animal irradiators.

2.2.1 Energy dependence

The irradiations to determine the relative response of alanine dosimeters were performed on the Small Animal Radiation Research Platform (SARRP) at UZ Leuven [60-62] with filtration of 0.15 mm Cu. The open field with dimensions of 13.6 x 13.6 cm² was used for all the irradiations on the SARRP. The irradiations were performed with the beams having the spectra that are shown in Figure 2-2.

To determine the relative response of the alanine dosimeters, a solid water phantom is produced using RW3 (PTW Freiburg, Freiburg, Germany), a water-equivalent material. This material consists of polystyrene with an addition of 2 % TiO_2 [64]. RW3 slabs of dimensions 5 x 5 x 0.5 cm³ were used in this study. In one of the slabs, a hole was drilled in the centre to place an alanine detector. Fourteen slabs are used for the whole phantom which gives the dimensions of 5 x 5 x 7 cm³ for the whole phantom. The alanine detector is placed at 0.5 cm depth. Figure 2-5 shows images of the RW3 slabs, and Table 2-4 shows the locations of the film and alanine detectors.

Figure 2-5: Left: 1 slab of the RW3 phantom containing the hole for the alanine detector. Right: a stack of 14 RW3 slabs containing film and alanine detectors.

Table 2-4: Locations of the detectors in the RW3 phantom.

Depth(cm)	Detector
0	Film
0.5	Film + alanine
1	Film
2	Film
3	Film
4	Film
5	Film

The detectors were placed perpendicular to the beam. The film at 0.5 cm depth is used to calculate the relative response of the alanine dosimeter. The film dosimeters are also used to measure the PDD described in 2.1.3. The film detectors had the dimensions of 5 x 5 cm².

The RW3 phantom was placed at a source to surface distance (SSD) of 26.5 cm. The positioning was done using the positioning lasers. The detectors were irradiated with the same exposure times given in Table 2-3.

2.2.2 Field size dependence

The irradiations to determine the relative response of alanine dosimeters in function of the field size were performed on the Precision X-RAD 225CX small animal irradiator [48, 49] in Maastro in Maastricht, The Netherlands. The detectors were irradiated with the beam of 225 kV using the 0.3 mm Cu filter.

Again the RW3 phantom was placed at a source to surface distance (SSD) of 26.5 cm. The alanine dosimeter was placed at 5 mm depth and 6 Gy was described to the alanine pellet. The

detectors in the RW3 phantom were placed as described in Table 2-4. The irradiation time was 101 s for each experiment. The parameters of the beams and field sizes used are given in Table 2-5. The parameters were calculated with SpekCalc [51-53]. Figure 2-6 shows the spectrum.

Table 2-5: Beam characteristics of the 225 kV energy beam used in this study on the X-RAD 225CX to investigate the influence of the field size. The parameters are calculated with SpekCalc [51-53].

Field size	Filtration (mm Al)	Filtration (mm Cu)	1st HVL (mm Al)	1st HVL (mm Cu)	Mean energy (keV)
10x10 mm² circular	0	0.3	11.5	0.946	85.476
15x15 mm² circular	0	0.3	11.5	0.946	85.476
20x20 mm² circular	0	0.3	11.5	0.946	85.476

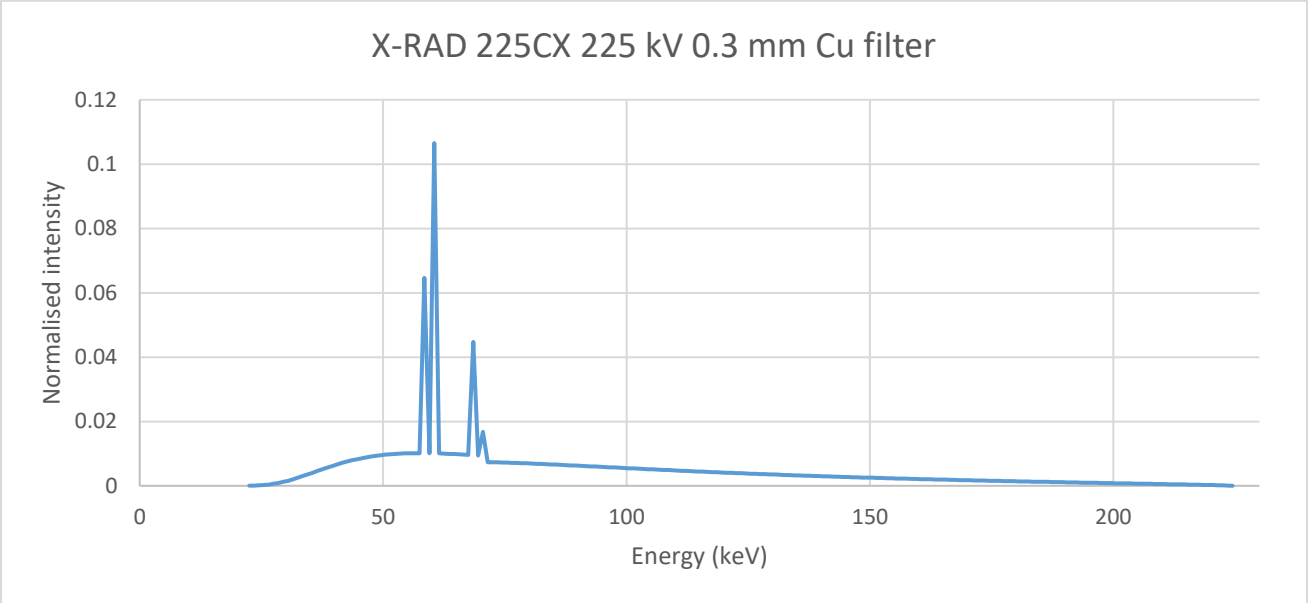

Figure 2-6: Spectrum of the X-RAD 225CX with 225 kV and 0.3 mm Cu filter

2.3 Alanine dosimetry

The alanine dosimetry procedure is based on the work of Anton [17].

2.3.1 Alanine detectors

In this work, cylindrical alanine pellets from Harwell Dosimeters (Oxfordshire, UK) [65] were used. The pellets have a diameter of 4.8 ± 0.1 mm and a height of 2.8 ± 0.1 mm and a

weight of 60 ± 2 mg. The pellets consist of 90.1 % of alanine and 9.9 % of paraffin as a binder. The bulk density of the alanine pellets is 1.2 g/cm³. All the alanine pellets are weighed with a Mettler Toledo XP6 microscale. The alanine pellets are stored in the laboratory with air-conditioning with temperatures around 19 °C and relative humidity below 40 %. The pellets were manipulated with vacuum tweezers to avoid the contamination of the pellets with the fingers. Alanine pellets of the batch AV584 were used in this study. Figure 2-7 shows an image of the alanine pellets.

Figure 2-7: Cylindrical alanine pellets [65].

2.3.2 Spectrometer

The alanine detectors were read out in a Bruker EMX^{micro} spectrometer with a 9-inch magnet [66]. This spectrometer is equipped with a high sensitivity resonator ER4119HS-W1. This is a continuous-wave spectrometer. The microwave bridge operated in the X-band (8 – 12 GHz). A heat exchanger was used (Bruker ER91) to monitor the temperatures of the power supply, the microwave bridge and the water-cooled magnet. The resonator had a quality factor up to 11300 and a guaranteed weak-pitch signal-to-noise ratio of 1500. The spectrometer is contained in the same air-conditioned room as the alanine detectors. Figure 2-8 shows a picture of the magnet and cavity.

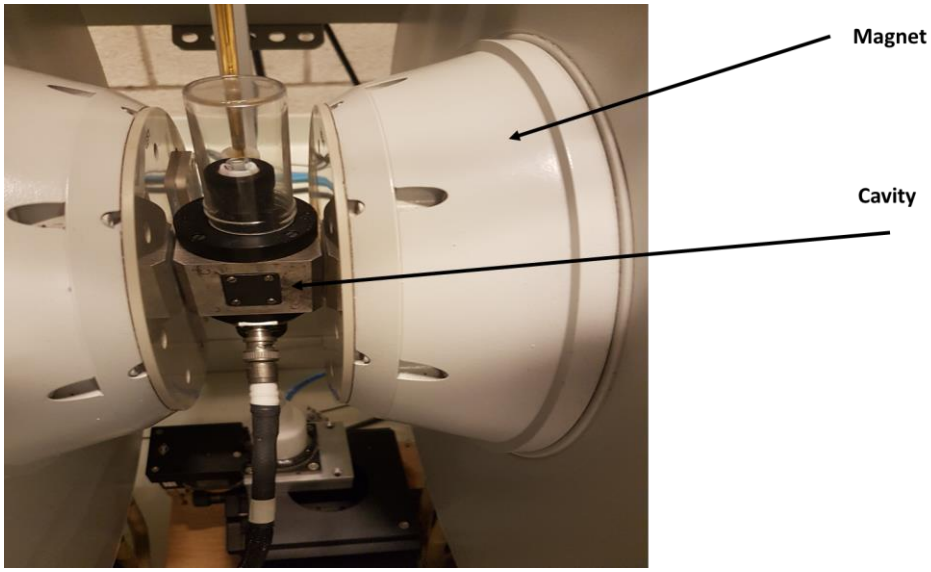

Figure 2-8: Magnet and cavity of the Bruker EMX^{micro} spectrometer.

2.3.3 Dosimeters positioning in the cavity

Based on the work by Anton [17], a reference sample was used in the measurement system to eliminate variations due to the spectrometer. This reference sample is placed in close vicinity of the alanine sample and always measured together with the sample and then used to normalise the measured spectra of the alanine sample. A popular choice for the reference material is synthetic ruby [11]. Another choice is chromium which is the one that is used in NuTeC.

The positioning device for the alanine dosimeters is also based on the work by Anton [17]. A schematic drawing is given in Figure 2-9.

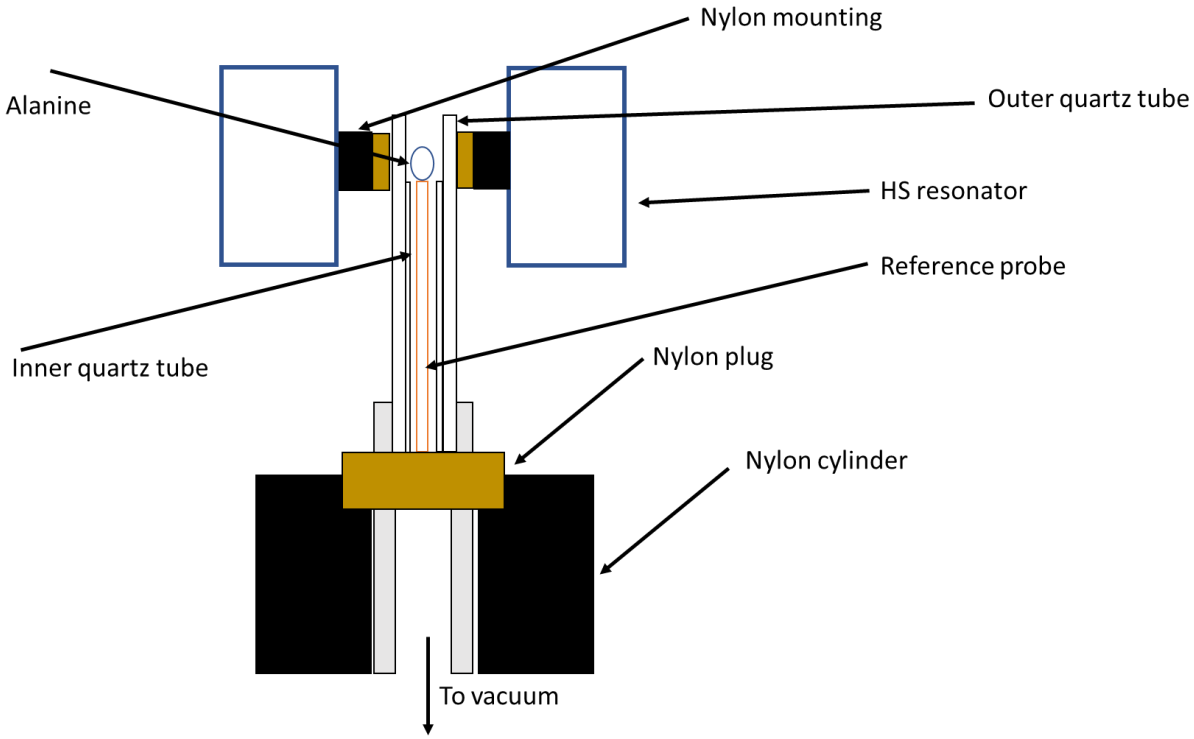

Figure 2-9: Schematic drawing of the positioning system of the alanine pellets with the reference sample in the cavity [17].

The holder for the alanine samples consists of two nested quartz tubes. The long outer tube is 15 cm long and has an inner diameter of 5.2 ± 0.1 mm with a wall thickness of 1 mm. The inner tube can slide and rotate within the outer tube. It has an outer diameter of 5.05 ± 0.13 mm. The alanine sample is put on the inner tube during measurement, and it rotates with the inner tube. The outer tube is attached to the resonator with the built-in collets and collet nuts while the inner tube is mounted on a nylon cylinder that is fixed on a goniometer driven by a stepper motor. The stepper motor is used to set the vertical and horizontal position of the inner tube and also for rotation of the sample during measurements. The inner tube is also fixed to a small vacuum pump that is used during measurements to stabilise the position of the alanine sample. The reference sample holder is placed in the inner tube and fixed to collets and collet nuts and a nylon plug on the bottom. The alanine sample is then put on the inner tube and close to the reference sample which is on the top of the reference sample holder. The optimal tube height was determined for the optimal signal intensity of the alanine sample which was around 22 mm.

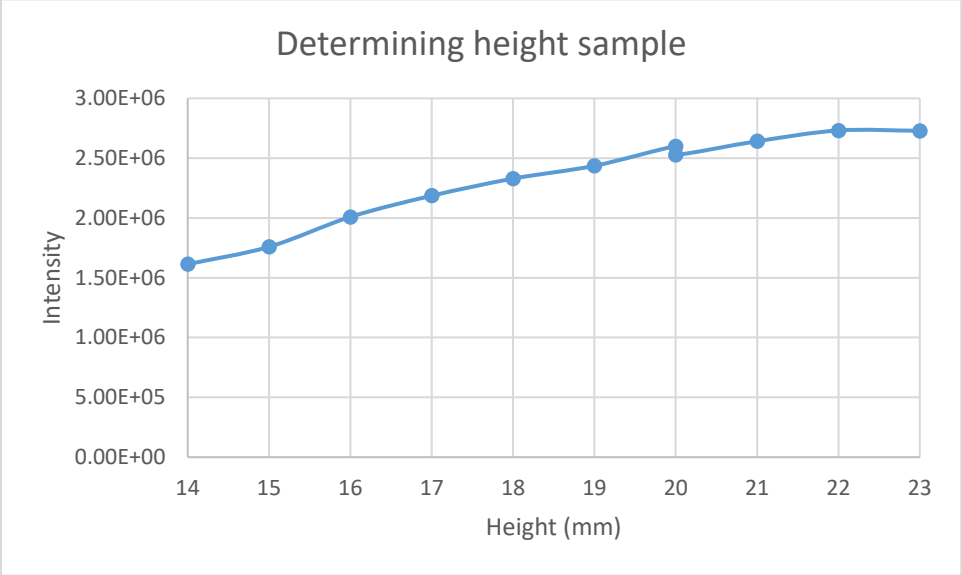

Figure 2-10: Determination of the optimal height of the sample in the cavity.

2.3.4 Spectrometer settings and readout procedure

The spectrometer was warmed up for about 1 hour before starting to measure. The EPR spectra were acquired as the first derivative of the absorption spectrum. The microwave frequency was 9.7 GHz with the microwave power set to 0.25 mW. The field was modulated with 0.5 mT with a modulation frequency of 100 kHz. The centre of the magnetic field was 348 mT and the sweep width was 30 mT. During each sweep, 2048 channels were sampled with a conversion time of 46 ms and time constant of 46 ms. The sweep time was 83.39 s. Five spectra were acquired for each alanine sample to compensate for any angular dependency [3, 17]. After each sweep, the alanine sample was rotated by 72 ° by the stepper motor. The vacuum pump was also triggered to ensure the rotation of the alanine pellet on the inner quartz tube. This process of rotation was automatized by an in-house written code [67]. The measurement of the five spectra took around 9-10 minutes.

2.3.5 Data analysis and dose calculation

Because the reading of the EPR spectra is not absolute, the amplitude of the EPR spectra has to be calibrated. For this purpose, NuTeC receives each year a set of dosimeters in the dose range of 0 – 25 Gy that are irradiated in a ^{60}Co reference beam in water against the primary water calorimetry standard at PTB [63]. These alanine pellets are used to calibrate and to monitor the stability of the alanine/EPR system in NuTeC.

The dose calculation is performed in a custom code written in MATLAB R2014a that is developed by PTB [17, 68] and it will be briefly described here.

The measured spectrum contains the signals of both the alanine (ala) and the reference (ref) material. Hereby, two base functions are fitted which corresponds with the coefficients A^{ala} and A^{ref}. One base function contains the signal of a pure alanine signal and the other base function contains the signal of the reference material and the background. The base function that contains the signal of the reference material was determined from the combined spectrum of unirradiated probes. The other base function that contains the pure alanine signal was determined by subtracting the summed spectrum of the unirradiated pellets from the combined spectrum of the irradiated alanine samples with 25 Gy that were irradiated in a ^{60}Co field described above. These pellets have to be measured on the same day as the test pellets (i.e. the alanine samples that the user desires to know the delivered dose). The five separate spectra for each alanine sample (taken at different angles with a 72° interval) were normalised and then the resulting frequency-normalised spectrum was fitted with a linear combination of both base functions and this yielded both coefficients A^{ala} and A^{ref} [17, 24].

The dose-normalised amplitude $\overline{A_D}$ which can be identified to the absorbed dose (D) can be described as [3]:

$$D = \overline{A_D} = \frac{\overline{A_m}}{\bar{m}} \cdot \overline{m^b} \cdot D^b \cdot \prod_l k_l \qquad (2.1)$$

and $\prod_l k_l$ is defined as:

$$\prod_l k_l = k_Q \cdot \frac{k_t \cdot k_f \cdot k_{pos} \cdot k_{sleeve}}{k_t^b \cdot k_f^b \cdot k_{pos}^b \cdot k_{sleeve}^b} \qquad (2.2)$$

The superscript “b” accounts for the base function derivation. $\overline{A_m}$ is the amplitude normalised to the mass. $\bar{m}$ is the average mass of the number of samples used during irradiation. For the calibration pellets irradiated by PTB, 4 pellets were used per irradiation while for the irradiation on small animal irradiators, 1 pellet was used. k_Q is the energy correction factor which depends on the energy used during irradiation. In this study, this factor is actually the variable that is investigated for low and medium kV X-rays. The correction factors were taken from [69].

k_t is the temperature correction factor.

$$k_T = 1 - c_T(T - T_0) \quad (2.3)$$

$c_T = 1.8 \cdot 10^{-3} K^{-1}$, T is the temperature of the alanine pellet during irradiation and T0 = 293.15 K. k_f is a fading correction factor.

$$k_f = e^{-c_t(t_{reading} - t_{irradiation})} \quad (2.4)$$

t is expressed in days and $c_t = \frac{7 \cdot 10^{-5}}{d}$

D^b is the dose that the alanine samples received to construct the base function (25 Gy). k^b_{sleeve} is a correction for the beam attenuation in the sleeve which is assumed unity. k_{pos} is the correction factor for the positioning which is also assumed unity because we assume a correct positioning of the alanine detector in the radiation beam for the depth.

The uncertainty of the alanine/EPR dosimetry system was calculated according to [68]. The main contributions of the uncertainty budget originate from the amplitude determination (± 45 mGy per pellet) and the homogeneity of the detector material (± 0.3 % per pellet). These 2 effects are independent of the dose.

2.4 Film dosimetry

2.4.1 Film detectors

GafChromic™ (Ashland Inc., Covington, Kentucky, United States) EBT3 films from lot #09151403 were used in this study. Films were cut to dimensions about 10 x 3 cm² for calibration. For the measurements of the PDD curves in water, they were cut about 9.2 x 9.2 cm² and to 5 x 5 cm² for the measurements of the relative response of alanine.

The films were handled according to the AAPM's Task Group report 55 [70]. They were stored in dark envelopes when not used for irradiation or scanning. They were handled with gloves to avoid fingerprints and the films were marked to keep track of the orientation [47].

2.4.2 Scanning procedure

The films were scanned on an Epson 10000XL flatbed scanner using the Epson driver. The scanner was fitted with the transparency adapter, and the scanning was done in transmission mode. Before scanning the scanner was warmed up with five consecutive scans. Images were scanned at a spatial resolution of 72 dpi for the irradiations at open field and a resolution of 150 dpi for the irradiations with field sizes of 2 x 2 cm² and smaller. The depth was 16 bit per colour and all the colour-corrections were turned off. This prevents the scanned data being modified to present an image optimized for display. The files were saved in TIFF format. The orientation of the film was maintained for all the films. Cardboard templates were used for accurate positioning and the films were positioned on the centre of the scanner to reduce the lateral response artefact (LRA) [71, 72] and to reduce the amount of light coming from the part of the scanner not covered by the film. The films were placed under a glass plate to avoid film curvature and to ensure a constant distance from light-source to film [73]. The filmstrips to produce the calibration curve of the lots were measured in a single scan to reduce scan-to-scan effects.

2.4.3 Calibration and analysis

Data and image analysis was done using the Film QA Pro software v5.0 (Ashland Inc., Covington, Kentucky, United States). The dose maps were calculated using the triple channel algorithm built-in the Film QA Pro software based on Micke et. al [74]. After the dose map was calculated, the green channel was used for the dosimetry. Calibration files were generated by measuring the calibration filmstrips with regions of interest approximately 3 x 2 cm² in the centre of the strips. The dose-response data for each colour channel was fitted using the simple rational function:

$$X(D) = a + b/(D - C) \tag{2.5}$$

with X(D) the response at dose D and a, b, c being constants.

The uncertainties of the measurements were determined according to the JCGM100 [75]. The uncertainty of the measured doses by the films was estimated at 2 %.

2.5 Experimentally defined relative response

The empirical value r which stands for the relative response is calculated as:

$$r = \frac{D_{w,x}}{D_{w,0}} \tag{2.6}$$

$D_{w,x}$ is the dose with at beam quality x and $D_{w,0}$ is the dose at a reference beam quality which is usually a ^{60}Co source. In this work, we used a different method to calculate the relative response because of no availability of a cobalt machine.

Alanine and radiochromic film detectors were placed as close as possible at the same location and depth. They were irradiated together by different kV X-ray beams. The relative response was then calculated as:

$$r = \frac{D_{meas_{alanine}}}{D_{meas_{film}} \; X \; \frac{D_{w,ala}}{D_{w,ref}}} \tag{2.7}$$

The film dosimeters were also investigated in this study which is described in 2.4. $D_{meas_{alanine}}$ and $D_{meas_{film}}$ is the dose measured by the alanine and film detectors respectively.

Another factor to take into account is the thickness of the alanine dosimeters. It is shown in [40] that the dose measured by the alanine pellet is the dose at the centre of the pellet. To obtain the delivered dose $D_{w,ala}$ at a depth of 1.39 ± 0.04 mm which is the centre of the pellet, a correction factor is required for $D_{w,ref}$. The ratio $D_{w,ala}/D_{w,ref}$ is calculated with Monte Carlo (MC) calculations which are explained in 2.6.

2.6 Simulations

The Monte Carlo (MC) simulations were performed with the EGSnrc Monte Carlo code system [76] using the DOSRZnrc user code [77]. This user code was chosen because it allows using cylindrical geometries like the cylindrical alanine detectors in this study. The PEGS4 user code was used to generate the cross-section data for water, alanine, PMMA and RW3

with the following energy ranges (in MeV) for photons and electrons. For electrons, the rest mass energy of 0.511 MeV was included.

- Lower electron range: AE = 0.512 MeV
- Upper electron range: UE = 2.511 MeV
- Lower photon range: AP = 0.001 MeV
- Upper photon range: UP = 2 MeV

The photon interaction coefficients were taken from the XCOM cross-section library [78]. The electron and photon transport cut-off parameters were chosen for all the simulations as follows:

- Electron cut-off: ECUT = 0.512 MeV
- Photon cut-off: PCUT = 0.001 MeV

Rayleigh scattering, bound Compton scattering, photoelectric absorption and fluorescent emission of characteristic X-rays were simulated. The geometries were created using the graphical user interface (GUI) of the RZ user codes [79]. The simulations were performed with enough histories so that the uncertainty was below 0.5 % in the scoring region. As almost all the simulations were done with kV energies the calculation times were not longer than a couple of hours.

For the alanine pellet, the medium density of 1.2 g/cm³ was used. For the alanine stopping power density effect correction, the simulations were performed using the correction based on the bulk density (1.2 g/cm³) as well as the correction based on the crystalline density (1.42 g/cm³) [30].

2.6.1 Alanine stopping power density correction option

One of the important parameters to choose for the simulations of alanine detectors is the choice of the alanine stopping power density correction option. In previous studies for MV photons and MeV electron beams [24, 26, 80], they used the **crystalline density of alanine** for the density correction. The crystalline density of alanine is the physical density of pure alanine (1.42 g/cm³). Whereas the actual density of the alanine pellets was 1.2 g/cm³ because the pellet also contains binder material and micro-air pockets during the pressing of the alanine pellet. The reason to use the crystalline density is explained because alanine is the

material that interacts with the ionising radiation and not the other constituents present in the alanine pellet.

The other option for alanine stopping power density correction is to use the **bulk density** (1.2 g/cm³) of the alanine pellet. This is the actual density of the detector and the reason to use this option is that it is a better representation of the actual detector in the simulations. In this study, both density correction options were used for the simulations.

2.6.2 Simulation for the relative response of alanine

The RW3 slab phantom is modelled as slabs of RW3 with dimensions 5 x 5 x 0.5 cm³ in DOSRZnrc. The alanine pellet was modelled at 0.5 cm depth in the centre of the RW3 slab. The spectra of the SARRP used for the simulations are shown in Figure 2-2. The spectra of the X-RAD 225CX used for the simulations are shown in Figure 2-11. These spectra were used as source inputs.

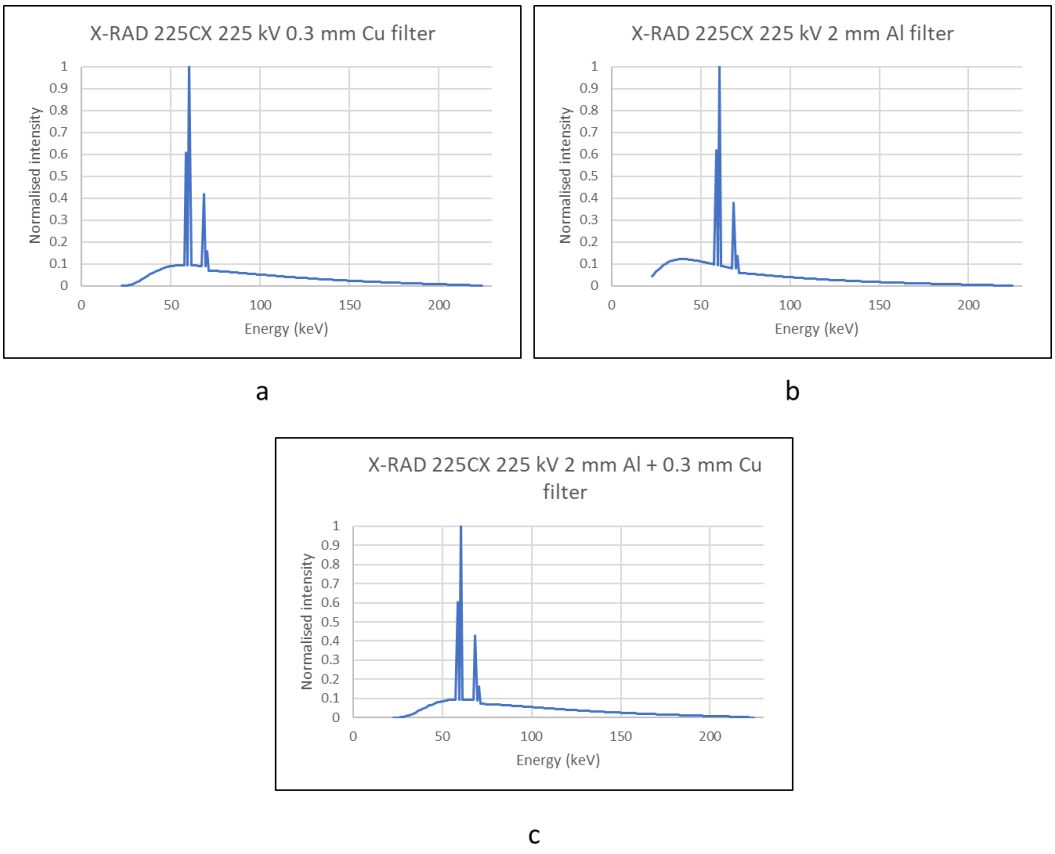

Figure 2-11: Used spectra of the X-RAD 225CX for the MC simulations. 225 kV was used for all simulations. (a) Spectrum with 0.3 mm Cu filter. (b) Spectrum with 2 mm Al filter. (c) Spectrum with 2 mm Al and 0.3 mm Cu filter.

To simulate with ^{60}Co beams, the spectra from Rogers et al. [81] is used which is distributed in the EGSnrc installation package.

For each beam, the simulation was performed 3 times:

- Using a dose scoring volume made of water to obtain D_w
- Using a dose scoring volume made of the atomic constituents of the alanine pellets with the bulk density to obtain D_{ala} **taking the density correction for the bulk density** of the alanine pellets (1.2 g/cm³).
- Using a dose scoring volume made of the atomic constituents of the alanine pellets with the bulk density to obtain D_{ala} **taking the density correction for crystalline alanine** (1.42 g/cm³).

The ratio D_{ala}/D_w was calculated for each quality and then referred to the corresponding D_{ala}/D_w ratio for ^{60}Co. the simulated relative response of the alanine pellets for the quality Q relative to ^{60}Co can be calculated as:

$$r_Q^{MC} = \frac{(\frac{D_{ala}}{D_W})_Q}{(\frac{D_{ala}}{D_W})_{Co}} \tag{2.8}$$

2.6.3 Simulation for the correction of the thickness of the alanine pellet

The film detector was placed on top of the alanine pellet. It was shown in [40] that the dose measured by the alanine pellet is the dose in the centre of the alanine detector. Thus, it is necessary to determine a correction for $D_{w,ref}$ to obtain the delivered dose at the centre of the alanine pellets $D_{w,ala}$ which is at 1.39 ± 0.04 mm. $D_{w,ala}/D_{w,ref}$ was calculated from MC simulations. Both the alanine stopping power density correction options (bulk density and crystalline alanine density) were used to calculate $D_{w,ala}/D_{w,ref}$.

2.6.4 Simulation of the PDD's

The PMMA water phantom was modelled as slabs of water with a diameter of 10 cm. The PMMA housing of the cube was not simulated because it was located too far from the dose scoring region with respect to the range of the particles included in the simulations to influence the results. A simulation including the PMMA cover yielded very similar results. The film detectors were also not explicitly simulated. The scoring region was defined in the beam centre where the film is located. The spectra of the beams from the SARRP from the described in Figure 2-2 were calculated with SpekCalc [51-53] and they were used as the source input. The source was defined as a point source with an SSD of 26.5 cm. Besides, the PDD's in the RW3 slab phantom were also simulated.

3 Results

3.1 Energy dependence film detectors

3.1.1 SARRP

The dose maps of the films used to measure the PDD's were recalculated with film calibration curves generated at 60 kV, 100 kV and 225 kV. The PDD's were recalculated for the different energies and the difference between the obtained dose values using the different calibration curves were plotted. The following figures show the difference for the PDD's obtained in the water tank.

- Figure 3-1 shows the difference of using different calibration curves on the PDD of 220 kV.
- Figure 3-2 shows the difference of using different calibration curves on the PDD of 100 kV.
- Figure 3-3 shows the difference of using different calibration curves on the PDD of 60 kV.

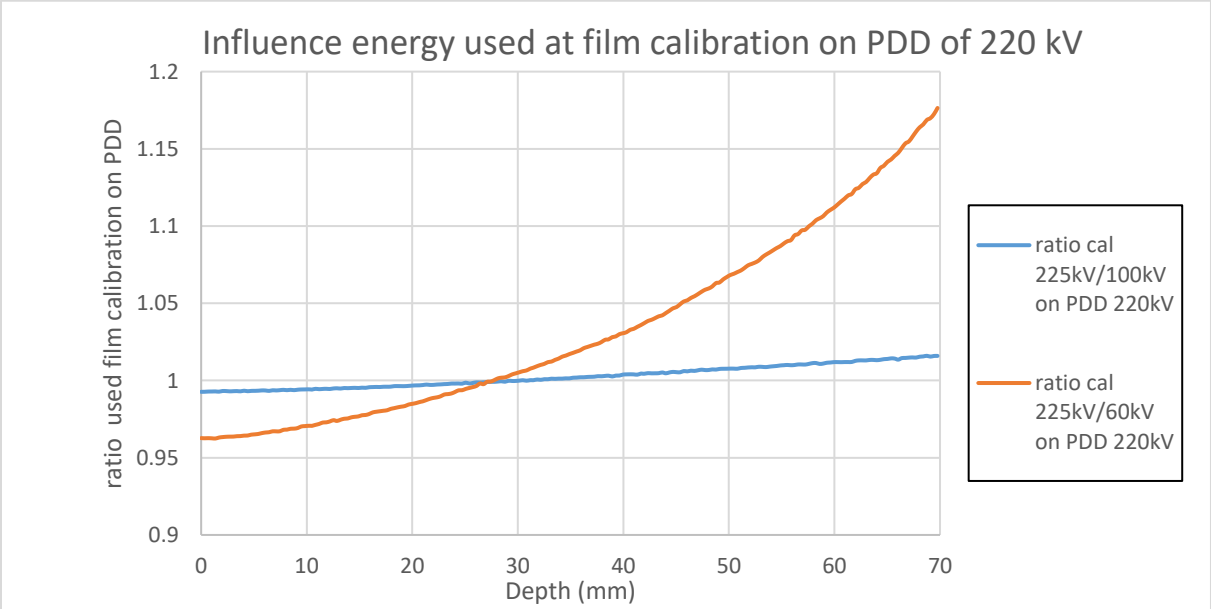

Figure 3-1:Effect of using different energies for the calibration curve on the film used to measure the PDD of 220 kV in water.

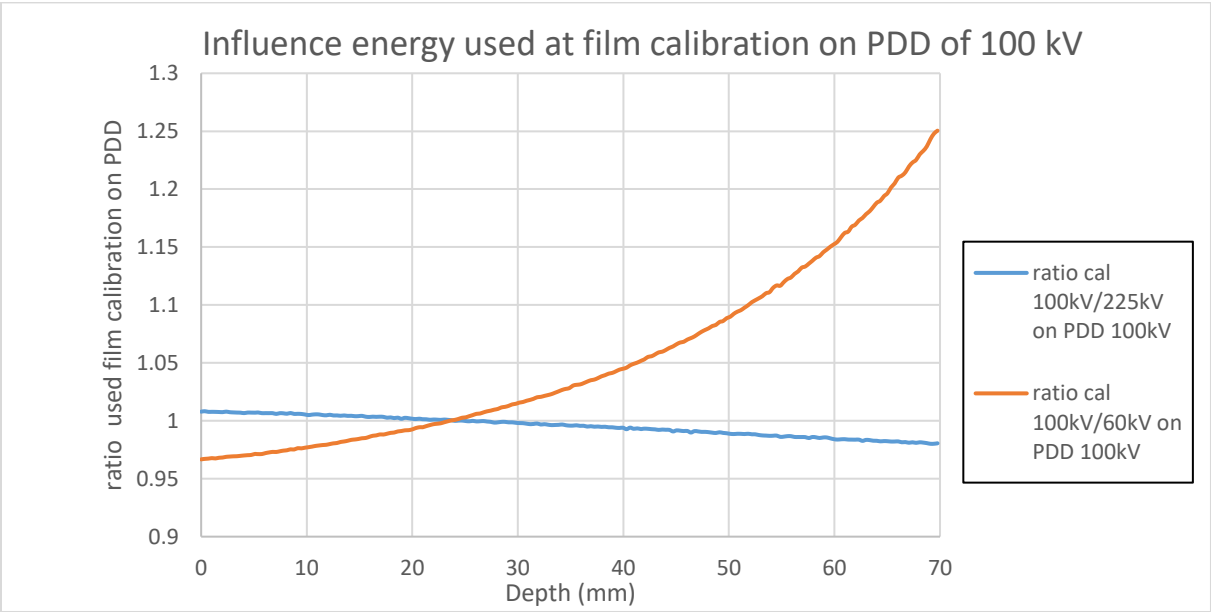

Figure 3-2: Effect of using different energies for the calibration curve on the film used to measure the PDD of 100 kV in water.

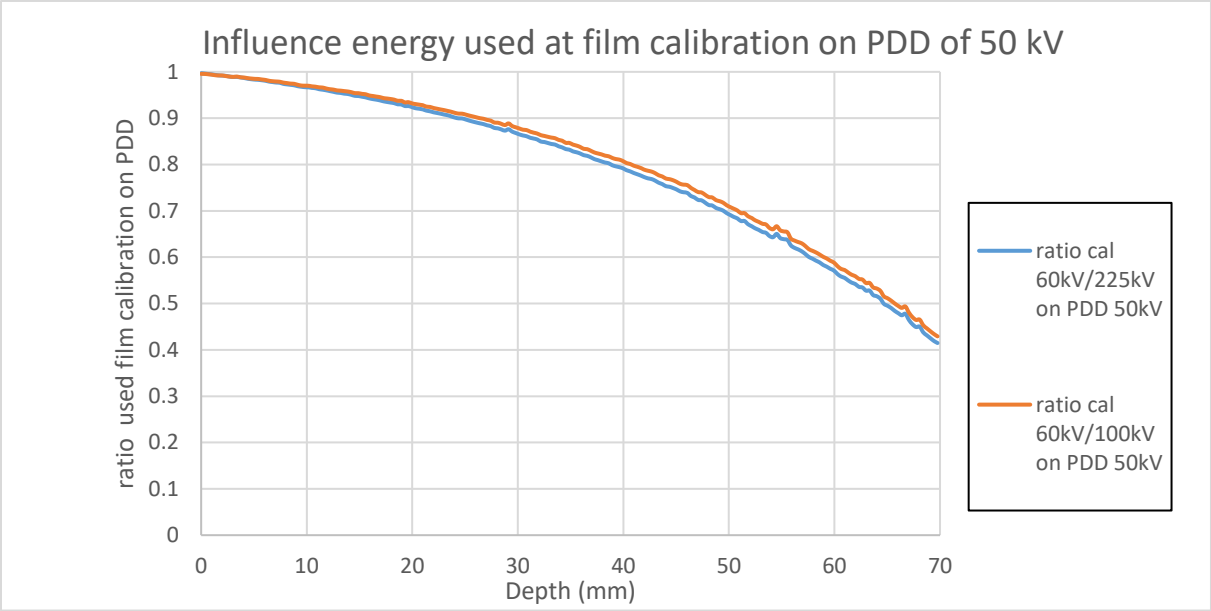

Figure 3-3: Effect of using different energies for the calibration curve on the film used to measure the PDD of 50 kV in water.

Very similar results are obtained for the films in the RW3 phantom.

For the PDD of 220 kV, there is a difference of 2 % when the dose map is recalculated with a 100 kV calibration curve. A similar result is observed on the PDD of 100 kV with the dose map recalculated with a 225 kV calibration curve. However, there is a huge difference when the 60 kV calibration curve is used to calculate the dose maps of the PDD's of 100 kV and 220 kV. Equally, a large difference is observed when the dose map of the film used for the

PDD of 50 kV is recalculated with 100 kV and 225 kV calibration curves. These results suggest that the film calibration curve of the corresponding energy (or as close as possible) should be used to generate the dose maps for lower kV X-rays.

3.2 PDD measurements with the films

The dose maps from the films were calculated using the calibration curves with the energies closest to the energy used to irradiate the film with unknown dose distribution (e.g. 60 kV calibration was used to calculate the dose map on a film irradiated with 50 kV).

3.2.1 SARRP

The PDD's were normalised at 10 mm depth.

Figure 3-4 shows the measured PDD's of the SARRP using the film in the water tank.

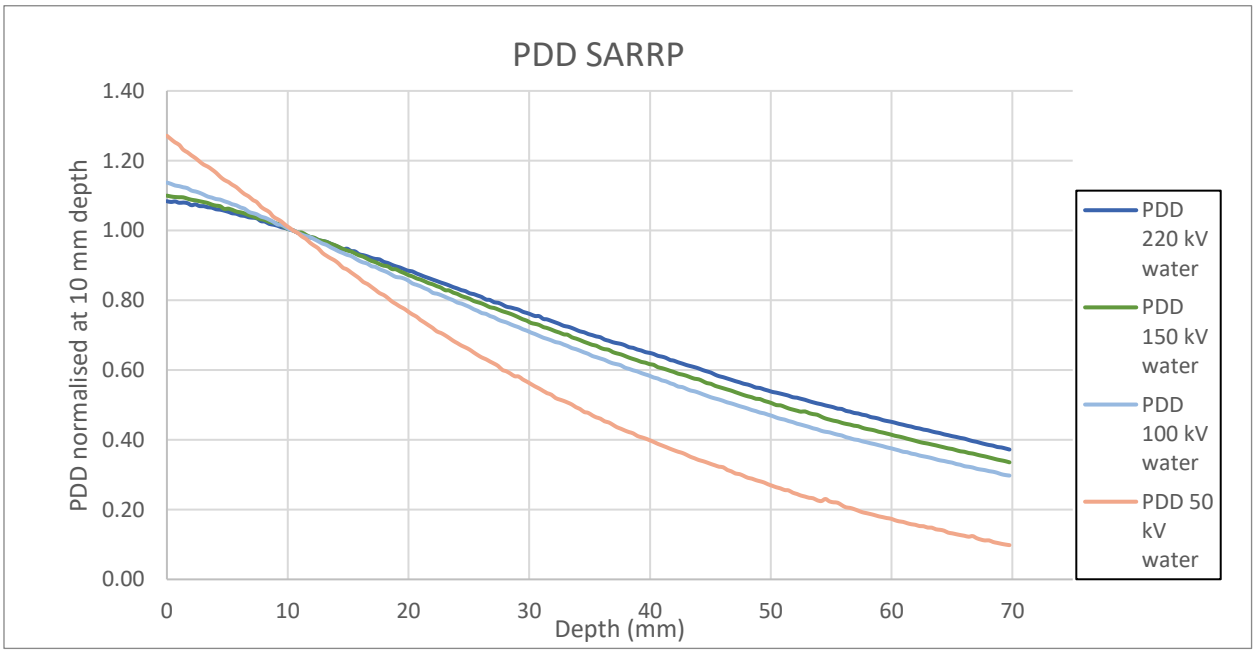

Figure 3-4: Measured PDD's in the water tank on the SARRP. The PDD's were normalised at 10 mm depth.

Figure 3-5 shows the measured PDD's of the SARRP in RW3. The depths were converted to the water-equivalent depth taking into account the density of RW3 (1.045 g/cm³).

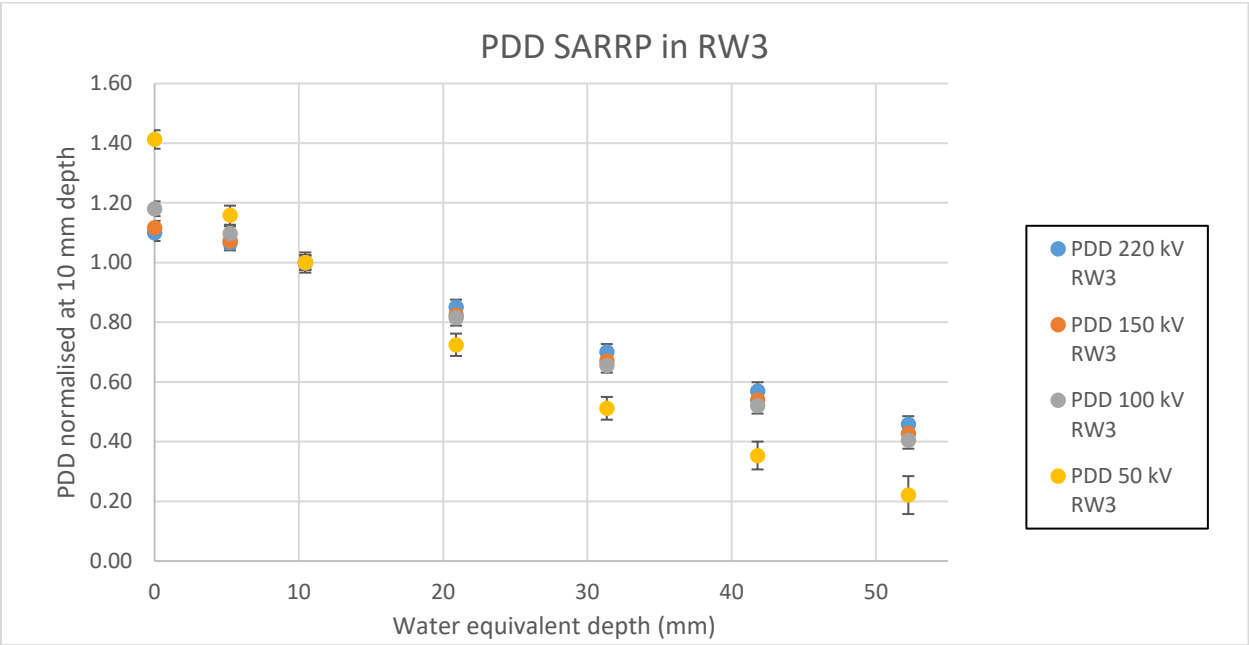

Figure 3-5: Measured PDD's in RW3 on the SARRP. The PDD's were normalised at 10 mm depth.

3.2.2 X-RAD 225CX

The PDD's were normalised at 10 mm depth.

Figure 3-6 shows the measured PDD's for different field sizes for the 225 kV beam with 0.3 mm Cu filtration.

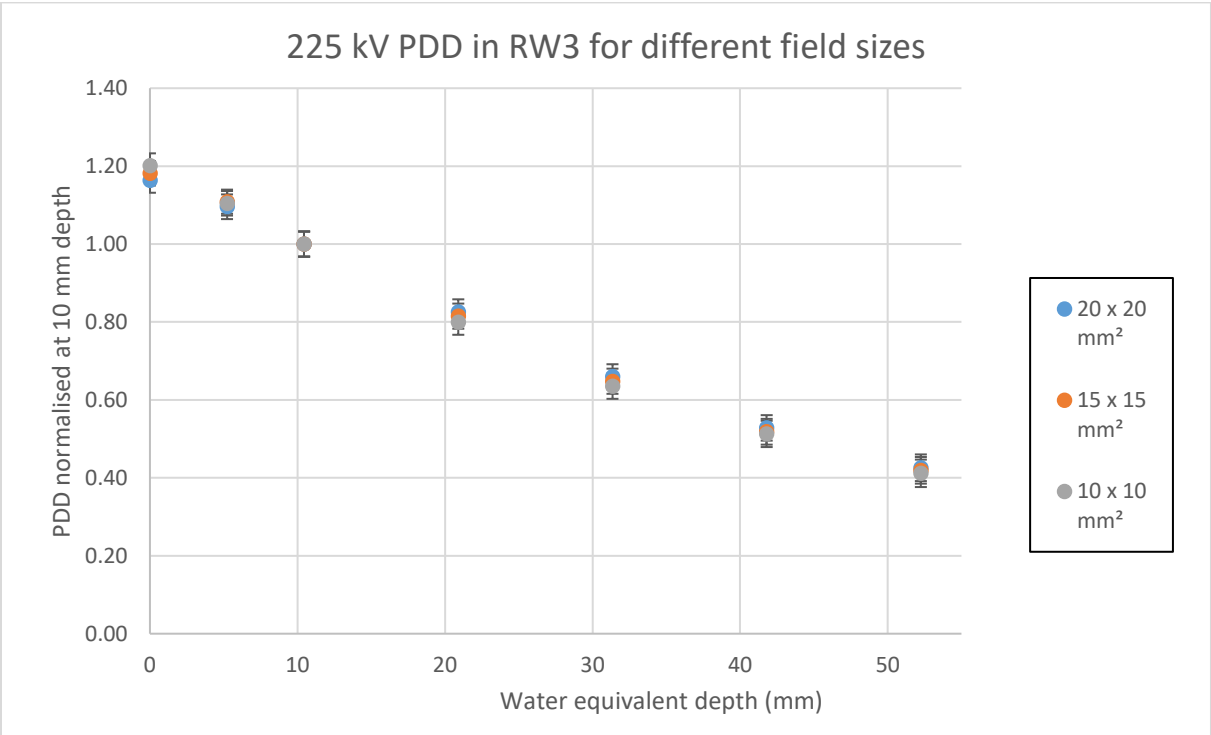

Figure 3-6: Measured PDD's for different field sizes for the 225 kV beam with 0.3 Cu filtration.

3.3 Energy dependence of alanine

The dose maps from the films were calculated using the calibration curves with the energies closest to the energy used to irradiate the film with unknown dose distribution (e.g. 60 kV calibration was used to calculate the dose map on a film irradiated with 50 kV).

The results obtained in this work were compared to Anton et al. [28]. Table 3-1 shows the characteristics of the beams used in their study.

Table 3-1: Beam characteristics used in the study by Anton et al. [28].

Voltage (kVp)	Filtration (mm Al)	Filtration (mm Cu)	1st HVL (mm Al)	1st HVL (mm Cu)	Mean energy (keV)
TW 30	0.5	0	0.359		19.3
TW 40	0.8	0	0.741		24.5
TW 50	1	0	0.94		28.7
TW 70	4	0	2.94		41.4
TW 100	4.5	0	4.41		51.9
TH 70	4	0	3.13		42.2
TH 100	4.5	0	4.63	0.18	52.4
TH 120	6	0	6.26	0.29	59.5
TH 140	9	0	8.21	0.46	67.1
TH 150	4	0.5	11.2	0.82	78
TH 200	4	1	14.39	1.59	99.6
TH 250	4	1.6	16.85	2.55	123.4
TH 280	4	3	18.7	3.43	147.7

For convenience purposes to the reader, the parameters of the beams used from the SARRP are shown again in Table 3-2.

Table 3-2: Beam characteristics of the energies used on the SARRP. The parameters are calculated with SpekCalc [51-53].

Energy (kV)	Filtration (mm Al)	Filtration (mm Cu)	1st HVL (mm Al)	1st HVL (mm Cu)	Mean energy (keV)
50	0	0.15	2.46	0.079	35.3
100	0	0.15	4.88	0.196	53.4
150	0	0.15	6.94	0.355	65.2
220	0	0.15	9.32	0.637	78.1

The correction for the thickness of the pellets was obtained from MC simulations. For the alanine stopping power density correction, both correction options were used (based on the bulk density of the pellets as well as crystalline alanine). Table 3-3 and Table 3-4 show the calculated thickness correction factors using the stopping power density correction based on the bulk density (1.2 g/cm^3) and crystalline alanine (1.42 g/cm^3) respectively in the MC simulations.

Table 3-3: Calculated thickness correction factors for the SARRP using the bulk density for the stopping power density correction for the MC simulations.

Energy (kV)	Mean energy (keV)	1st HVL (mm Al)	$D_{w,ala}/D_{w,ref}$	Unc. $D_{w,ala}/D_{w,ref}$ (rel)	Unc. $D_{w,ala}/D_{w,ref}$ (%)
50	35.3	2.46	0.884	0.003	0.317
100	53.4	4.88	0.905	0.003	0.312
150	65.2	6.94	0.925	0.003	0.314
220	78.1	9.32	0.932	0.003	0.317

Table 3-4: Calculated thickness correction factors for the SARRP using the crystalline alanine density for the stopping power density correction for the MC simulations.

Energy (kV)	Mean energy (keV)	1st HVL (mm Al)	$D_{w,ala}/D_{w,ref}$	Unc. $D_{w,ala}/D_{w,ref}$ (rel)	Unc. $D_{w,ala}/D_{w,ref}$ (%)
50	35.3	2.46	0.951	0.004	0.425
100	53.4	4.88	0.962	0.004	0.407
150	65.2	6.94	0.970	0.004	0.409
220	78.1	9.32	0.972	0.004	0.412

We observe that the calculated factors using the bulk density correction are lower than the factors calculated with the crystalline alanine correction. This is expected because the density is different in both corrections (1.2 g/cm³ vs 1.42 g/cm³). This gets more pronounced at lower energies.

3.3.1 Results using the bulk density correction

Figure 3-7 and Figure 3-8 show the calculated relative responses in function of the mean energy and the HVL while Table 3-5 shows the tabulated results for the SARRP and Table 3-6 the tabulated results from Anton et al. [28]. For the alanine stopping power density correction, it was based on the bulk density (1.2 g/cm³) of the alanine pellets. The relative response is defined in equation (2.7).

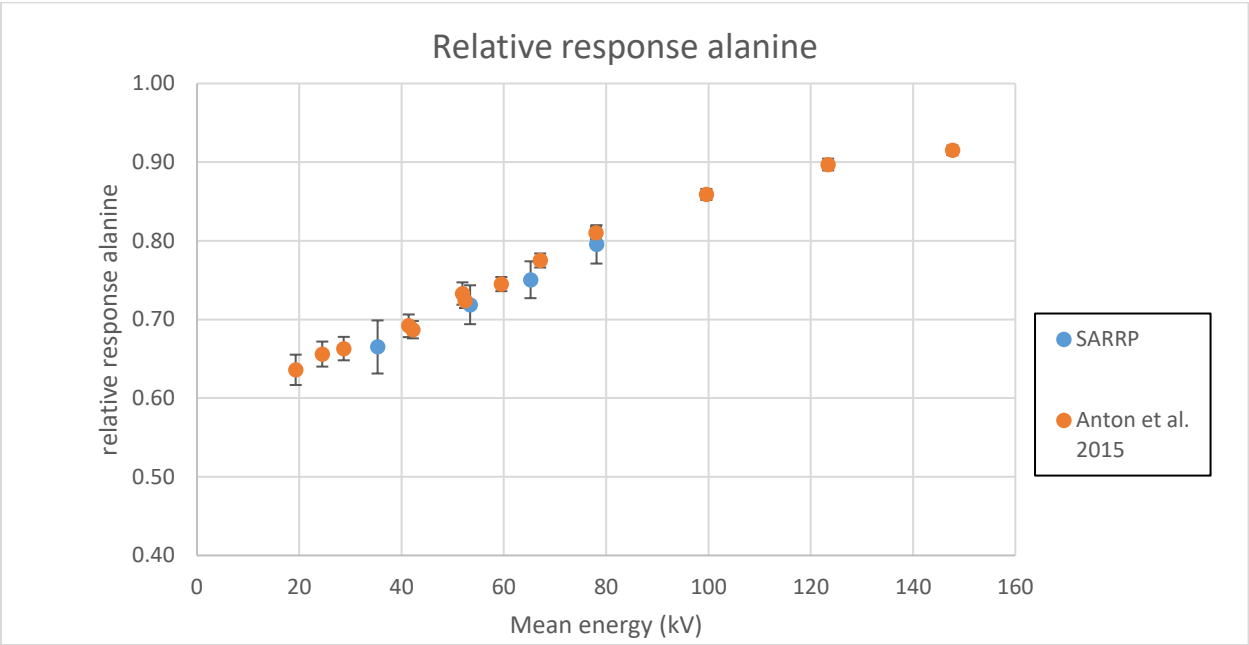

Figure 3-7: Measured relative response of alanine dosimeters in function of the mean energy of the X-rays spectra. The thickness correction is calculated with MC simulations using the bulk density for the alanine stopping power density correction.

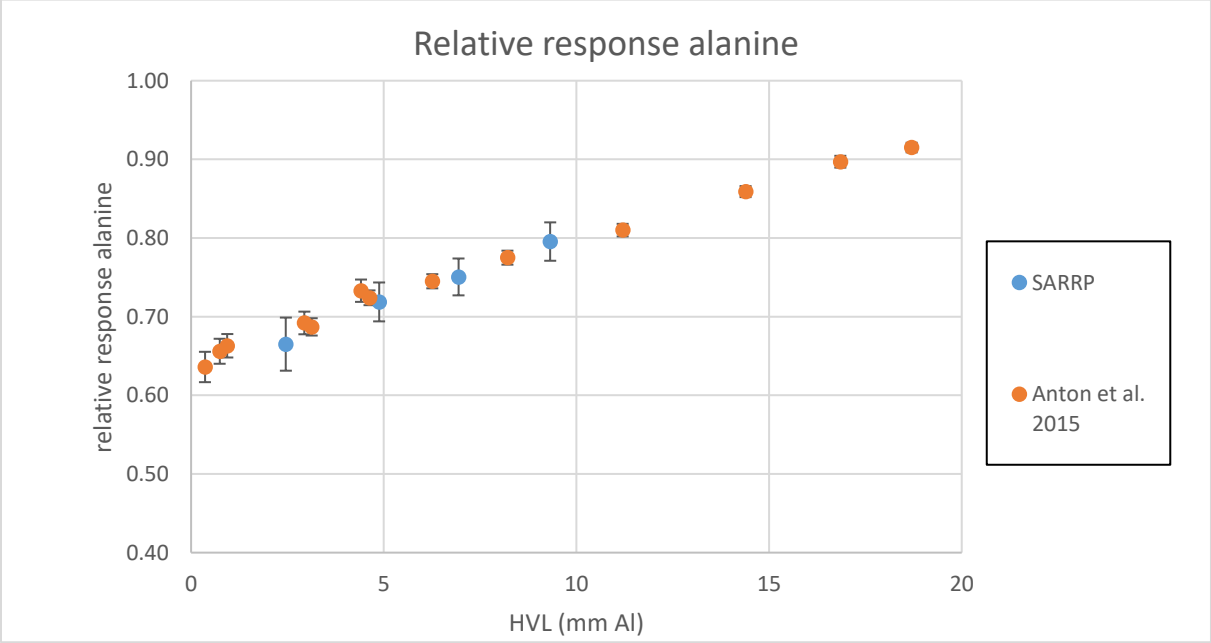

Figure 3-8: Measured relative response of alanine dosimeters in function of the half value layer of the X-rays spectra. The thickness correction is calculated with MC simulations using the bulk density for the alanine stopping power density correction.

Table 3-5: Measured relative response of alanine dosimeters for the SARRP. The thickness correction is calculated with MC simulations using the bulk density for the alanine stopping power density correction.

Energy(kV)	E mean (keV)	1st HVL (mm Al)	r (without thickness correction)	r (with thickness correction)	Unc. r (rel)	Unc. r (%)
50	35.3	2.46	0.588	0.665	0.034	3.377
100	53.4	4.88	0.650	0.719	0.025	2.472
150	65.2	6.94	0.694	0.751	0.023	2.343
220	78.1	9.32	0.742	0.795	0.024	2.441

Table 3-6: Measured relative response of alanine dosimeters from the study by Anton et al. [28].

Voltage (kVp)	Mean energy (keV)	r	Unc. r (rel)	Unc. r (%)
TW 30	19.3	0.636	0.019	1.93
TW 40	24.5	0.656	0.016	1.59
TW 50	28.7	0.663	0.015	1.49
TW 70	41.4	0.692	0.014	1.44
TW 100	51.9	0.733	0.014	1.42
TH 70	42.2	0.687	0.011	1.1
TH 100	52.4	0.724	0.009	0.94
TH 120	59.5	0.745	0.009	0.9
TH 140	67.1	0.775	0.009	0.89
TH 150	78	0.81	0.008	0.8
TH 200	99.6	0.859	0.007	0.7
TH 250	123.4	0.897	0.008	0.75
TH 280	147.7	0.915	0.006	0.61

The relative response drops from 1 at ^{60}Co to 0.795 at 220 kV beams and it drops further to 0.67 at 50 kV beams. When plotted in the mean energy as well as the HVL, the results obtained in this study are in agreement with the results from the study by Anton et al. [28]. Certainly, if the uncertainty is taken into account.

3.3.2 Results using the crystalline alanine density correction

Figure 3-9 and Figure 3-10 show the calculated relative responses in function of the mean energy and the HVL while Table 3-7 shows the tabulated results for the SARRP. For the alanine stopping power density correction, it was based on the density of crystalline alanine (1.42 g/cm^3). The relative response is defined in equation (2.7).

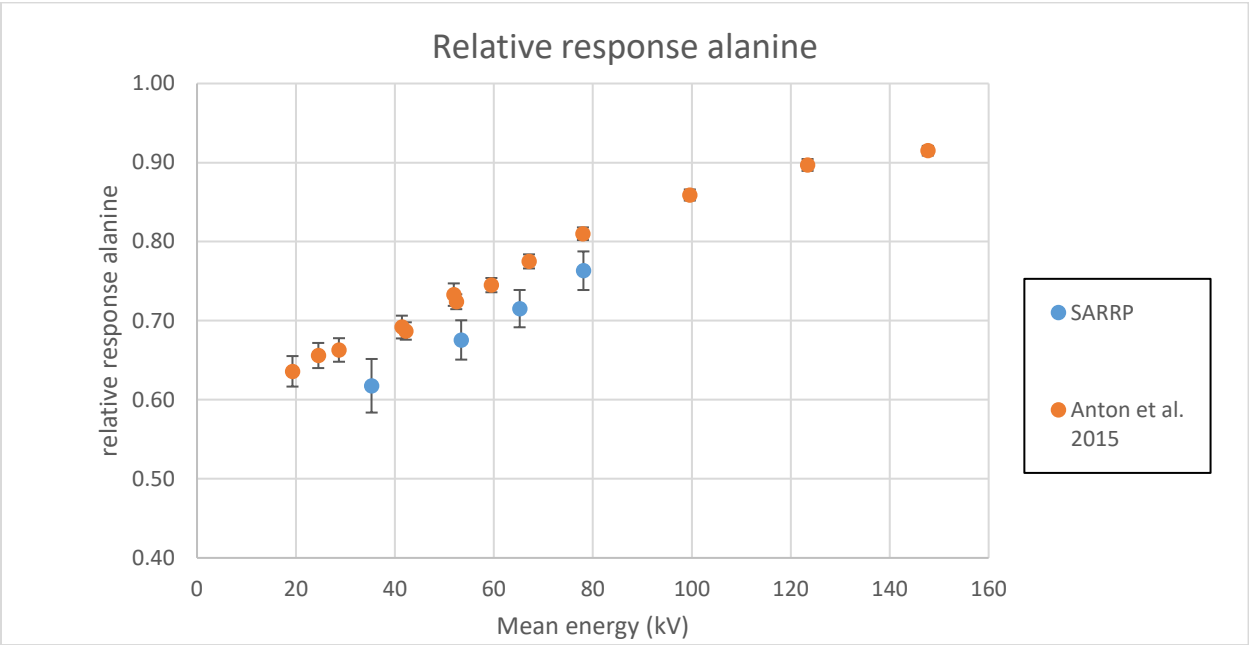

Figure 3-9: Measured relative response of alanine dosimeters in function of the mean energy of the X-rays spectra. The thickness correction is calculated with MC simulations using the density of crystalline alanine for the alanine stopping power density correction.

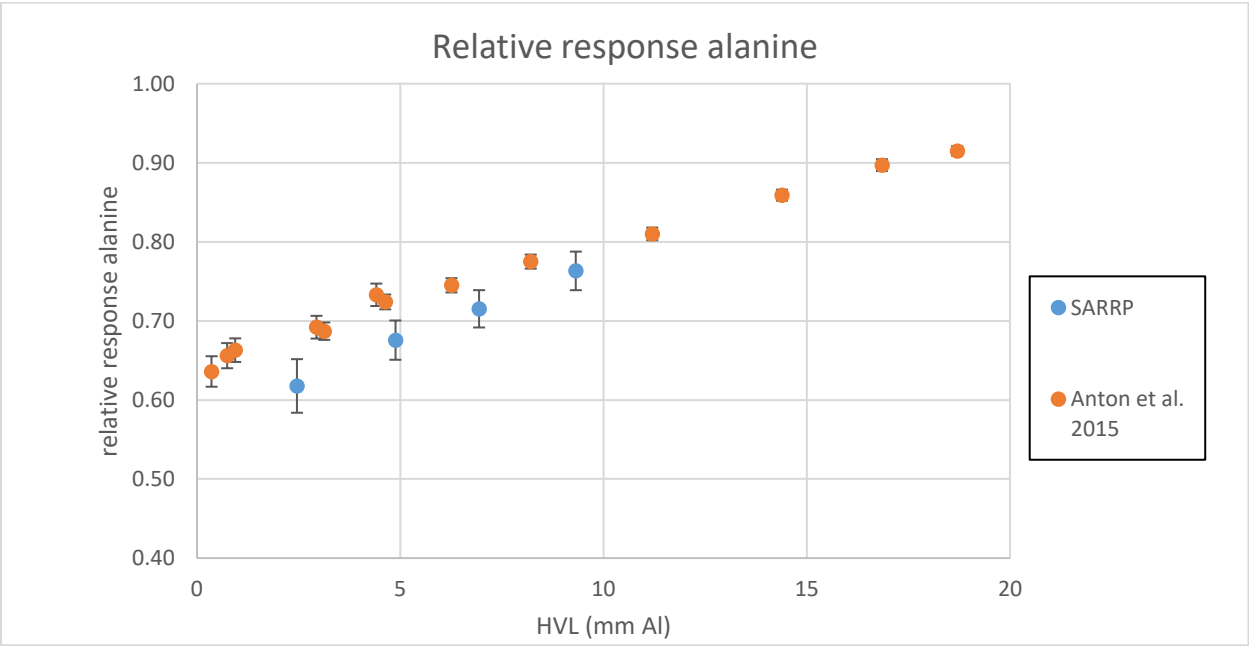

Figure 3-10: Measured relative response of alanine dosimeters in function of the HVL of the X-rays spectra. The thickness correction is calculated with MC simulations using the density of crystalline alanine for the alanine stopping power density correction.

Table 3-7: Measured relative response of alanine dosimeters for the SARRP. The thickness correction is calculated with MC simulations using the density of crystalline alanine for the alanine stopping power density correction.

Energy(kV)	Mean energy (keV)	1st HVL (mm Al)	r (without thickness correction)	r (with thickness correction)	Unc. r (rel)	Unc. r (%)
50	35.3	2.46	0.588	0.618	0.034	3.389
100	53.4	4.88	0.650	0.676	0.025	2.486
150	65.2	6.94	0.694	0.715	0.024	2.358
220	78.1	9.32	0.742	0.763	0.024	2.441

Compared to the results obtained using the bulk density correction, the results do not agree with Anton et al. [28]. The calculated relative response values are systematically lower than the results from Anton et al. [28]. It was decided to rely on the results obtained using the correction based on the bulk density for the alanine stopping power density correction.

3.4 Effect of the variation of the field size on the response of the alanine detectors

The dose maps from the films were calculated using the calibration curves with the energies closest to the energy used to irradiate the film with unknown dose distribution (e.g. 60 kV calibration was used to calculate the dose map on a film irradiated with 50 kV).

The correction for the thickness of the pellets was obtained from MC simulations. For the alanine stopping power density correction, both correction options were used (based on the bulk density of the pellets as well as crystalline alanine). Table 3-8 and Table 3-9 show the calculated thickness correction factors using the stopping power density correction based on the bulk density (1.2 g/cm³) and crystalline alanine (1.42 g/cm³) respectively in the MC simulations.

Table 3-8: Calculated thickness correction factors for the X-RAD 225CX for the 225 22kV beams using the bulk density for the stopping power density correction for the MC simulations.

Energy (kV)	Field size (mm²)	Mean energy (keV)	1st HVL (mm Al)	$D_{w,ala}/D_{w,ref}$	Unc. $D_{w,ala}/D_{w,ref}$ (rel)	Unc. $D_{w,ala}/D_{w,ref}$ (%)
225	10x10 circular	85.5	11.5	0.939	8.20E-04	0.082
225	15 x 15 circular	85.5	11.5	0.941	1.21E-03	0.121
225	20x20 circular	85.5	11.5	0.945	1.58E-03	0.158

Table 3-9: Calculated thickness correction factors for the X-RAD 225CX for the 225 kV beam using the crystalline alanine density for the stopping power density correction for the MC simulations.

Energy (kV)	Field size (mm²)	Mean energy (keV)	1st HVL (mm Al)	$D_{w,ala}/D_{w,ref}$	Unc. $D_{w,ala}/D_{w,ref}$ (rel)	Unc. $D_{w,ala}/D_{w,ref}$ (%)
225	10x10 circular	85.5	11.5	0.969	5.89E-04	0.059
225	15 x 15 circular	85.5	11.5	0.972	8.68E-04	0.087
225	20x20 circular	85.5	11.5	0.975	1.28E-03	0.128

Again we observe that the calculated factors using the bulk density correction are lower than the factors calculated with the crystalline alanine correction.

3.4.1 Results using the bulk density correction

Figure 3-11 and Figure 3-12 show the calculated relative responses in function of the mean energy and the HVL. Figure 3-13 shows the relative response in function of the field size and Table 3-10 shows the tabulated results for the X-RAD 225CX. For the alanine stopping power density correction, it was based on the bulk density (1.2 g/cm³) of the alanine pellets. The relative response is defined in equation (2.7).

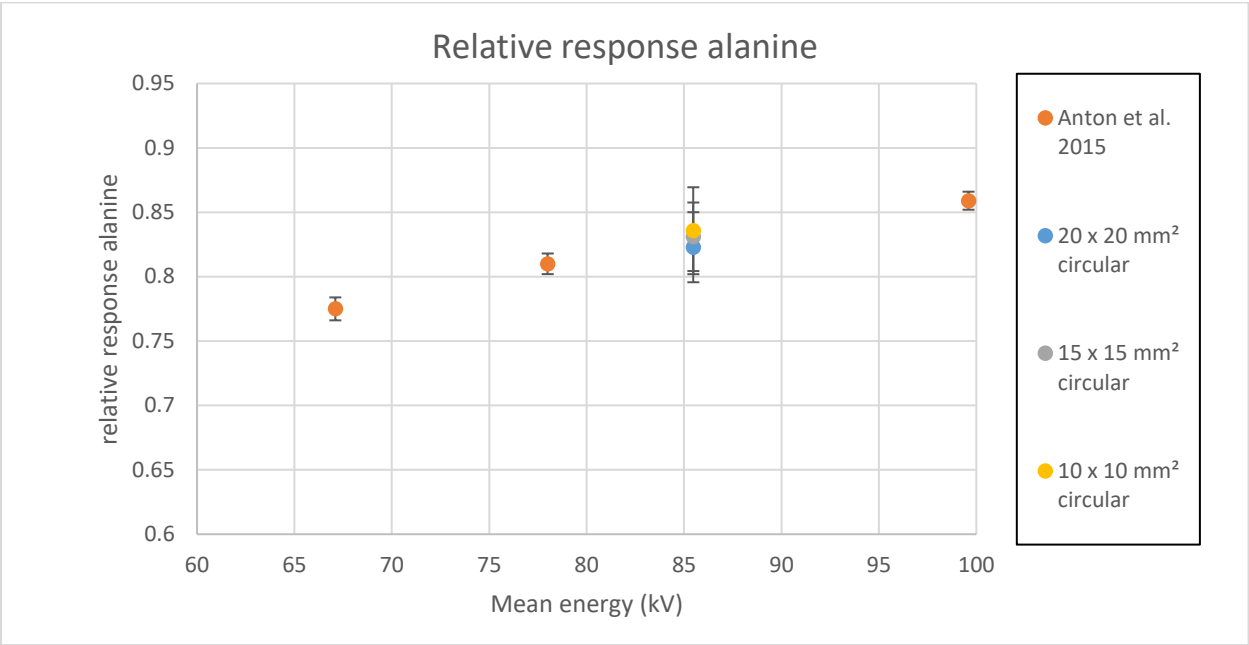

Figure 3-11: Measured relative response of alanine dosimeters in function of the mean energy of the X-rays spectra. The thickness correction is calculated with MC simulations using the bulk density for the alanine stopping power density correction.

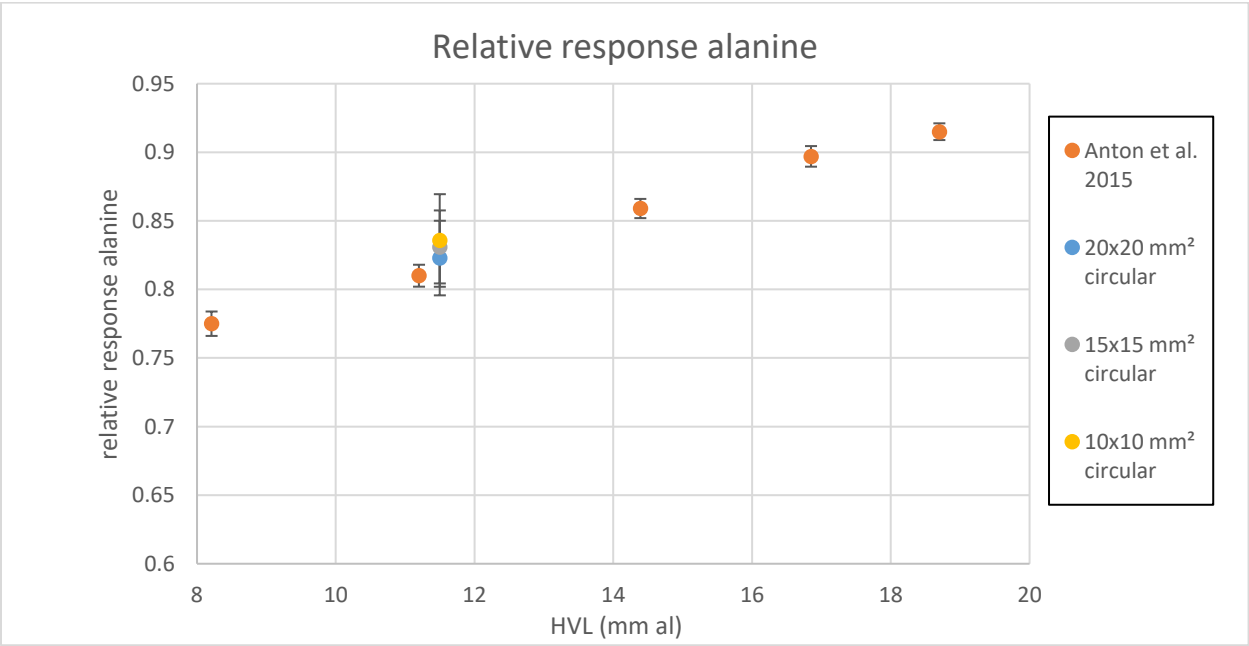

Figure 3-12: Measured relative response of alanine dosimeters in function of the half value layer of the X-rays spectra. The thickness correction is calculated with MC simulations using the bulk density for the alanine stopping power density correction.

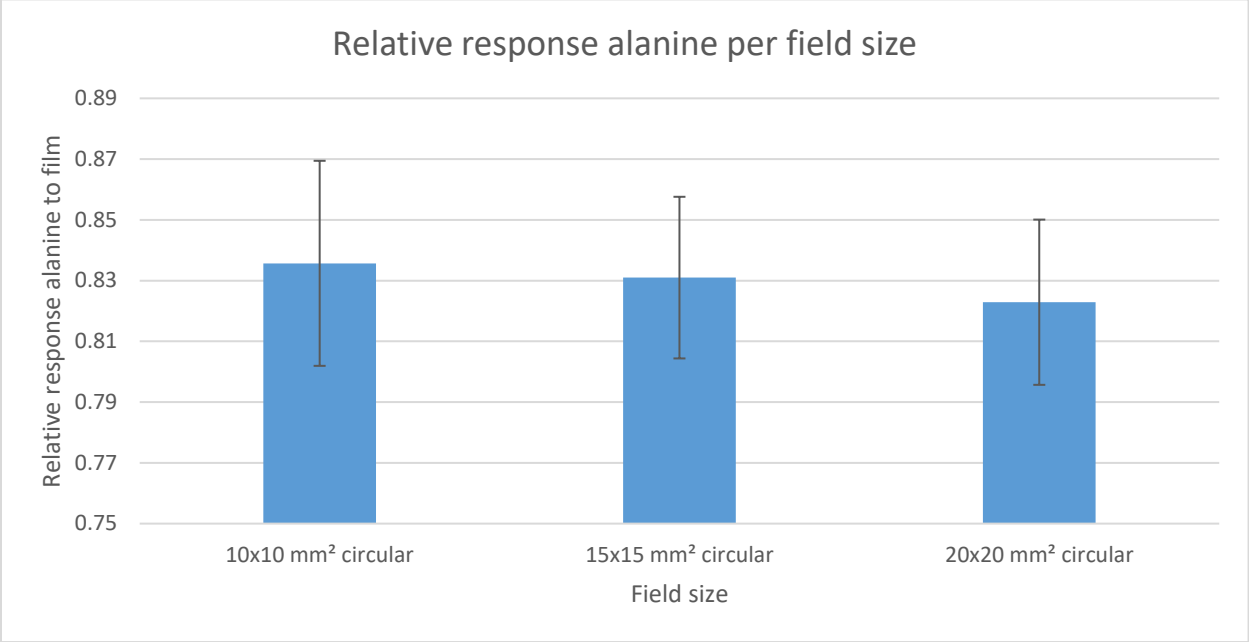

Figure 3-13: Measured relative response of alanine dosimeters in function of the field size of the beams. The thickness correction is calculated with MC simulations using the bulk density for the alanine stopping power density correction.

Table 3-10: Measured relative response of alanine dosimeters for the X-RAD 225CX. The thickness correction is calculated with MC simulations using the bulk density for the alanine stopping power density correction.

Field size	E mean (keV)	1st HVL (mm Al)	r (without thickness correction)	r (with thickness correction)	Unc. r (rel)	Unc. r (%)
10x10 mm² circular	85.5	11.5	0.784	0.836	0.034	3.375
15x15 mm² circular	85.5	11.5	0.780	0.831	0.027	2.661
20x20 mm² circular	85.5	11.5	0.772	0.823	0.027	2.720

The relative response increases with 1.5 % with decreasing field sizes from 20 x 20 mm² to 10 x 10 mm². This could be explained due to less contribution from scatter in these smaller fields. Thus there are fewer photons involved with lower energy which has a lower relative response in smaller fields.

3.4.2 Results using the crystalline alanine density correction

Figure 3-14 and Figure 3-15 show the calculated relative responses in function of the mean energy and the HVL. Figure 3-16 shows the relative response in function of the field size and Table 3-11 shows the tabulated results for the X-RAD 225CX. For the alanine stopping power

density correction, it was based on the density of crystalline alanine (1.42 g/cm³). The relative response is defined in equation (2.7).

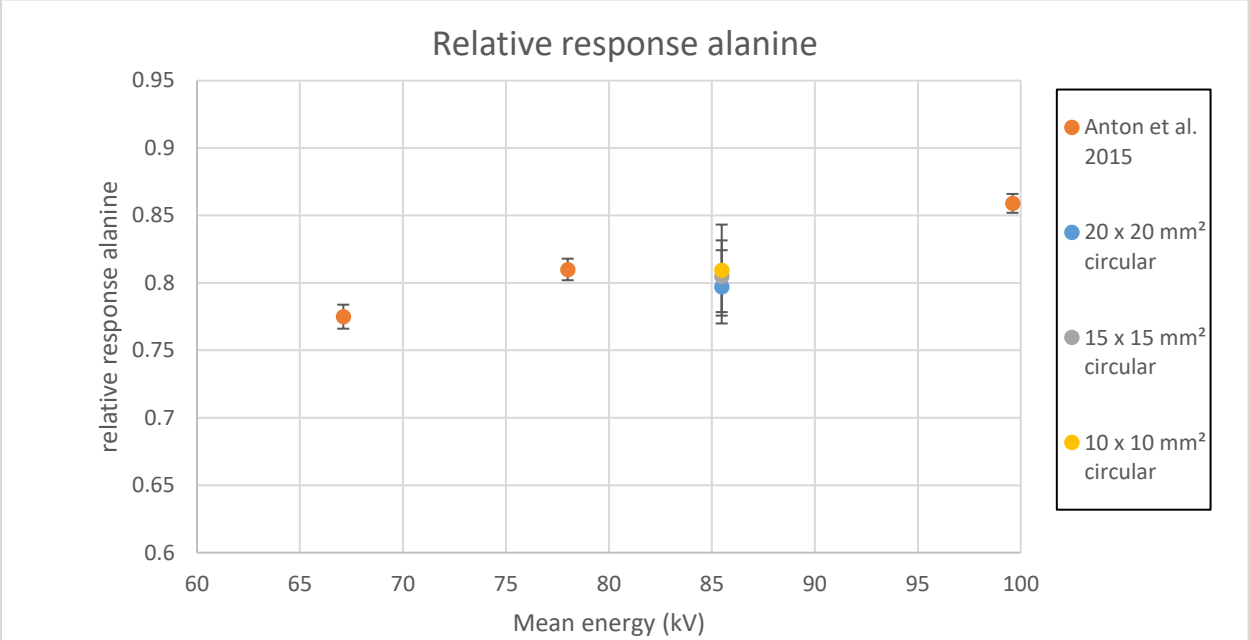

Figure 3-14: Measured relative response of alanine dosimeters in function of the mean energy of the X-rays spectra. The thickness correction is calculated with MC simulations using the density of crystalline alanine for the alanine stopping power density correction.

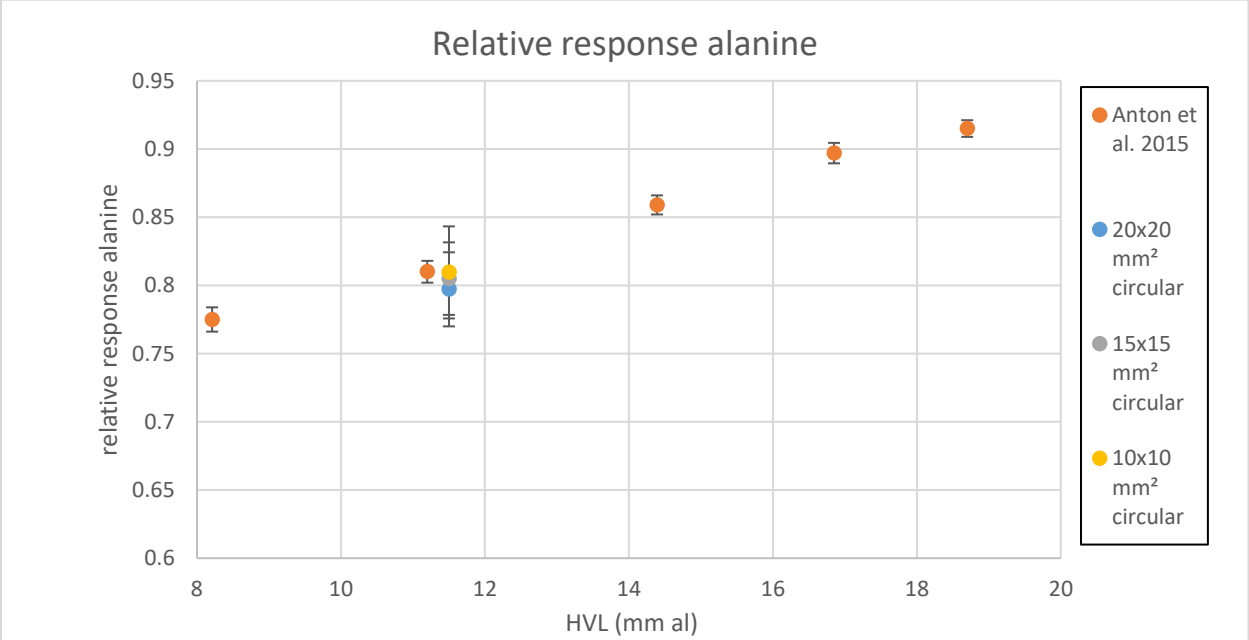

Figure 3-15: Measured relative response of alanine dosimeters in function of the half value layer of the X-rays spectra. The thickness correction is calculated with MC simulations using the density of crystalline alanine for the alanine stopping power density correction.

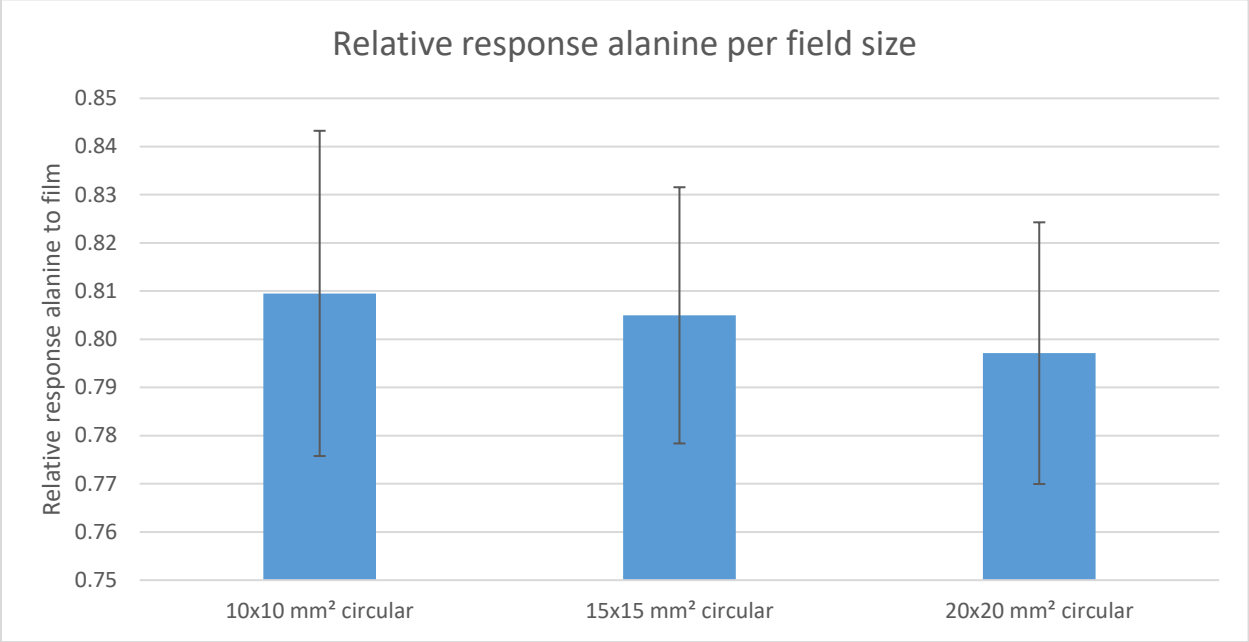

Figure 3-16: Measured relative response of alanine dosimeters in function of the field size of the beams. The thickness correction is calculated with MC simulations using the density of crystalline alanine for the alanine stopping power density correction.

Table 3-11: Measured relative response of alanine dosimeters for the X-RAD 225CX. The thickness correction is calculated with MC simulations using the density of crystalline alanine for the alanine stopping power density correction.

Field size	E mean (keV)	1st HVL (mm Al)	r (without thickness correction)	r (with thickness correction)	Unc. r (rel)	Unc. r (%)
10x10 mm² circular	85.5	11.5	0.784	0.810	0.034	3.375
15x15 mm² circular	85.5	11.5	0.780	0.805	0.027	2.659
20x20 mm² circular	85.5	11.5	0.772	0.797	0.027	2.716

Again, the relative response values calculated using the density correction based on the crystalline alanine density are lower than those based on the bulk density. The relative response increases with 1.5 % with decreasing field sizes from 20 x 20 mm² to 10 x 10 mm².

3.5 MC simulations

On the X-RAD 225CX, simulations were also performed with the open field and the 40 x 40 mm² besides the beams described in Table 2-5. Simulations were also performed using beams

with 2 mm Al filter and a filtration consisting of 2 mm Al and 0.3 mm Cu. The parameters were calculated with SpekCalc [51-53]. The spectra are shown in Figure 2-11.

3.5.1 Comparison of alanine stopping power density correction option

The open field has dimensions of 13.6 x 13.6 cm². Table 3-12 shows the results of the comparisons of both density correction option for the beams used on the SARRP. Table 3-13 shows the results for the beams on the X-RAD 225CX with 0.3 mm Cu filtration and Table 3-14 shows the results with 2 mm Al filtration and Table 3-15 shows the results with the filtration consisting of 2 mm Al and 0.3 mm Cu.

Table 3-12: Comparison of the density correction options for the beams used on the SARRP.

Field size	Mean energy (kV)	HVL (mm Al)	Voltage (kVp)	$Corr_{Bulk\_d}/Corr_{Cryst\_d}$	Unc. (rel)	Unc. (%)
Open field (SARRP)	35.3	2.46	50	0.962	0.002	0.246
Open field (SARRP)	53.4	4.88	100	0.975	0.002	0.239
Open field (SARRP)	65.2	6.94	150	0.985	0.002	0.239
Open field (SARRP)	78.1	9.32	220	0.985	0.002	0.241

Table 3-13: Comparison of the density correction options for the beams used on the X-RAD 225CX with 0.3 mm Cu filtration.

Field size (mm²)	Mean energy (kV)	HVL (mm Al)	Voltage (kVp)	$Corr_{Bulk\_d}/Corr_{Cryst\_d}$	Unc. (rel)	Unc. (%)
Open field (X-RAD 225CX)	85.5	11.50	225	0.991	0.002	0.245
40 x 40 square (X-RAD 225CX)	85.5	11.50	225	0.991	0.002	0.183
20 x 20 circular (X-RAD 225CX)	85.5	11.50	225	0.996	0.001	0.121
15 x 15 circular (X-RAD 225CX)	85.5	11.50	225	0.993	0.001	0.092
10 x 10 circular (X-RAD 225CX)	85.5	11.50	225	0.993	0.001	0.063

Table 3-14: Comparison of the density correction options for the beams used on the X-RAD 225CX with 2 mm filtration.

Field size (mm²)	Mean energy (kV)	HVL (mm Al)	Voltage (kVp)	$Corr_{Bulk\_d}/Corr_{Cryst\_d}$	Unc. (rel)	Unc. (%)
Open field (X-RAD 225CX)	73.0	7.22	225	0.985	0.002	0.240
40 x 40 square (X-RAD 225CX)	73.0	7.22	225	0.984	0.002	0.239
20 x 20 circular (X-RAD 225CX)	73.0	7.22	225	0.984	0.001	0.111
15 x 15 circular (X-RAD 225CX)	73.0	7.22	225	0.983	0.001	0.085
10 x 10 circular (X-RAD 225CX)	73.0	7.22	225	0.983	0.001	0.058

Table 3-15: Comparison of the density correction options for the beams used on the X-RAD 225CX with filtration consisting of 2 mm Al and 0.3 mm Cu.

Field size (mm²)	Mean energy (kV)	HVL (mm Al)	Voltage (kVp)	$Corr_{Bulk\_d}/Corr_{Cryst\_d}$	Unc. (rel)	Unc. (%)
Open field (X-RAD 225CX)	87.5	11.96	225	0.998	0.002	0.245
40 x 40 square (X-RAD 225CX)	87.5	11.96	225	0.995	0.002	0.183
20 x 20 circular (X-RAD 225CX)	87.5	11.96	225	0.995	0.001	0.121
15 x 15 circular (X-RAD 225CX)	87.5	11.96	225	0.996	0.001	0.092
10 x 10 circular (X-RAD 225CX)	87.5	11.96	225	0.995	0.000	0.044

The choice of using a density correction option (bulk density or crystalline alanine density) starts to influence once the mean energy drops below 80 kV. Above 80 kV, the ratio ($Corr_{Bulk\_d}/Corr_{Cryst\_d}$) is higher than 0.99. Below 80 kV, it drops to 0.985 and below 60 kV the ratio drops even further to 0.975. Below 50 kV, it has a major influence where the ratio drops further to 0.962. The field size does not seem to have a major influence as no trend can be observed when the field size decreases from 13.6 x 13.6 cm² to 1 x 1 cm².

3.5.2 Simulated relative response of alanine detectors

Energy dependence

The simulated relative response is defined in equation (2.8). Figure 3-17 and Figure 3-18 show the simulated relative response values using the bulk density for the alanine stopping power density correction. The field size was the open field in these simulations. Table 3-16 and Table 3-17 show the tabulated results from the MC simulations in this study and the results from Anton et al. [28] respectively. Figure 3-19 shows the comparison between the simulated and experimental results where the bulk density is used for the alanine stopping power density correction for the results in this study.

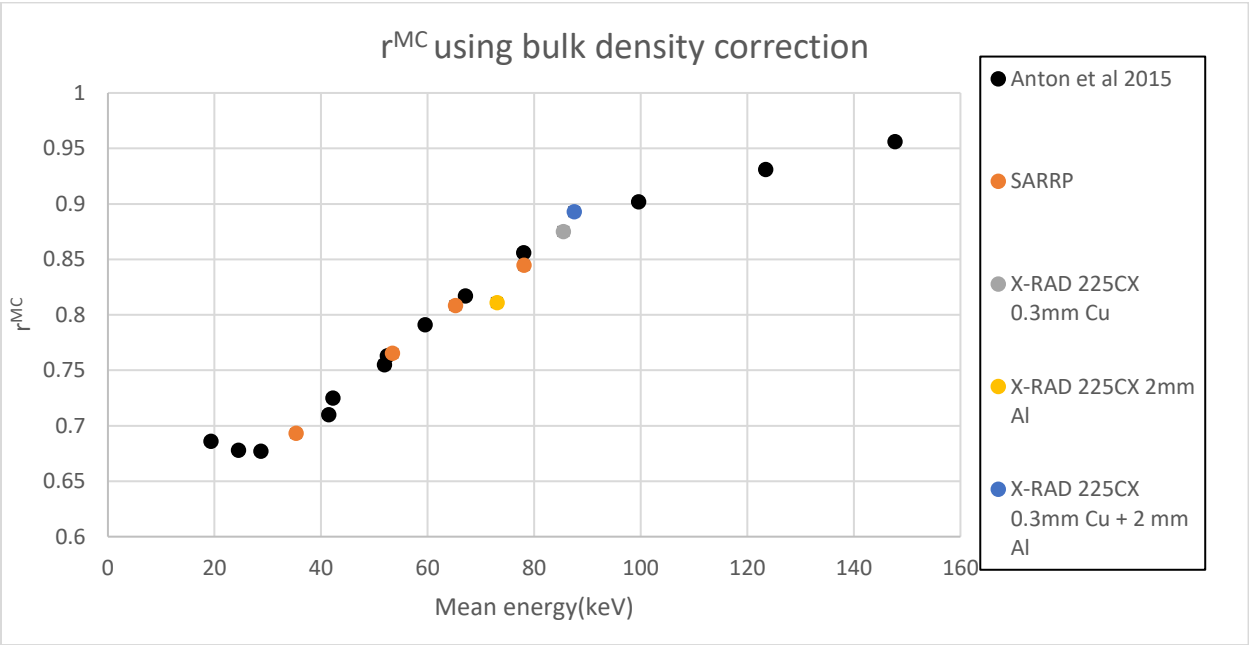

Figure 3-17: Simulated relative response values in function of the mean energy of the photon spectra using the bulk density for the alanine stopping power density correction.

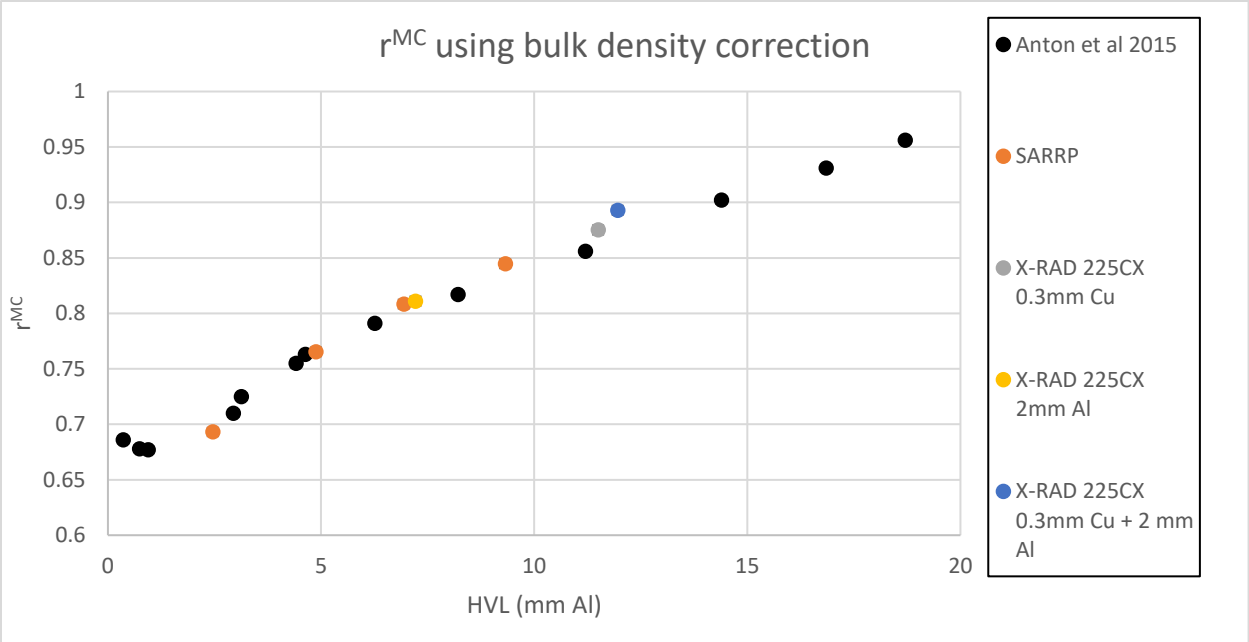

Figure 3-18: Simulated relative response values in function of the half value layer of the photon spectra using the bulk density for the alanine stopping power density correction.

Table 3-16: Simulated relative response values of the beams used in this study.

Machine	Mean energy (keV)	1st HVL (mm Al)	r^{MC}	Unc. r^{MC} (%)
SARRP	35.3	2.46	0.693	0.382
SARRP	53.4	4.88	0.765	0.393
SARRP	65.2	6.94	0.808	0.399
X-RAD 225CX	73.0	7.22	0.811	0.412
SARRP	78.1	9.32	0.845	0.402
X-RAD 225CX	85.5	11.5	0.875	0.410
X-RAD 225CX	87.5	11.96	0.893	0.411

Table 3-17: Results of the simulated relative response values from Anton et al. [28]

Voltage (kVp)	Mean energy (keV)	1st HVL (mm Al)	r^{MC}	Unc. r^{MC} (%)
TW 30	19.3	0.359	0.686	0.3
TW 40	24.5	0.741	0.678	0.3
TW 50	28.7	0.94	0.677	0.3
TW 70	41.4	2.94	0.71	0.3
TW 100	51.9	4.41	0.755	0.4
TH 70	42.2	3.13	0.725	0.3
TH 100	52.4	4.63	0.763	0.3
TH 120	59.5	6.26	0.791	0.3
TH 140	67.1	8.21	0.817	0.3
TH 150	78	11.2	0.856	0.3
TH 200	99.6	14.39	0.902	0.3
TH 250	123.4	16.85	0.931	0.3
TH 280	147.7	18.7	0.956	0.3

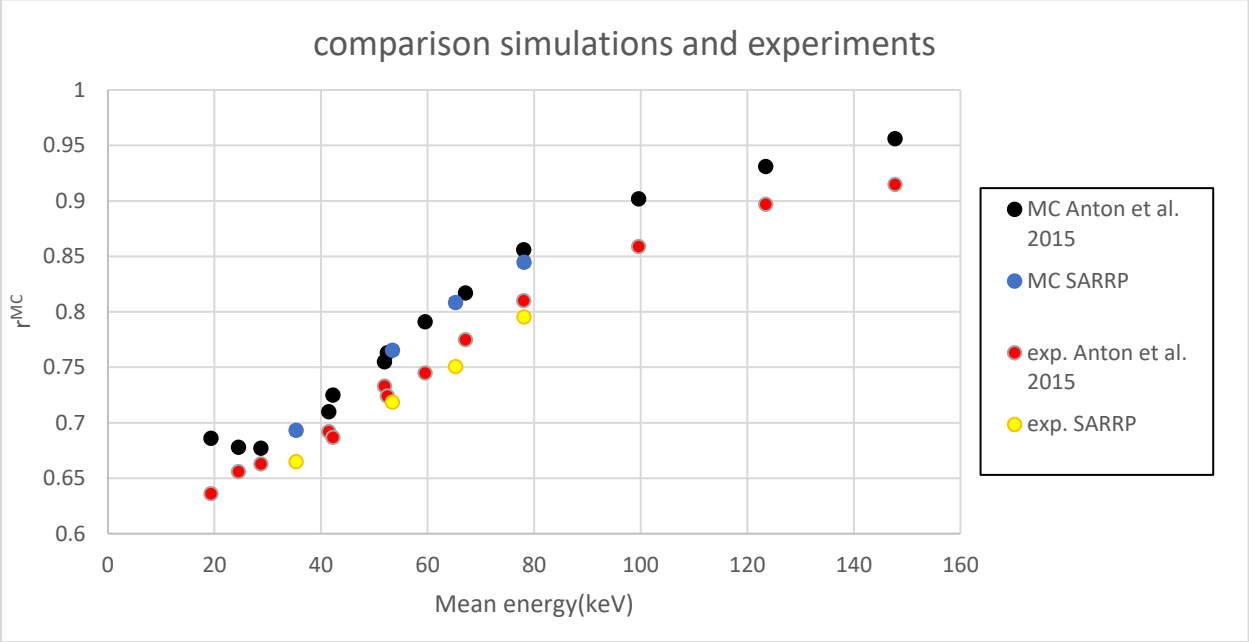

Figure 3-19: Comparison of experimental and simulation results in function of the mean energy of the spectra.

The simulated results agree well with the results from Anton et al. [28] when the bulk density is used for the stopping power density correction. As explained in 3.5.1, the effect of using the crystalline alanine density for the stopping power correction results in higher values obtained from simulations. When simulations are performed using the crystalline alanine density for the correction, the results are systematically higher than the results from Anton et al. [28].

The simulation results do not agree with the experimental results. This is the same with our values and those from Anton et al. [28]. This can be explained because the simulation results represent a ratio of absorbed dose values while the dosimetry performed with EPR dosimetry is due to the concentration of free radicals in the sample. This was reported in previous studies [29, 30].

The number of radicals generated per unit absorbed dose decreases for lower photon energies. This effect can be described as the intrinsic efficiency of alanine pellets.

Field size dependence

The simulated relative response is defined in equation (2.8). Figure 3-20 shows the simulated results of the relative response in function of the field size and Table 3-18 shows the tabulated results. Figure 3-21 shows the comparison between the simulated and experimental results.

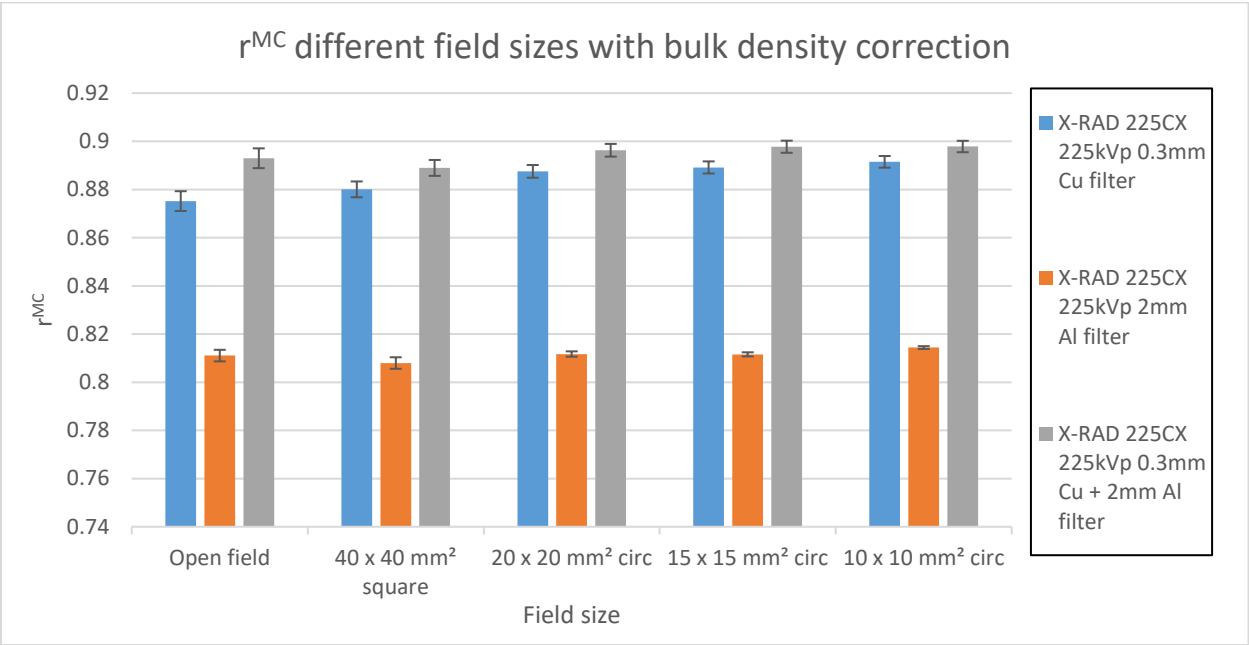

Figure 3-20: Simulated relative response values of the beams from the X-RAD 225CX using the bulk density for the alanine stopping power density correction.

Table 3-18: Simulated relative response values of the beams from the X-RAD 225CX using the bulk density for the alanine stopping power density correction.

Field size	Mean energy (keV)	1st HVL (mm Al)	r^{MC}	Unc. r^{MC} (%)
Open field	85.5	11.5	0.875	0.410
40 x 40 mm² square			0.880	0.329
20 x 20 mm²circular			0.888	0.264
15 x 15 mm² circular			0.889	0.252
10 x 10 mm² circular			0.891	0.242
Open field	73	7.21	0.811	0.412
40 x 40 mm² square			0.808	0.240
20 x 20 mm²circular			0.812	0.112
15 x 15 mm² circular			0.812	0.085
10 x 10 mm² circular			0.814	0.058
Open field	87.5	11.95	0.893	0.411
40 x 40 mm² square			0.889	0.329
20 x 20 mm² circular			0.896	0.264
15 x 15 mm² circular			0.898	0.252
10 x 10 mm² circular			0.898	0.238

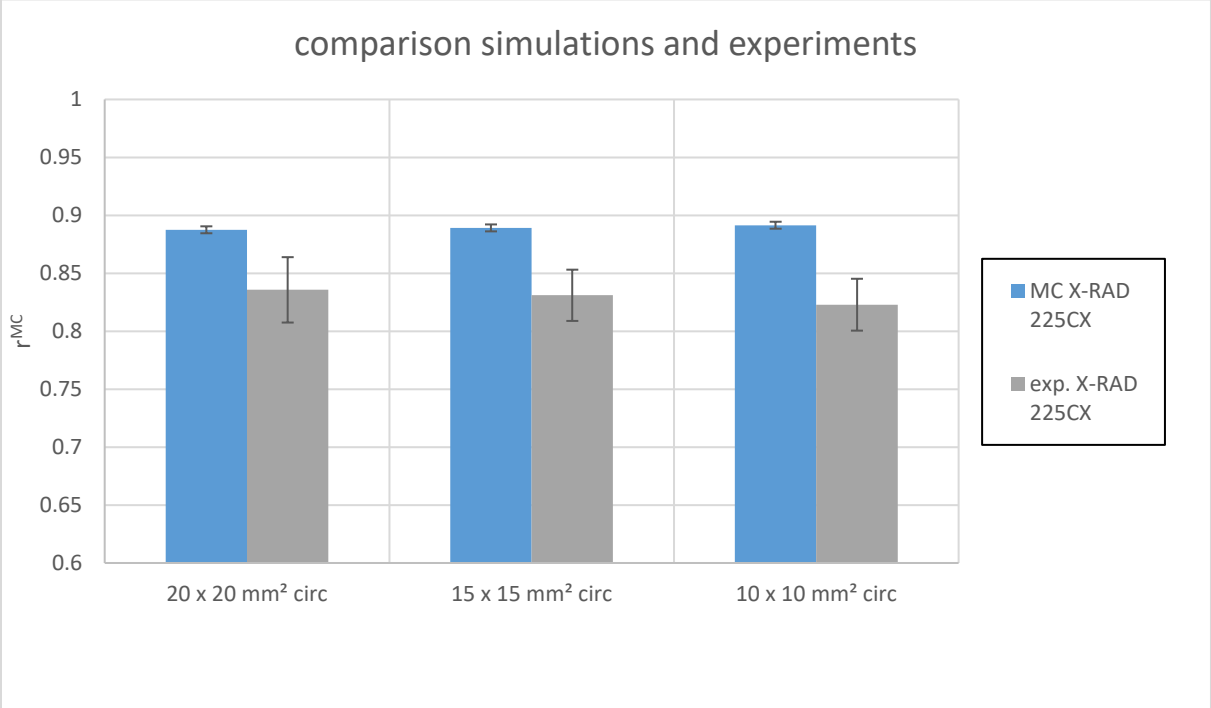

Figure 3-21: Simulated and measured relative responses of the beams from the X-RAD 225CX.

The simulated results show that the relative response increases with decreasing field size as observed with the experimental results. The relative response increases with 2 % from the open field (13.6 x 13.6 cm²) to the 1 x 1 cm² field size.

When comparing with the experimental results, the experimental results are systematically lower than the simulated results. This is caused due to the intrinsic efficiency of the alanine pellets.

3.5.3 Comparison of measured and simulated PDD's

SARRP

The following figures show the comparison between simulated and measured PDD's for the SARRP in the water tank and RW3. The PDD's are normalised at 10 mm depth.

Simulations in water

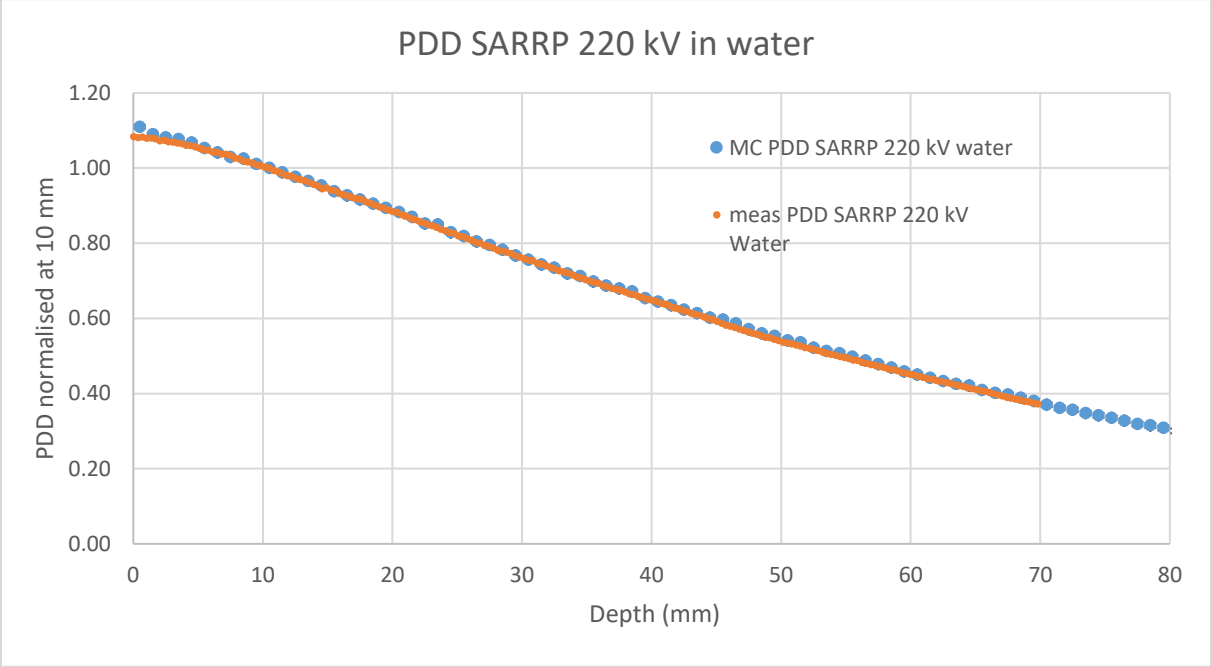

Figure 3-22: Simulated and measured PDD's for the 220 kV beam in the water tank.

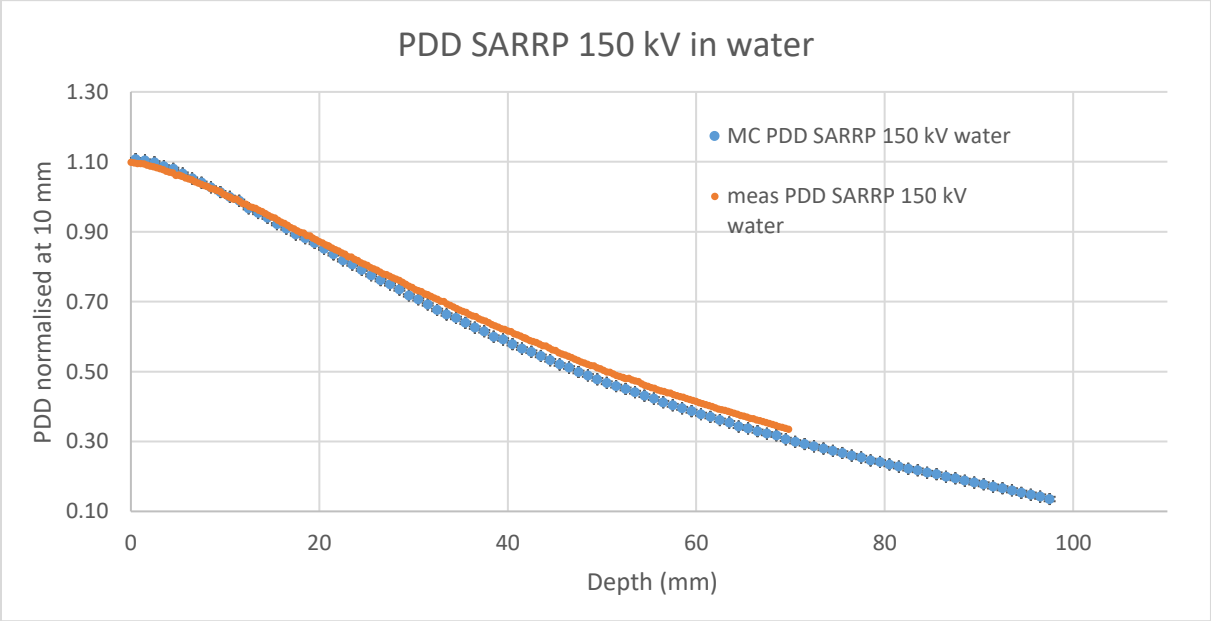

Figure 3-23: Simulated and measured PDD's for the 150 kV beam in the water tank.

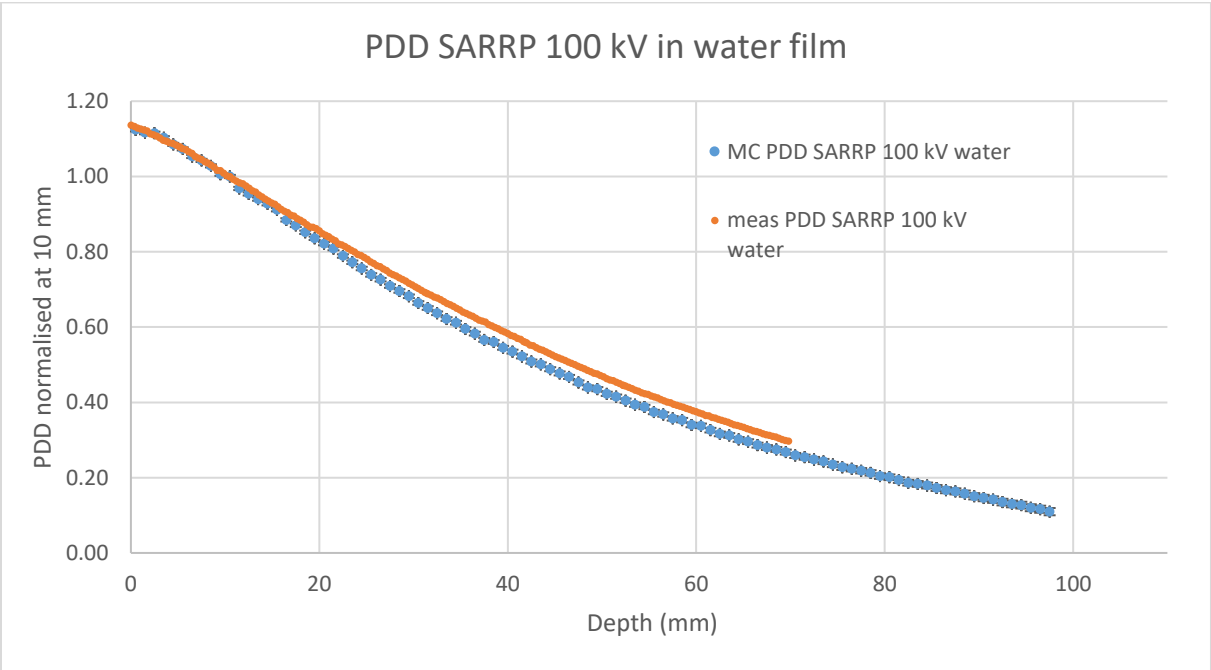

Figure 3-24: Simulated and measured PDD's for the 100 kV beam in the water tank.

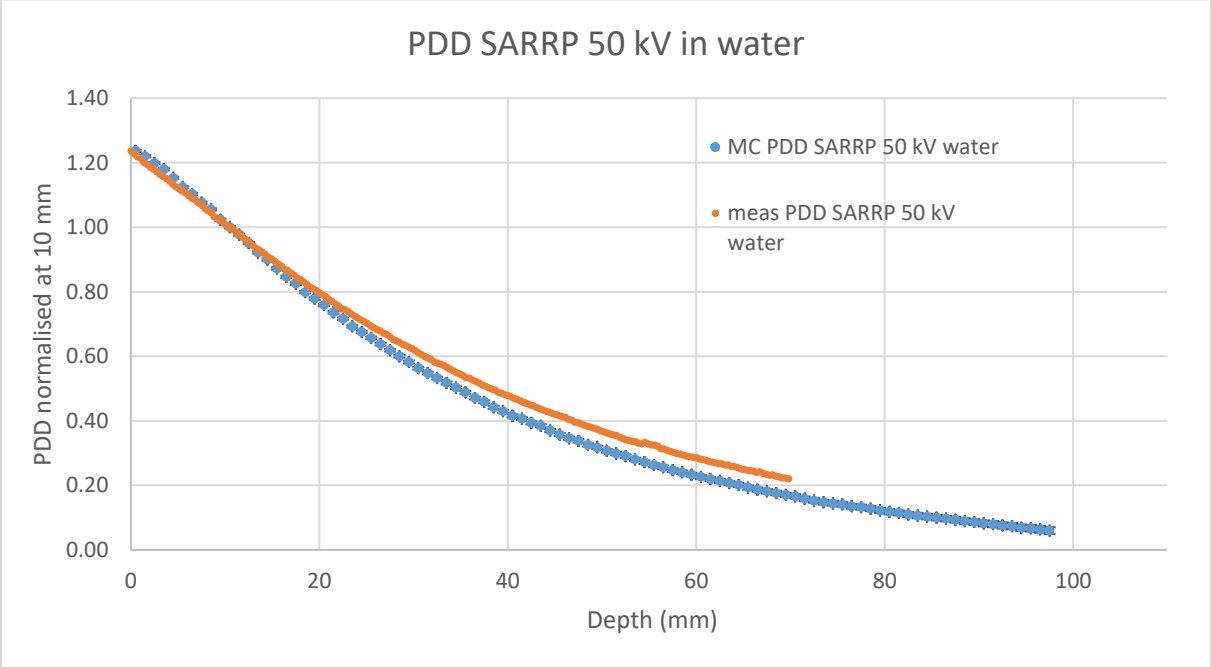

Figure 3-25: Simulated and measured PDD's for the 50 kV beam in the water tank.

The simulated and measured PDD's agree for 220 kV but the agreement gets worse when the energy is lower. For 100 kV and 50 kV they do not agree well. This could be explained due to the self-absorption effect of the film detectors because the film was placed parallel to the beam direction.

RW3

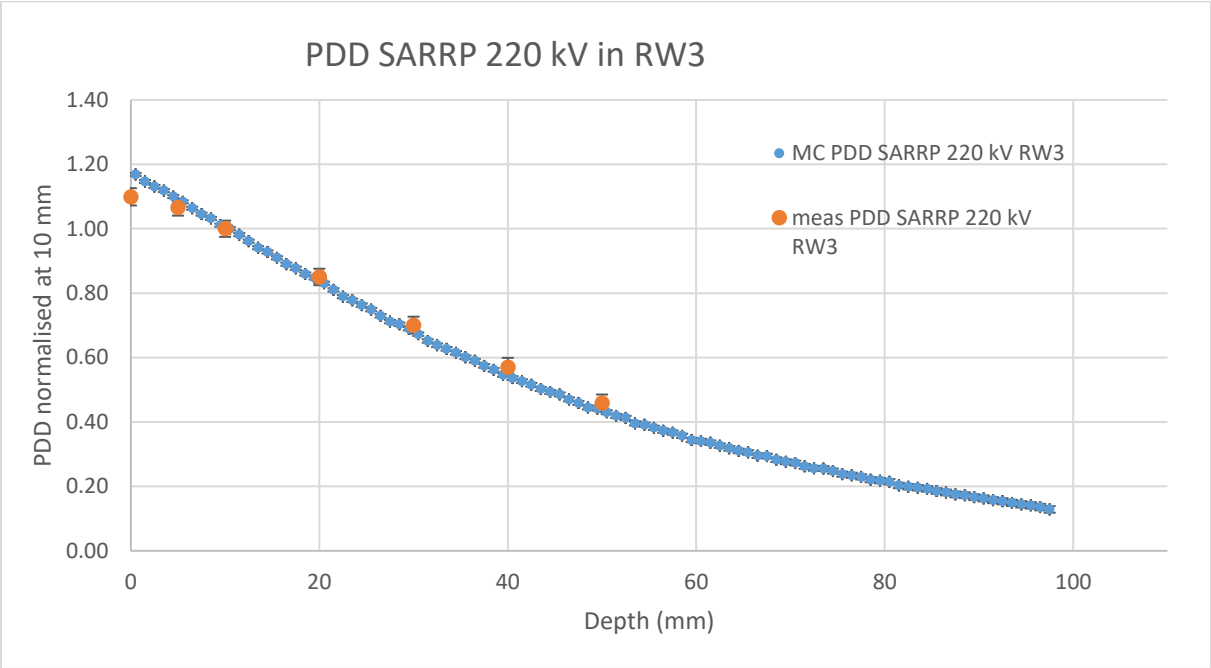

Figure 3-26: Simulated and measured PDD's for the 220 kV beam in RW3.

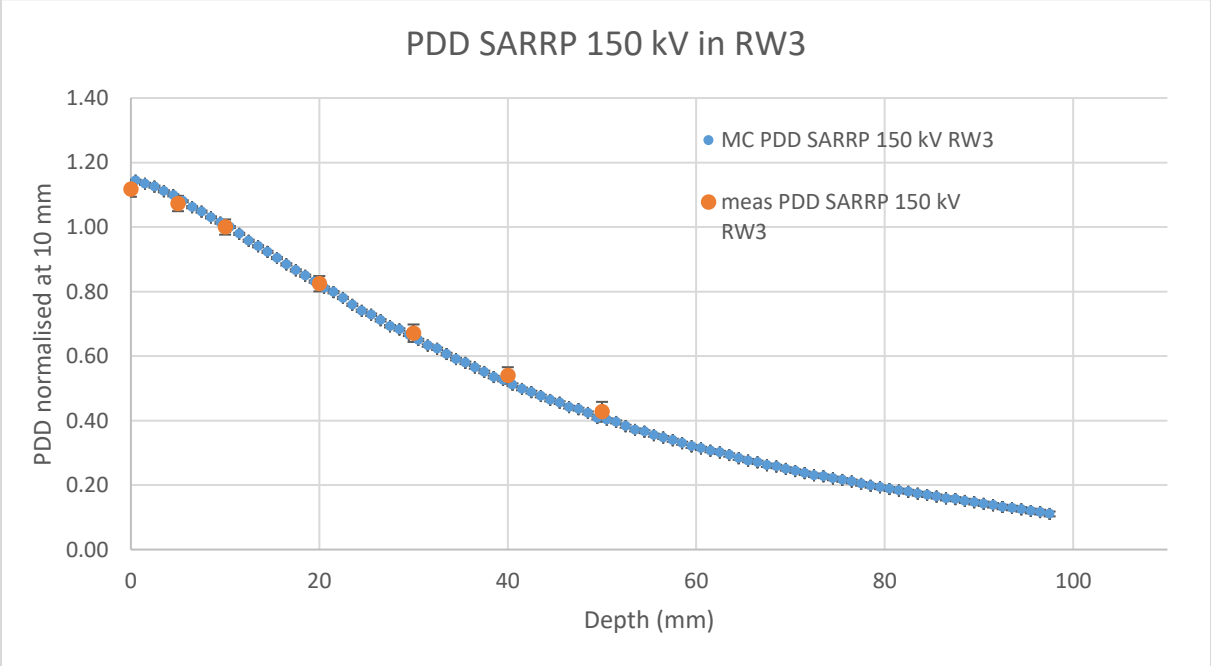

Figure 3-27: Simulated and measured PDD's for the 150 kV beam in RW3.

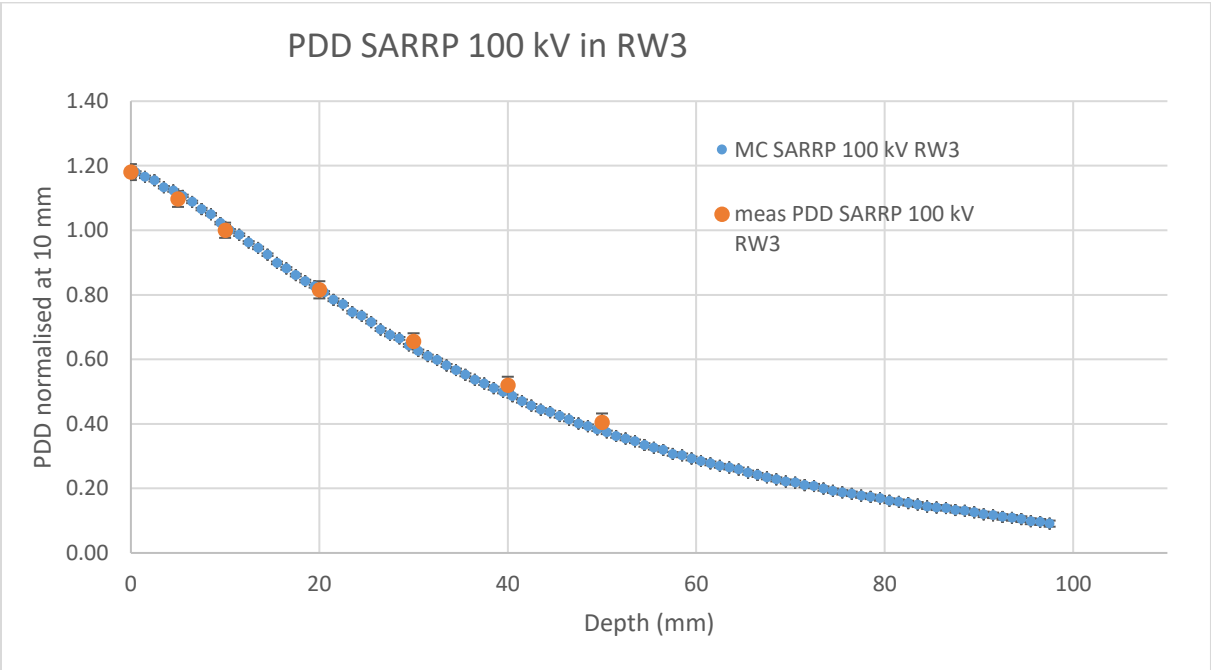

Figure 3-28: Simulated and measured PDD's for the 100 kV beam in RW3.

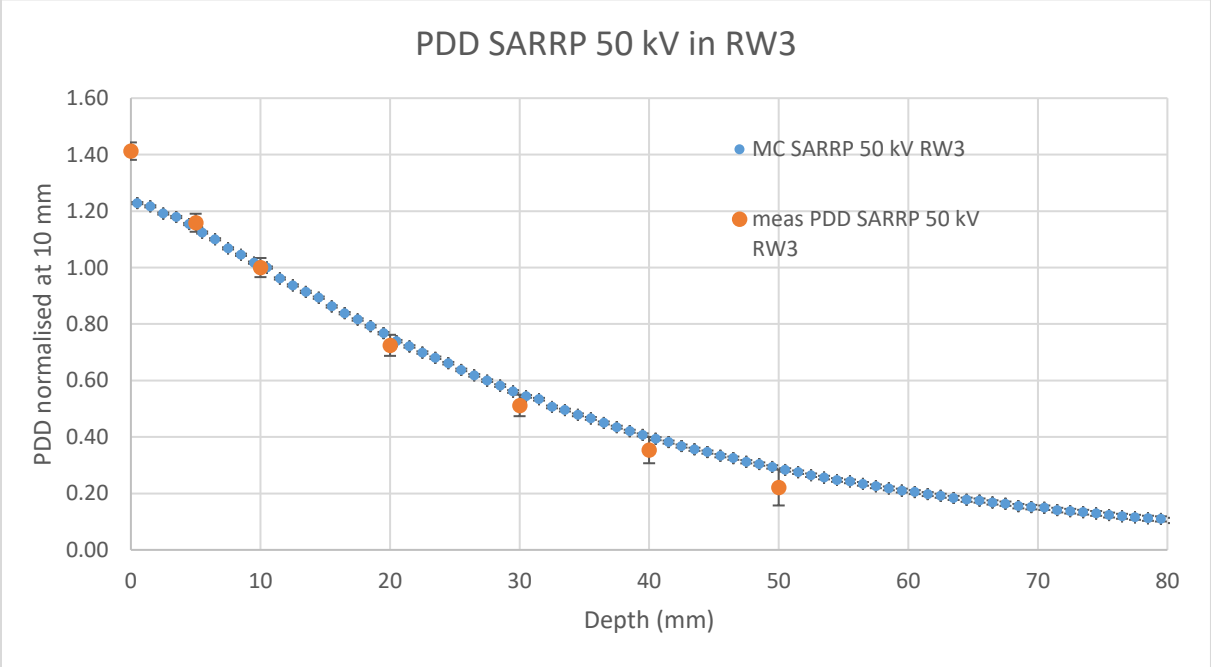

Figure 3-29: Simulated and measured PDD's for the 50 kV beam in RW3.

The simulated and measured PDD's agree within uncertainty.

X-RAD 225CX

The following figures show the comparison between simulated and measured PDD's for the X-RAD 225CX in RW3. The PDD's are normalised at 10 mm depth.

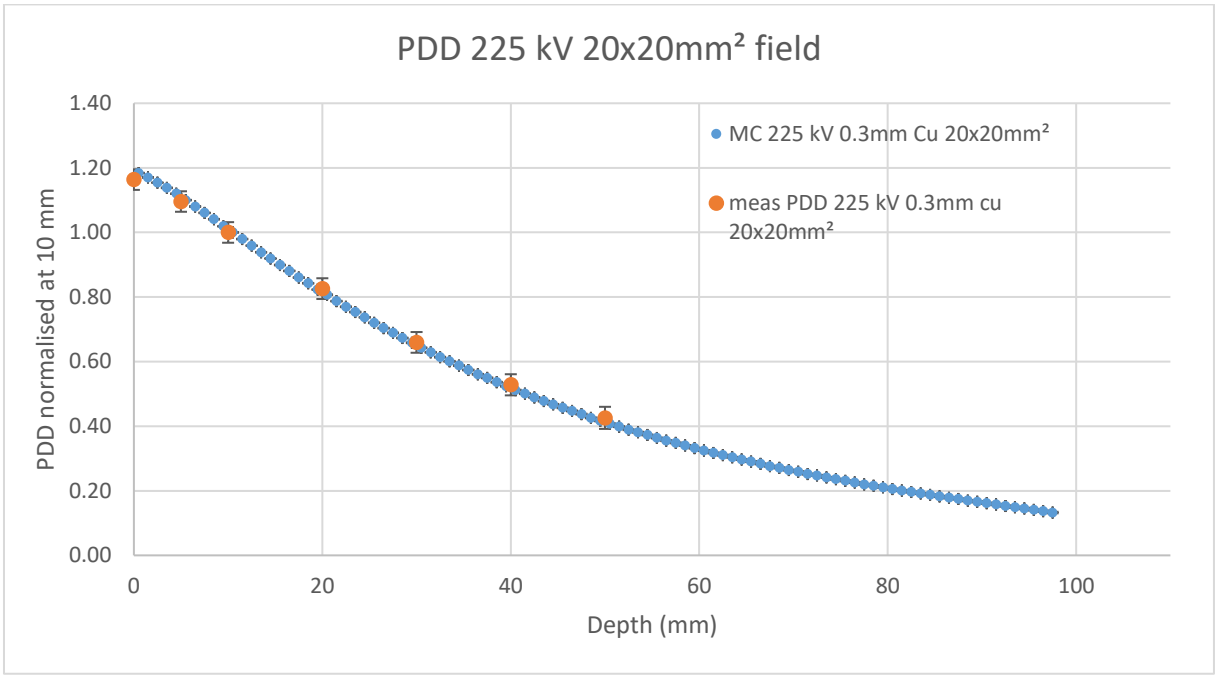

Figure 3-30: Simulated and measured PDD's for the 225 kV beam with a field size of 20 x 20 mm².

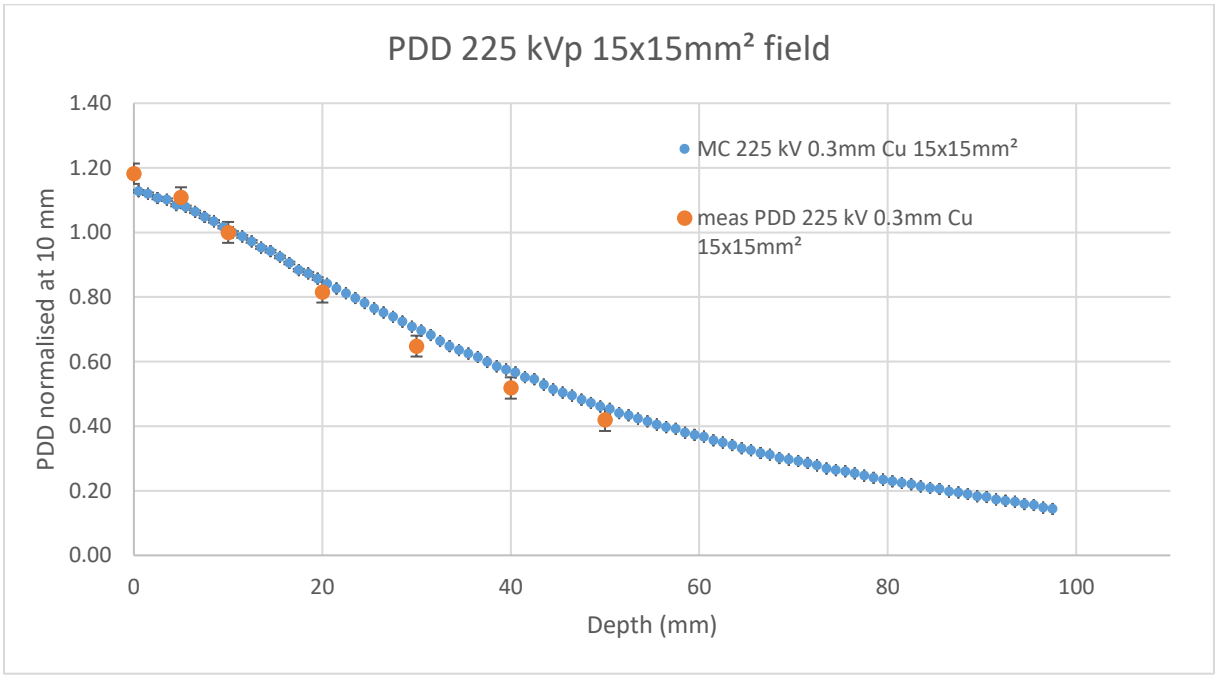

Figure 3-31: Simulated and measured PDD's for the 225 kV beam with a field size of 15 x 15 mm².

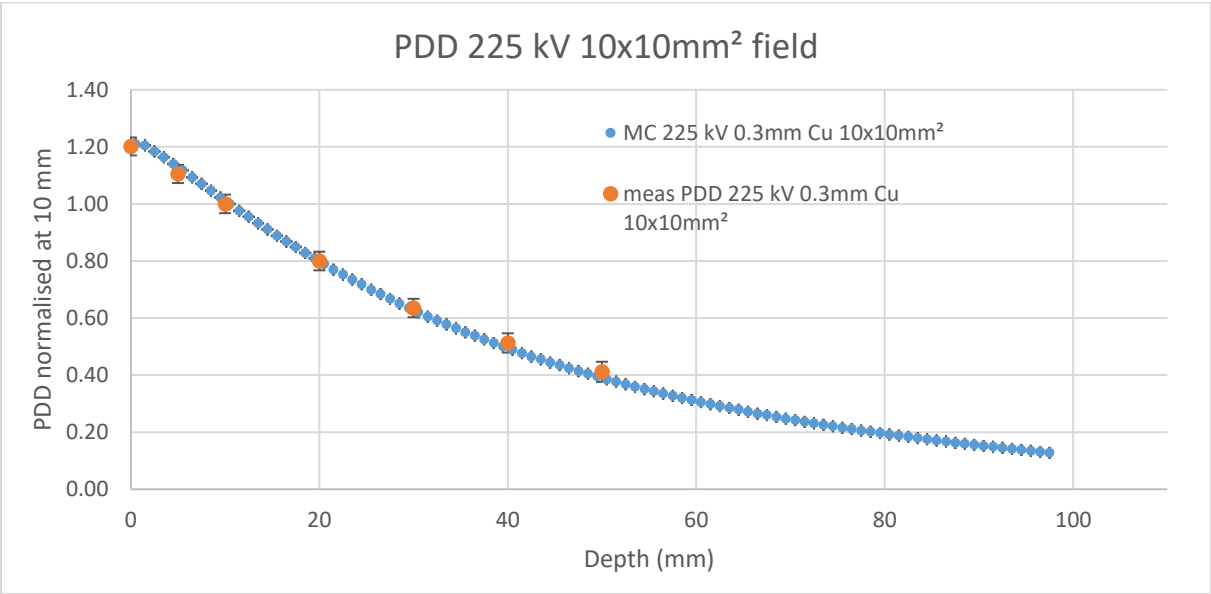

Figure 3-32: Simulated and measured PDD's for the 225 kV beam with a field size of 15 x 15 mm².

The simulated and measured PDD's agree within uncertainty.

4 Discussion

In this study, we investigated the relative response of alanine dosimeters in 50 – 225 kV X-rays and small fields. Alanine and film detectors were irradiated with kV X-rays beams with open fields on small animal irradiators and also with small field sizes down to 1 x 1 cm². Cylindrical alanine pellets with a diameter of 4.8 ± 0.1 mm and a height of 2.8 ± 0.1 mm were used in this study for the alanine/EPR dosimetry while Gafchromic^{TM} EBT3 films were used for the film dosimetry. The choice of using radiochromic films was that it gave the possibility to irradiate all the detectors in one session. The other reason was that there was no possibility to irradiate in a ^{60}Co beam. The film detector was placed directly on top of the alanine detector. The dose measured by the alanine pellet was compared to the dose measured by the film detector after correcting for the difference of the depths of both detectors. The dose measured by the alanine pellet is the dose at the centre of the pellet and this was taken into account by calculating $D_{w,ala}/D_{w,ref}$ with MC simulations. Then, the relative response in this study was described in equation (2.7). The energy dependence of the film detectors was also investigated with the results presented in 3.1. PDD's were measured in water and RW3 with film dosimeters. Calibration curves were generated with films irradiated at 60 kV, 100 kV and 225 kV and these calibration curves were then used to calculate the dose distributions of the films used to determine the relative response of the alanine detectors as well as for the PDD measurements.

Simulations were performed using the EGSnrc code system [76] with the DOSRZnrc user code [77]. The PDD's were simulated in water and RW3 and the results were compared to the experiments. The relative response was also simulated using two options for the alanine stopping power density correction:

- Based on the bulk density of the alanine pellet (1.2 g/cm³)
- Based on the density of crystalline alanine (1.42 g/cm³)

The simulated relative response of beam quality Q is calculated relative to a ^{60}Co beam. The simulated relative response is defined in equation (2.8).

4.1 Energy dependence film detectors

It is known that radiochromic films have the advantage that they present only a weak energy dependence from kV to MV photon beams [54-57]. However, in the kV range, it has been reported that there is an energy dependence, certainly when going below 100 kV [58, 59]. When observing the results from the PDD measurements, it can be observed that there is an influence when the energy used for the irradiations to make the calibration curve is different from the irradiated film that is investigated. Between 225 kV and 100 kV, the difference is between 1.5 % - 2 %. But if the energy of the beam drops below 100 kV (e.g. 225 kV to 60 kV or 100 kV to 60 kV), the difference is more than 20 %. These kinds of results were also observed in [59]. From these results, it can be concluded that to perform accurate film dosimetry for kV photon energies, the energy used for film calibration should be the same or very similar to the energy used for dosimetry of the irradiated films with unknown dose distribution.

When comparing the experimental results to the simulation results, they agree for all energies except for the beam at 50 kV for the PDD's measured in water. This could be due to the self-absorption of the film dosimeters as the film was placed parallel to the beam direction. For the PDD's in RW3, the agreement was fine where the films were placed perpendicular to the film beam direction.

4.2 Relative response of alanine detectors

4.2.1 Energy dependence

For MV beams, the relative response of alanine dosimetry is already well documented [24]. For kV beams, investigations were also performed [28-30, 42]. It was shown that the relative response in kV beam qualities drops down to 0.64 for 30 kV beams, relative to ^{60}Co radiation.

In this study, we used a different approach to define the relative response of alanine dosimetry. When comparing to ^{60}Co, two irradiations must be performed. One irradiation in beam quality Q (that you are investigating) and another irradiation in a ^{60}Co beam. This

means that the uncertainty of the delivered dose in both irradiations must be taken into account.

In this study, the measured doses by the alanine dosimeters were compared to film measurements placed at the same location as the alanine detectors as close as possible. In this way, only 1 irradiation is needed to perform the study for a certain beam quality.

One of the issues comparing measurements with kV beams is the usage of beams with different parameters in various studies. Many different types of filtrations can be used to make the spectra softer or harder. This makes the peak voltage an unsuitable parameter for comparisons. Another option to use for comparisons is to use parameters like the mean energy or the HVL of the spectra of the X-ray beams.

The results in this study show that the relative response drops to 0.66 for the spectra of 50 kV having 35 kV mean energy. The results agree well with Anton et al. [28] and also with Silvestre Patallo et al. [43]. It seems feasible to use the film detectors as the comparison against the alanine pellets if the correct energy is used for the calibration curves of the films to calculate the corresponding dose maps. The results in this study show that it is feasible to characterise the response of alanine dosimeters in the function of the mean energy or the HVL as done by Silvestre Patallo et al. [43].

The simulated results agree with Anton et al. [40] if the bulk density (1.2 g/cm^3) is used for the alanine stopping power density correction. It was reported that for MV beams and MeV electrons it is better to use the crystalline alanine density (1.42 g/cm^3) for the stopping power density correction [24], but the results in this study imply that for kV beams it is better to use the bulk density. This can be explained because the bulk density is the actual physical density (1.2g/cm^2) of the alanine pellets rather than using the crystalline density (1.42 g/cm^2) which is higher. The justification of using the crystalline density because it is the only part that interacts with the ionising radiation is not validated with our results.

In this study, as well as in Anton's results, the simulated and experimental results do not agree as explained in 3.5.2. The number of radicals generated per unit absorbed dose decreases for kV beams and this effect can be described as the intrinsic efficiency that cannot be simulated by MC simulations. However, it seems that the drop is quite constant as we observe a difference of about 4.5 % between the simulated and experimental results. To be able to compare simulation and experimental results, the effect of the intrinsic efficiency must be

known. This was investigated by Olko et al. [82, 83] and they concluded that the number of radicals generated per unit of absorbed dose remained constant for ^{60}Co radiation, electrons and MV X-rays. However, the number of radicals decreased per unit absorbed dose for kV X-rays. Since alanine/EPR dosimetry is based on the detection of the concentration of free radicals, this must be known to reproduce these results by MC simulations.

4.2.2 Field size dependence

Smaller irradiations fields are more and more used these days in the field of radiotherapy and certainly in the preclinical research. There are several problems with dosimetry in small fields such as the steep gradient of the radiation field, volume averaging effect, lack of charged particle equilibrium, partial occlusion of the radiation source and beam alignment [44].

Alanine detectors also suffer from effects such as the volume averaging effect. It was shown that the dose measured by the alanine pellet is the dose at the centre of the pellet if there is a constant dose gradient [40].

The results of this study show that the response of the alanine detectors increases slightly with decreasing field size for kV X-rays. This could be explained due to the loss of scatter and therefore fewer photons with lower energy interacting with the alanine pellet. This means that photons of higher energy interact with the alanine pellet and so the response increases.

4.2.3 Summary

In general, it can be concluded that the response of the alanine detectors can be characterised in these conditions with a general parameter such as the mean energy or the HVL. This makes it feasible to use alanine/EPR dosimetry in the preclinical radiotherapy research and electronic brachytherapy sources.

5 Conclusion

The relative response of the alanine dosimeters changes for kV X-rays and smaller fields. The relative response drops down to 0.665 for X-rays with mean energies of 35.3 keV while the relative response increases 1.5 % for decreasing field sizes to 10 x 10 mm². It is possible to characterise the response of the detectors in function of certain beam parameters such as the mean energy or the HVL of the X-ray spectra. This way it is feasible to use alanine detectors for dosimetry QA of small animal irradiators used in preclinical radiotherapy research.

6 References

[1] B. Yalvac *et al.*, "Results of external audits for basic and complex dosimetry for photon and electron beams from Oct 2016.," in *34th BHPA Symposium*, Aalst, Belgium, 2019/02/01 2019. [Online]. Available: http://hdl.handle.net/1942/27928.

[2] B. Yalvac *et al.* "Mailed Auditing." UHasselt. https://www.uhasselt.be/UH/NUTEC-Medical-dosimetry/Mailed-auditing.html (accessed 2019/10/30.

[3] B. Schaeken *et al.*, "Implementation of alanine/EPR as transfer dosimetry system in a radiotherapy audit programme in Belgium," *Radiother Oncol,* vol. 99, no. 1, pp. 94-6, Apr 2011, doi: 10.1016/j.radonc.2011.01.026.

[4] F. Verhaegen *et al.*, "Small animal radiotherapy research platforms," *Phys Med Biol,* vol. 56, no. 12, pp. R55-83, Jun 21 2011, doi: 10.1088/0031-9155/56/12/R01.

[5] D. Liu *et al.*, "Spectroscopic characterization of a novel electronic brachytherapy system," *Phys Med Biol,* vol. 53, no. 1, pp. 61-75, Jan 7 2008, doi: 10.1088/0031-9155/53/1/004.

[6] M. J. Rivard *et al.*, "Calculated and measured brachytherapy dosimetry parameters in water for the Xoft Axxent X-Ray Source: an electronic brachytherapy source," *Med Phys,* vol. 33, no. 11, pp. 4020-32, Nov 2006, doi: 10.1118/1.2357021.

[7] M. Dinsmore *et al.*, "A new miniature x-ray source for interstitial radiosurgery: device description," *Med Phys,* vol. 23, no. 1, pp. 45-52, Jan 1996, doi: 10.1118/1.597790.

[8] W. W. Bradshaw *et al.*, "The Use of Alanine as a Solid Dosimeter," *Radiation Research,* vol. 17, no. 1, 1962, doi: 10.2307/3571206.

[9] G. R. Eaton *et al.*, *Quantitative EPR*. Springer Vienna, 2010.

[10] O. F. Sleptchonok *et al.*, "Advancements in accuracy of the alanine dosimetry system. Part 1. The effects of environmental humidity," *Radiation Physics and Chemistry,* vol. 57, no. 2, pp. 115-133, 2000, doi: 10.1016/s0969-806x(99)00338-2.

[11] V. Nagy *et al.*, "Advancements in accuracy of the alanine EPR dosimetry system Part III: Usefulness of an adjacent reference sample," *Radiation Physics and Chemistry,* vol. 59, no. 4, pp. 429-441, Oct 2000, doi: Doi 10.1016/S0969-806x(00)00275-9.

[12] M. Z. Heydari *et al.*, "Alanine Radicals. 2. The Composite Polycrystalline Alanine EPR Spectrum Studied by ENDOR, Thermal Annealing, and Spectrum Simulations," *The Journal of Physical Chemistry A,* vol. 106, no. 38, pp. 8971-8977, 2002/09/01 2002, doi: 10.1021/jp026023c.

[13] K. V. Ettinger, "Free radical dosimetry techniques and their suitability for precise and accurate measurements of radiation," *International Journal of Radiation Applications and Instrumentation. Part A. Applied Radiation and Isotopes,* vol. 40, no. 10-12, pp. 865-870, 1989, doi: 10.1016/0883-2889(89)90008-7.

[14] D. F. Regulla *et al.*, "Dosimetry by ESR spectroscopy of alanine," *The International Journal of Applied Radiation and Isotopes,* vol. 33, no. 11, pp. 1101-1114, 11/1982 1982, doi: 10.1016/0020-708x(82)90238-1.
[15] P. H. G. Sharpe *et al.*, "The effect of irradiation temperatures between ambient and 80°C on the response of alanine dosimeters," *Radiation Physics and Chemistry,* vol. 78, no. 7-8, pp. 473-475, 2009, doi: 10.1016/j.radphyschem.2009.03.028.
[16] J. M. Arber *et al.*, "Fading characteristics of irradiated alanine pellets: The importance of pre-irradiation conditioning," *Applied Radiation and Isotopes,* vol. 44, no. 1-2, pp. 19-22, 1993, doi: 10.1016/0969-8043(93)90190-l.
[17] M. Anton, "Development of a secondary standard for the absorbed dose to water based on the alanine EPR dosimetry system," *Appl Radiat Isot,* vol. 62, no. 5, pp. 779-95, May 2005, doi: 10.1016/j.apradiso.2004.10.009.
[18] V. Nagy *et al.*, "Advancements in accuracy of the alanine EPR dosimetry system," *Radiation Physics and Chemistry,* vol. 59, no. 4, pp. 429-441, 2000, doi: 10.1016/s0969-806x(00)00275-9.
[19] A. Gago-Arias *et al.*, "Development of an alanine dosimetry system for radiation dose measurements in the radiotherapy range," *Journal of Instrumentation,* vol. 10, no. 08, pp. T08004-T08004, Aug 2015, doi: 10.1088/1748-0221/10/08/T08004.
[20] B. A. Goodman *et al.*, "Radiation Dosimetry Using Alanine and Electron Paramagnetic Resonance (EPR) Spectroscopy: A New Look at an Old Topic," *Applied Magnetic Resonance,* vol. 48, no. 2, pp. 155-173, 2016, doi: 10.1007/s00723-016-0855-8.
[21] M. F. Desrosiers *et al.*, "Absorbed-dose/dose-rate dependence studies for the alanine-EPR dosimetry system," *Radiation Physics and Chemistry,* vol. 78, no. 7-8, pp. 461-463, 2009, doi: 10.1016/j.radphyschem.2009.03.025.
[22] M. F. Desrosiers *et al.*, "An Absorbed-Dose/Dose-Rate Dependence for the Alanine-EPR Dosimetry System and Its Implications in High-Dose Ionizing Radiation Metrology," *J Res Natl Inst Stand Technol,* vol. 113, no. 2, pp. 79-95, Mar-Apr 2008, doi: 10.6028/jres.113.007.
[23] H. Kudoh *et al.*, "Response of alanine dosimeters at very high dose rate," *Applied Radiation and Isotopes,* vol. 48, no. 4, pp. 497-499, 1997, doi: 10.1016/s0969-8043(96)00281-3.
[24] M. Anton *et al.*, "Difference in the relative response of the alanine dosimeter to megavoltage x-ray and electron beams," *Phys Med Biol,* vol. 58, no. 10, pp. 3259-82, May 21 2013, doi: 10.1088/0031-9155/58/10/3259.
[25] M. Anton *et al.*, "Response of the alanine/ESR dosimetry system to MV X-rays relative to (60)Co radiation," *Phys Med Biol,* vol. 53, no. 10, pp. 2753-70, May 21 2008, doi: 10.1088/0031-9155/53/10/020.
[26] G. G. Zeng *et al.*, "An experimental and Monte Carlo investigation of the energy dependence of alanine/EPR dosimetry: I. Clinical x-ray beams," *Phys Med Biol,* vol. 49, no. 2, pp. 257-70, Jan 21 2004, doi: 10.1088/0031-9155/49/2/006.
[27] E. S. Bergstrand *et al.*, "An investigation of the photon energy dependence of the EPR alanine dosimetry system," *Phys Med Biol,* vol. 48, no. 12, pp. 1753-71, Jun 21 2003, doi: 10.1088/0031-9155/48/12/306.

[28] M. Anton *et al.*, "Relative response of the alanine dosimeter to medium energy x-rays," *Phys Med Biol,* vol. 60, no. 15, pp. 6113-29, Aug 7 2015, doi: 10.1088/0031-9155/60/15/6113.
[29] E. Waldeland *et al.*, "The energy dependence of lithium formate and alanine EPR dosimeters for medium energy x rays," *Med Phys,* vol. 37, no. 7, pp. 3569-75, Jul 2010, doi: 10.1118/1.3432567.
[30] G. G. Zeng *et al.*, "The response of alanine to a 150keV X-ray beam," *Radiation Physics and Chemistry,* vol. 72, no. 5, pp. 537-540, 4/2005 2005, doi: 10.1016/j.radphyschem.2004.05.044.
[31] S. Onori *et al.*, "Use of commercial alanine and TL dosemeters for dosimetry intercomparisons among Italian radiotherapy centres," *Radiat Prot Dosimetry,* vol. 120, no. 1-4, pp. 226-9, 2006, doi: 10.1093/rpd/nci632.
[32] C. De Angelis *et al.*, "Use of alanine for dosimetry intercomparisons among Italian radiotherapy centers," *Appl Radiat Isot,* vol. 62, no. 2, pp. 261-5, Feb 2005, doi: 10.1016/j.apradiso.2004.08.019.
[33] P. H. G. Sharpe *et al.*, "Progress towards an alanine/ESR therapy level reference dosimetry service at NPL," *Applied Radiation and Isotopes,* vol. 47, no. 11-12, pp. 1171-1175, Nov-Dec 1996, doi: Doi 10.1016/S0969-8043(96)00174-1.
[34] P. H. G. Sharpe *et al.*, "Alanine dosimetry at NPL - the development of a mailed reference dosimetry service at radiotherapy dose levels," International Atomic Energy Agency (IAEA), 1011-4289, 1999. [Online]. Available: http://inis.iaea.org/search/search.aspx?orig_q=RN:30019778
[35] S. Heukelom *et al.*, "NCS Report 25: Process management and quality assurance for intracranial stereotactic treatment," NCS, Delft, 2015-10-01 2015. Accessed: 2018-09-13 10:13:30.
[36] T. Garcia *et al.*, "Dose verification and calibration of the Cyberknife® by EPR/alanine dosimetry," *Radiation Measurements,* vol. 46, no. 9, pp. 952-957, 2011, doi: 10.1016/j.radmeas.2011.03.031.
[37] G. Budgell *et al.*, "A national dosimetric audit of IMRT," *Radiother Oncol,* vol. 99, no. 2, pp. 246-52, May 2011, doi: 10.1016/j.radonc.2011.03.016.
[38] H. Yamaguchi *et al.*, "Development of postal dosimetry service using an alanine dosimeter in Japan," *Radiation Measurements,* 2020, doi: 10.1016/j.radmeas.2020.106339.
[39] P. Diez *et al.*, "A multicentre audit of HDR/PDR brachytherapy absolute dosimetry in association with the INTERLACE trial (NCT015662405)," *Phys Med Biol,* vol. 62, no. 23, pp. 8832-8849, Nov 9 2017, doi: 10.1088/1361-6560/aa91a9.
[40] M. Anton *et al.*, "Response of the alanine/ESR dosimeter to radiation from an Ir-192 HDR brachytherapy source," *Phys Med Biol,* vol. 60, no. 1, pp. 175-93, Jan 7 2015, doi: 10.1088/0031-9155/60/1/175.
[41] B. Schaeken *et al.*, "Experimental determination of the energy response of alanine pellets in the high dose rate 192Ir spectrum," *Phys Med Biol,* vol. 56, no. 20, pp. 6625-34, Oct 21 2011, doi: 10.1088/0031-9155/56/20/007.
[42] A. Nasreddine *et al.*, "Absorbed dose to water determination for kilo-voltage X-rays using alanine/EPR dosimetry systems," *Radiation Physics and Chemistry,* 2020, doi: 10.1016/j.radphyschem.2020.108938.
[43] I. Silvestre Patallo *et al.*, "Development and implementation of an end-to-end test for absolute dose verification of small animal pre-clinical irradiation

research platforms," *International Journal of Radiation Oncology*Biology*Physics,* 2020, doi: 10.1016/j.ijrobp.2020.03.001.
[44] I. A. E. AGENCY, *Dosimetry of Small Static Fields Used in External Beam Radiotherapy* (Technical Reports Series, no. 483). Vienna: INTERNATIONAL ATOMIC ENERGY AGENCY, 2017.
[45] M. C. Saylor *et al.*, "A thin film recording medium for use in food irradiation," *International Journal of Radiation Applications and Instrumentation. Part C. Radiation Physics and Chemistry,* vol. 31, no. 4-6, pp. 529-536, 1988, doi: 10.1016/1359-0197(88)90222-6.
[46] R. D. H. Chu *et al.*, "GafchromicTM dosimetry media: A new high dose, thin film routine dosimeter and dose mapping tool," *International Journal of Radiation Applications and Instrumentation. Part C. Radiation Physics and Chemistry,* vol. 35, no. 4-6, pp. 767-773, 1990, doi: 10.1016/1359-0197(90)90313-7.
[47] S. Devic *et al.*, "Reference radiochromic film dosimetry: Review of technical aspects," *Phys Med,* vol. 32, no. 4, pp. 541-56, Apr 2016, doi: 10.1016/j.ejmp.2016.02.008.
[48] F. Verhaegen *et al.*, "A review of treatment planning for precision image-guided photon beam pre-clinical animal radiation studies," *Z Med Phys,* vol. 24, no. 4, pp. 323-34, Dec 2014, doi: 10.1016/j.zemedi.2014.02.004.
[49] R. Clarkson *et al.*, "Characterization of image quality and image-guidance performance of a preclinical microirradiator," *Med Phys,* vol. 38, no. 2, pp. 845-56, Feb 2011, doi: 10.1118/1.3533947.
[50] C. M. Ma *et al.*, "AAPM protocol for 40-300 kV x-ray beam dosimetry in radiotherapy and radiobiology," *Med Phys,* vol. 28, no. 6, pp. 868-93, Jun 2001, doi: 10.1118/1.1374247.
[51] G. G. Poludniowski *et al.*, "Calculation of x-ray spectra emerging from an x-ray tube. Part I. electron penetration characteristics in x-ray targets," *Med Phys,* vol. 34, no. 6, pp. 2164-74, Jun 2007, doi: 10.1118/1.2734725.
[52] G. G. Poludniowski, "Calculation of x-ray spectra emerging from an x-ray tube. Part II. X-ray production and filtration in x-ray targets," *Med Phys,* vol. 34, no. 6, pp. 2175-86, Jun 2007, doi: 10.1118/1.2734726.
[53] G. Poludniowski *et al.*, "SpekCalc: a program to calculate photon spectra from tungsten anode x-ray tubes," *Phys Med Biol,* vol. 54, no. 19, pp. N433-8, Oct 7 2009, doi: 10.1088/0031-9155/54/19/N01.
[54] G. Massillon-Jl *et al.*, "Energy Dependence of the New Gafchromic EBT3 Film:Dose Response Curves for 50 KV, 6 and 15 MV X-Ray Beams," *International Journal of Medical Physics, Clinical Engineering and Radiation Oncology,* vol. 01, no. 02, pp. 60-65, 2012, doi: 10.4236/ijmpcero.2012.12008.
[55] P. Lindsay *et al.*, "Investigation of energy dependence of EBT and EBT-2 Gafchromic film," *Medical Physics,* vol. 37, no. 2, pp. 571-576, 2010, doi: 10.1118/1.3291622.
[56] A. Rink *et al.*, "Energy dependence (to) of radiochromic films assessed using a real-time optical dosimeter," *Medical Physics,* vol. 34, no. 2, pp. 458-463, 2007, doi: 10.1118/1.2431425.
[57] M. J. Butson *et al.*, "Scanning orientation effects on Gafchromic EBT film dosimetry," *Australas Phys Eng Sci Med,* journal article vol. 29, no. 3, pp. 281-4, Sep 2006, doi: 10.1007/bf03178579.

[58] G. Massillon-Jl *et al.*, "Relative efficiency of Gafchromic EBT3 and MD-V3 films exposed to low-energy photons and its influence on the energy dependence," *Phys Med,* vol. 61, pp. 8-17, May 2019, doi: 10.1016/j.ejmp.2019.04.007.
[59] S. Devic *et al.*, "Dose measurements nearby low energy electronic brachytherapy sources using radiochromic film," *Phys Med,* vol. 64, pp. 40-44, Aug 2019, doi: 10.1016/j.ejmp.2019.05.017.
[60] E. Tryggestad *et al.*, "A comprehensive system for dosimetric commissioning and Monte Carlo validation for the small animal radiation research platform," *Phys Med Biol,* vol. 54, no. 17, pp. 5341-57, Sep 7 2009, doi: 10.1088/0031-9155/54/17/017.
[61] J. Wong *et al.*, "High-resolution, small animal radiation research platform with x-ray tomographic guidance capabilities," *Int J Radiat Oncol Biol Phys,* vol. 71, no. 5, pp. 1591-9, Aug 1 2008, doi: 10.1016/j.ijrobp.2008.04.025.
[62] H. Deng *et al.*, "The small-animal radiation research platform (SARRP): dosimetry of a focused lens system," *Phys Med Biol,* vol. 52, no. 10, pp. 2729-40, May 21 2007, doi: 10.1088/0031-9155/52/10/007.
[63] A. Krauss, "The PTB water calorimeter for the absolute determination of absorbed dose to water in60Co radiation," *Metrologia,* vol. 43, no. 3, pp. 259-272, Jun 2006, doi: 10.1088/0026-1394/43/3/008.
[64] M. Cameron *et al.*, "Comparison of phantom materials for use in quality assurance of microbeam radiation therapy," *J Synchrotron Radiat,* vol. 24, no. Pt 4, pp. 866-876, Jul 1 2017, doi: 10.1107/S1600577517005641.
[65] H. Dosimeters. "Harwell Alanine." http://www.harwell-dosimeters.co.uk/harwell-alanine/ (accessed 06/03/2020, 2020).
[66] Bruker. "EMXmicro." Bruker. https://www.bruker.com/products/mr/epr/emxmicro.html (accessed 2020-04-22, 2020).
[67] D. Gybels, "Sample positioning and temperature guarding of a resonance spectrometer," Bachelor Paper, Faculty of Industrial Engineering, Hasselt University, Diepenbeek, 2018.
[68] M. Anton, "Uncertainties in alanine/ESR dosimetry at the Physikalisch-Technische Bundesanstalt," *Phys Med Biol,* vol. 51, no. 21, pp. 5419-40, Nov 7 2006, doi: 10.1088/0031-9155/51/21/003.
[69] M. Anton *et al.*, *Alanine dosimetry - uncertainty components* (PTB-Dos-55). 2009.
[70] A. Niroomand-Rad *et al.*, "Radiochromic film dosimetry: recommendations of AAPM Radiation Therapy Committee Task Group 55. American Association of Physicists in Medicine," *Med Phys,* vol. 25, no. 11, pp. 2093-115, Nov 1998, doi: 10.1118/1.598407.
[71] D. Lewis *et al.*, "Correcting lateral response artifacts from flatbed scanners for radiochromic film dosimetry," *Med Phys,* vol. 42, no. 1, pp. 416-29, Jan 2015, doi: 10.1118/1.4903758.
[72] D. Poppinga *et al.*, "A new correction method serving to eliminate the parabola effect of flatbed scanners used in radiochromic film dosimetry," *Med Phys,* vol. 41, no. 2, p. 021707, Feb 2014, doi: 10.1118/1.4861098.
[73] D. Lewis *et al.*, "Correcting scan-to-scan response variability for a radiochromic film-based reference dosimetry system," *Med Phys,* vol. 42, no. 10, pp. 5692-701, Oct 2015, doi: 10.1118/1.4929563.

[74] A. Micke *et al.*, "Multichannel film dosimetry with nonuniformity correction," *Med Phys,* vol. 38, no. 5, pp. 2523-34, May 2011, doi: 10.1118/1.3576105.
[75] I. BIPM *et al.*, "JCGM 100: Evaluation of measurement data–Guide to the expression of uncertainty in measurement," *International Organization for Standardization,* 2008.
[76] I. Kawrakow *et al.*, "The EGSnrc code system: Monte Carlo simulation of electron and photon transport NRCC Report PIRS-701," National Research Council Canada, 2017. [Online]. Available: http://nrc-cnrc.github.io/EGSnrc/doc/pirs701-egsnrc.pdf
[77] D. W. O. Rogers *et al.*, "NRC user codes for EGSnrc Technical Report PIRS-702," National Research Council Canada, 2017. [Online]. Available: https://nrc-cnrc.github.io/EGSnrc/doc/pirs702-egsnrc-codes.pdf
[78] M. Berger *et al.*, "XCOM: photon cross sections data, NIST standard reference database 8 (XGAM) Technical Report (Gaithersburg, MD: National Institute of Standards and Technology)," 1998. [Online]. Available: www.nist.gov/pml/data/xcom/index.cfm
[79] E. Mainegra-Hing, "User Manual for egs inprz, a GUI for the NRC RZ user-codes NRCC Report PIRS-801(RevB)," National Research Council Canada, 2013. [Online]. Available: https://nrc-cnrc.github.io/EGSnrc/doc/pirs801-egsinprz.pdf
[80] S. Voros *et al.*, "Relative response of alanine dosemeters for high-energy electrons determined using a Fricke primary standard," *Phys Med Biol,* vol. 57, no. 5, pp. 1413-32, Mar 7 2012, doi: 10.1088/0031-9155/57/5/1413.
[81] D. W. O. Rogers *et al.*, *Calculation of electron contamination in a 60Co therapy beam*. International Atomic Energy Agency (IAEA): IAEA, 1988.
[82] P. Olko *et al.*, "Microdosimetric one hit detector model for calculation of dose and energy response of some solid state detectors," *Radiat Prot Dosimetry,* vol. 99, no. 1-4, pp. 381-2, 2002, doi: 10.1093/oxfordjournals.rpd.a006811.
[83] P. Olko, "The microdosimetric one-hit detector model for calculating the response of solid state detectors," *Radiation Measurements,* vol. 35, no. 3, pp. 255-267, Jun 2002.

FACULTEIT WETENSCHAPPEN
Kasteelpark Arenberg 11 bus 2100
3001 LEUVEN (HEVERLEE), BELGIË
tel. + 32 16 32 14 01
www.kuleuven.be